AD626529

TR 65-124

TECHNICAL REPORT NO. 65-124

COMPARISON OF SEISMOGRAPH SYSTEMS AT UBSO

CLEARINGHOUSE
FOR FEDERAL SCIENTIFIC AND
TECHNICAL INFORMATION
Hardcopy | Microfiche
$3.00 | $0.75 | 83 pp as
ARCHIVE COPY
Code 1

DDC
RECEIVED
JAN 21 1966
DDC-IRA F

Sponsored by

Advanced Research Projects Agenc
Nuclear Test Detection Office
ARPA Order No. 624

DISTRIBUTION OF THIS
DOCUMENT IS UNLIMITED.

GEOTECH

THE GEOTECHNICAL CORPORATION

3401 SHILOH ROAD GARLAND, TEXAS

TECHNICAL REPORT NO. 65-124

COMPARISON OF SEISMOGRAPH SYSTEMS AT UBSO

by

Frank F. Seymour

Sponsored by

Advanced Research Projects Agency
Nuclear Test Detection Office
ARPA Order No. 624

TELEDYNE INDUSTRIES, INC.
GEOTECH DIVISION
3401 Shiloh Road
Garland, Texas

3 November 1965

IDENTIFICATION

AFTAC Project No: VT/5054
Project Title: Operation of BMSO and UBSO
ARPA Order No: 624
ARPA Project Code No: 5810
Name of Contractor: The Geotechnical Corporation
Date of Contract: 1 July 1963
Amount of Contract: $568,521
Amount of Supplemental
Agreements to the Contract:

Supplemental Agreement No. 1:	$ ---
Supplemental Agreement No. 2:	$248,512
Supplemental Agreement No. 3:	$190,000
Supplemental Agreement No. 4:	$ 86,400
Supplemental Agreement No. 5:	$ 86,400
Supplemental Agreement No. 6:	$487,471

Amount of total Contract: $1,667,304
Contract Number: AF 33(657)-12373
Contract Expiration Date: 30 April 1966
Program Manager: B. B. Leichliter, BR8-8102

CONTENTS

ILLUSTRATIONS

ILLUSTRATIONS, Continued

ILLUSTRATIONS Continued

ILLUSTRATIONS, Continued

ILLUSTRATIONS, Continued

* * * * * * * * * * * * * * * * *

TABLES

TABLES, Continued

ABSTRACT

Five seismograph systems that are routinely operated at the Uinta Basin Seismological Observatory were evaluated to determine their relative capabilities in detecting teleseismic P-wave arrivals. This evaluation includes a detailed analysis of microseismic background noise, signal characteristics, and signal-to-noise ratios, as recorded on a single element of the surface array of seismographs, both the filtered and unfiltered summation of the outputs of the elements of the surface array, the shallow-hole, and the deep-hole seismograph systems. In addition, system magnitude residuals relative to magnitudes reported by the USC&GS as well as apparent arrival time residuals are presented.

COMPARISON OF SEISMOGRAPH SYSTEMS AT UBSO

1. INTRODUCTION

This report is a compilation of several comparative studies designed to evaluate the relative capabilities and characteristics of the surface array, the deep-hole (DH), and the shallow-hole (SH) seismograph systems at the Uinta Basin Seismological Observatory (UBSO). A previous study in a Geotech Technical Report (TR 64-101) indicated that the optimum depth of operation for the DH seismometer at UBSO is approximately 1980 meters (6500 feet). Initially, we planned to operate the DH seismometer at the optimum depth for an extended interval of time in order to gather data specifically for use in this study; however, because of higher priority tests being performed by other groups, it was not practical. We reviewed the available data and selected an interval of time (16 August through 15 September 1964) during which the seismometer was operated at a depth (2700.5 meters (8860 feet)) that was as close as possible to the optimum depth. Therefore, all results derived from this study are applicable only to these conditions of operation.

Of the 614 teleseismic events recorded during this interval, 200 events that were recorded by all systems were selected for signal-to-noise comparison.

1.1 AUTHORITY

This is a report of the work done under Analysis Assignment SEB-3-64 as a part of Contract AF 33(657)-12373, dated 1 July 1963, and six supplemental agreements. The work was started under Project VT/1124 and because of the assignment of higher priority to other work, was completed under Project VT/5054. The Air Force Technical Applications Center (AFTAC) has technical supervision of the contract as a part of Project VELA-UNIFORM, which is under the overall direction of the Advanced Research Projects Agency (ARPA). Analysis Assignment SEB-3-64 is included in this report as appendix 1.

Figure 1. Diagrammatic sketch of the area surrounding the Uinta Basin Seismological Observatory

1.2 PURPOSE

UBSO is located in Uintah County, Utah, about 12 miles south-southwest of the town of Vernal. Surface-array, deep-hole, and shallow-hole seismographs are part of an extensive complement of instrumentation at the observatory. A generalized sketch of the area showing the location of the observatory and the configuration of the array of short-period vertical seismographs is included as figure 1.

The purpose of this study was to evaluate the relative capabilities of the different systems in detecting teleseismic P-wave arrivals and to determine the difference in signal and noise characteristics as recorded by the various systems. This evaluation includes comparisons of signal and noise characteristics, signal-to-noise ratios, apparent signal first-motion determination, and calculated magnitudes for the systems studied.

2. INSTRUMENTATION

Four seismograph systems were evaluated during the course of this study. These are:

System 1

A single vertical, short-period, Johnson-Matheson (JM) seismometer; an element of the surface array (Z1).

System 2

A vertical, short-period, Deep-Hole Seismometer, Model 11167 operated 57.3 meters (188 feet) below the surface (SH).

System 3

A vertical, short-period, Deep-Hole Seismometer, Model 11167, operated 2700.5 meters (8860 feet) below the surface (DH).

System 4

All 10 short-period vertical elements of the surface array, the arithmetic summation of the outputs of the 10 elements (ST), and a filtered summation of the 10 elements (SF).

For the detection portion of this study (section 4.5), ST and SF were considered to be components of system 4; however, detailed signal and noise measurements were taken from both seismographs for the quantitative evaluations.

The frequency response norms and tolerances for each seismograph studied are shown in figure 2; however, tolerances have not been established for the SF system. Frequency response checks were taken daily on the SH and DH systems as part of an evaluation program being done under another contract. The average frequency response for the SH and DH systems and the standard Benioff frequency response are shown in figure 3. No attempt was made to adjust day-to-day variation in the DH and SH responses. The standard Benioff frequency response was selected as a datum and all SH and DH trace amplitude measurements made during this study were corrected to this datum. Ground displacement calculations were made using the appropriate daily frequency-response data. Frequency-response checks of the standard JM surface-array instruments are made once a month and the parameters are kept within the specified tolerances (figure 2). The Z1 and ST systems are operated with identical parameters. Bandpass filtering is introduced into the SF system, resulting in a different set of frequency response parameters.

3. ANALYSIS OF SEISMOGRAMS

Two types of analyses of the seismograms were performed; i.e., simulated "on-line" analysis and detailed analysis of the microseismic background noise. During the on-line analysis, each of the 31 seismograms was analyzed 5 times. All traces were masked except those of the system being analyzed; e.g., only the trace which represented Z1 was visible during the analysis of system 1. The time of each teleseismic P or P' phase arrival, the associated period and amplitude measurements, and the direction of first motion were recorded on a special analysis form. As a matter of convention, period and amplitude measurements were taken from the largest pulse within the first few cycles of the signal. The half-period (T/2) of the largest pulse was measured

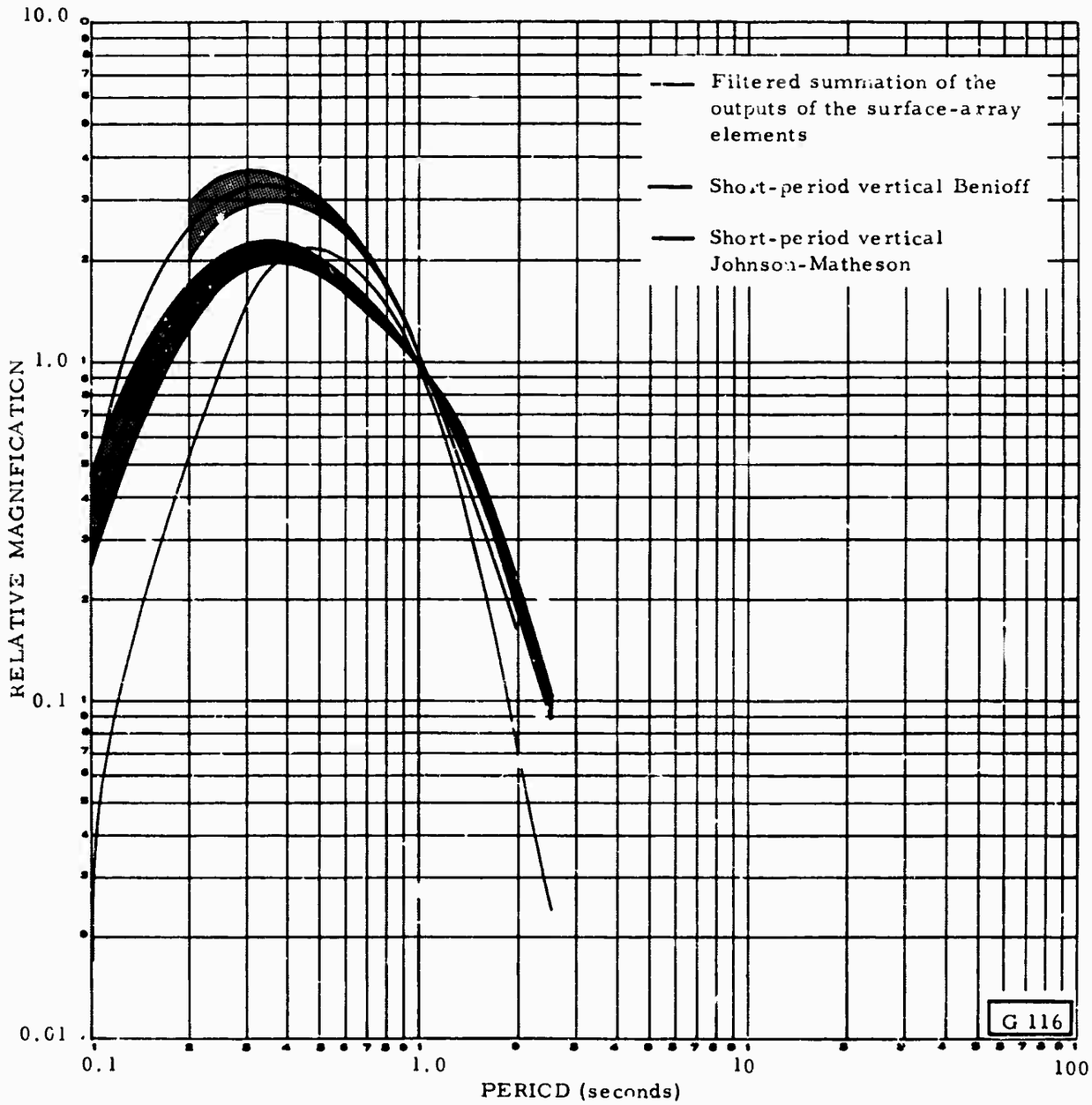

Figure 2. Standard frequency-response norms and tolerances for the UBSO systems included in the study

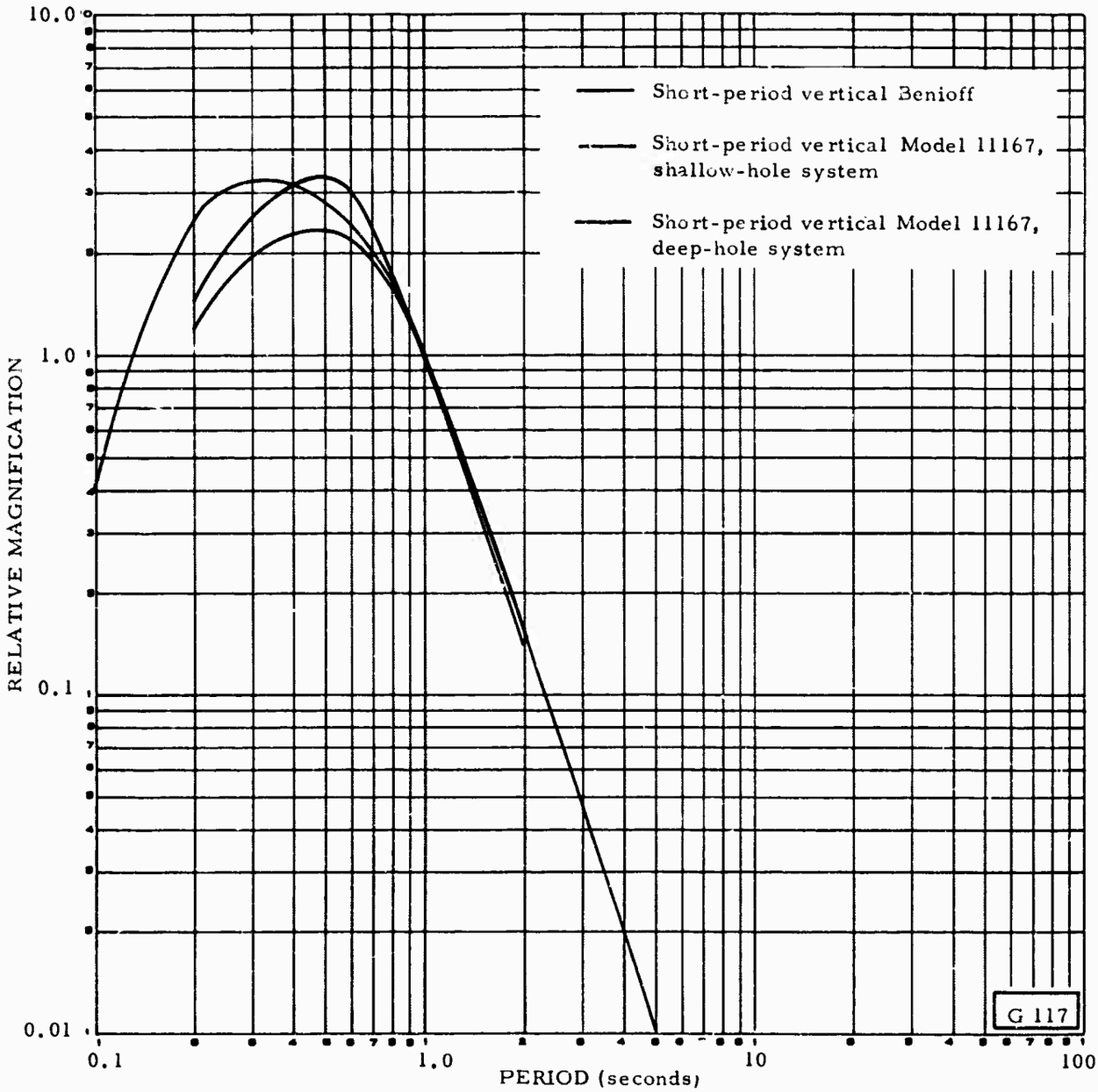

Figure 3. Average frequency responses for the shallow-hole and deep-hole systems and the standard Benioff response

and converted to full period before statistical analysis was performed. When system 4 was analyzed, period and amplitude measurements were made on Z1, ST, and SF.

After each seismogram had been analyzed for seismic events, an analysis of the background noise as recorded by each of the five seismographs (Z1, ST, SF, SH, and DH) was performed. Using 200 signals that were recorded by all five components, the half-period and associated amplitude of each half-cycle of the microseismic background noise in the 10 seconds preceding the arrival of the signal was measured. The wind speed at the time of the measurement was also recorded. Because of the infrequent occurrence of wind at speeds above 15-20 mph, sufficient data were not available for an evaluation of the variation in background noise level as a function of wind speed.

4. DATA REDUCTION AND EVALUATION

4.1 SIGNAL CHARACTERISTICS

The occurrence of each signal was verified (see section 4.5) and the ground motion of each verified signal as recorded on each system was calculated using the following equation.

$$A = \frac{\alpha \times 10^3}{k g_t}$$

where:

A = Peak-to-peak ground displacement in millimicrons.

α = Peak-to-peak pulse amplitude in millimeters when the seismogram is enlarged 10 times.

k = Magnification in thousands at the calibration frequency.

g_t = Correction factor applied to obtain true magnification at the signal frequency; obtained from the seismograph frequency-response curve.

The distribution of signal amplitudes was determined for each system by grouping all occurrences into constant amplitude ratio increments. This convention was adopted because of the large number of signal occurrences in the lower amplitude ranges. The resulting frequency distributions are shown in figures 4 through 7. All signals with amplitudes too large to measure are included in the highest amplitude cell; i.e., all amplitudes greater than or equal to 204.8 mμ. In addition, a comparison was made to determine the relationship of the amplitudes recorded on the SH, DH, and ST systems relative to a single seismograph Z1 of the surface array. For each signal that was recorded by Z1 and any of the other systems, the ratio of the peak-to-peak ground motion relative to Z1, was computed. These data are shown in figures 8 through 10.

Theoretical predictions show that the ratio of DH to Z1 amplitudes should be about 0.4; however, several values appear to be anomalously large. The scatter of data and the large ratio values in figures 8 and 9 can be attributed, at least partially, to the fact that a given signal as recorded on the various seismographs is not affected identically by the background noise. On some seismographs, the signal may be enhanced, whereas on other seismographs, the noise might have a deleterious effect on the recorded amplitude. The mean amplitude ratio value, 0.53, for DH is in close agreement with the value (0.48) reported in TR 64-101.

The accuracy of estimates of the ground displacement resulting from seismic signals is very sensitive to the accuracy with which the dominant frequencies of the signals are determined. For signal periods between 0.2 and 1.0 seconds, the period correction factors ($\frac{1}{g_t}$) are less than 1.0; for periods greater than 1.0 second, the factors are greater than 1.0. Therefore, if two systems, operating with similar frequency responses and at identical magnifications at 1 cps, record the same trace amplitude but at different periods, the computed ground motion for a given signal recorded by the two seismographs may vary as much as 100 percent. Because of frequency-response characteristics, the SH and DH systems are more sensitive to periods less than 1.0 second than are either the Z1 or ST systems. As a result, the DH and SH systems frequently exhibited shorter periods associated with a given signal than either of the other systems. The percentages of the observations for which the signal

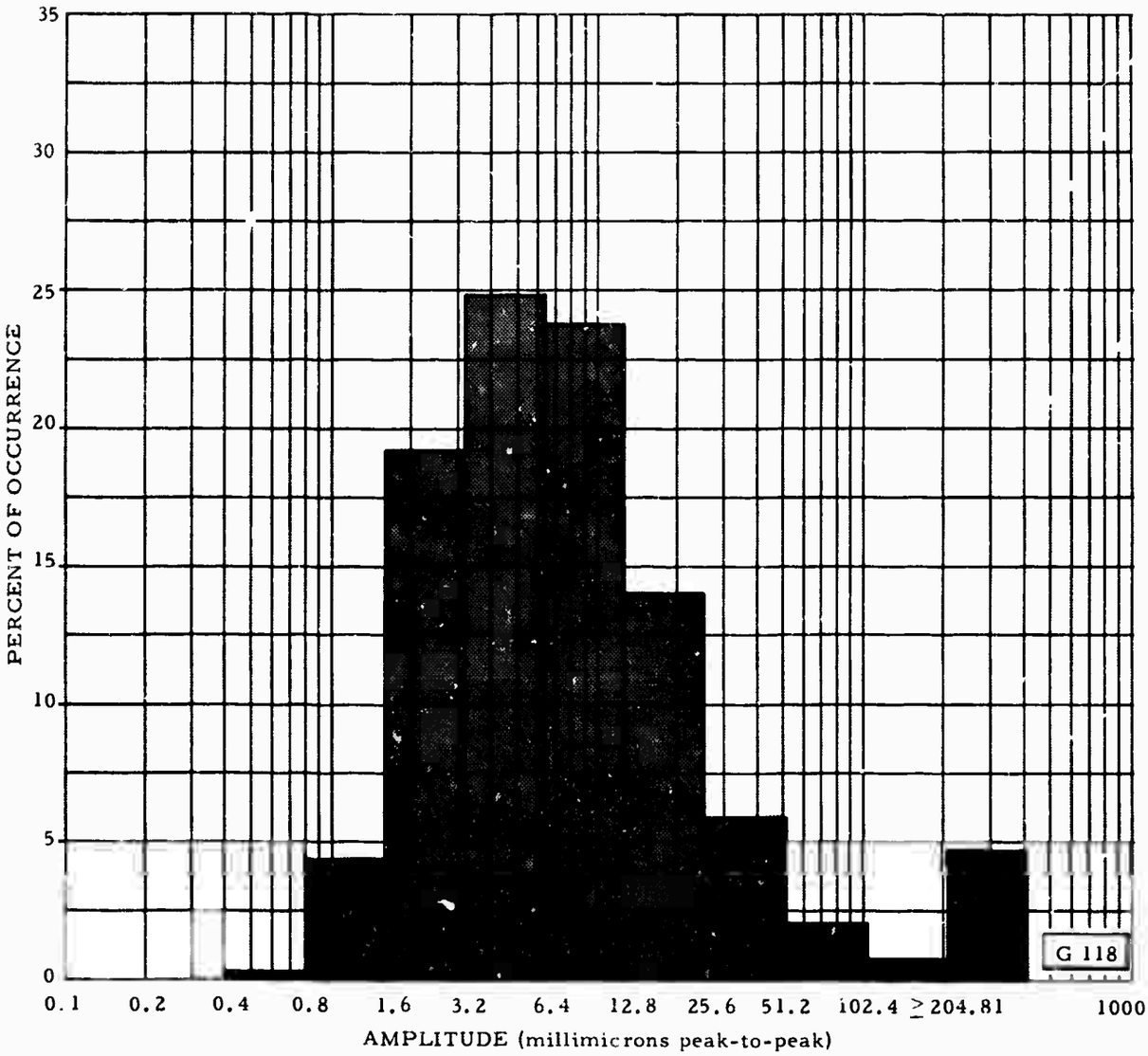

Figure 4. Frequency distribution of amplitudes of 541 signals that were recorded by a single element of the surface array (Z1)

Figure 5. Frequency distribution of amplitudes of 325 signals that were recorded by the shallow-hole (SH) system

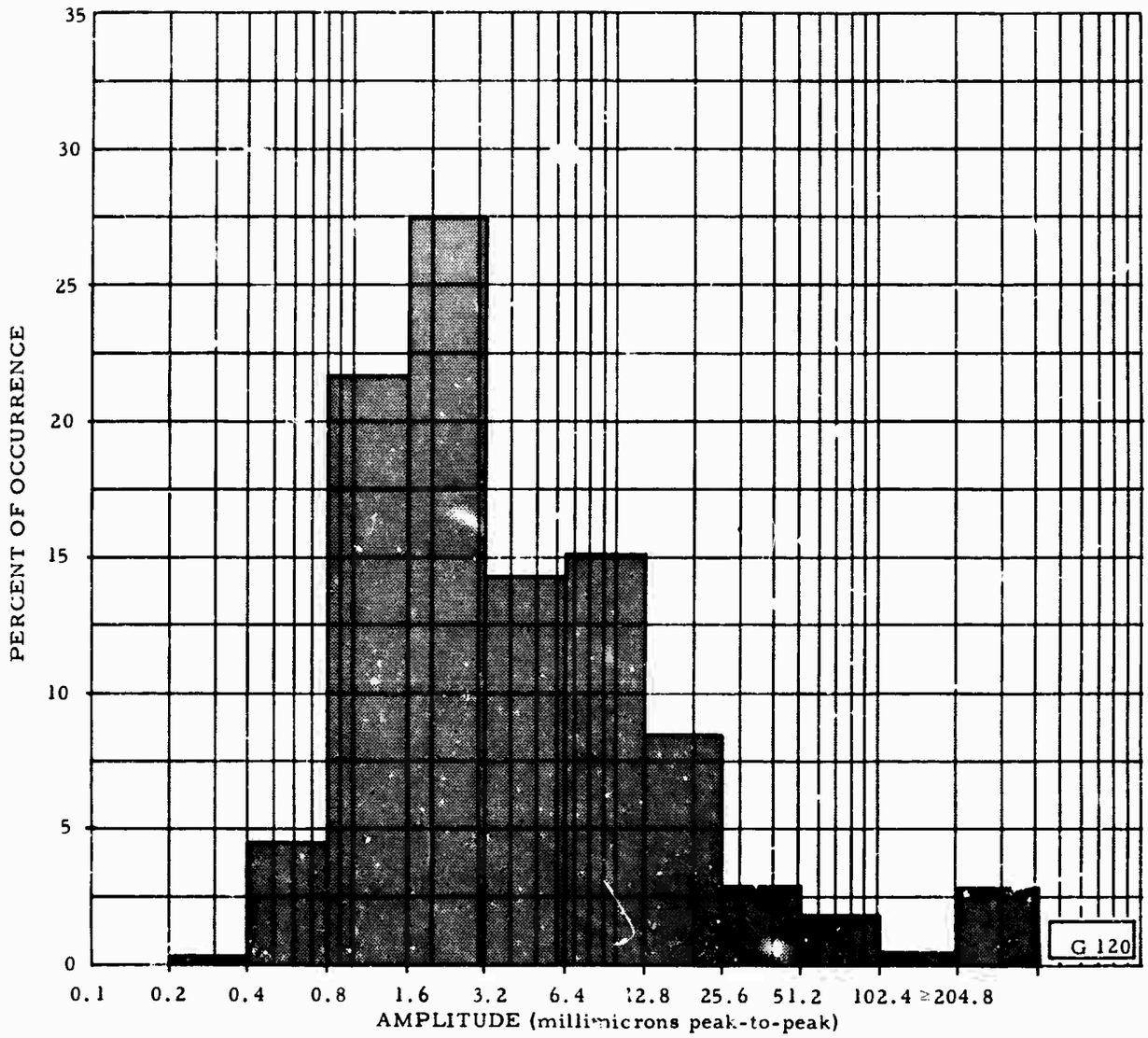

Figure 6. Frequency distribution of amplitudes of 378 signals that were recorded by the deep-hole (DH) system

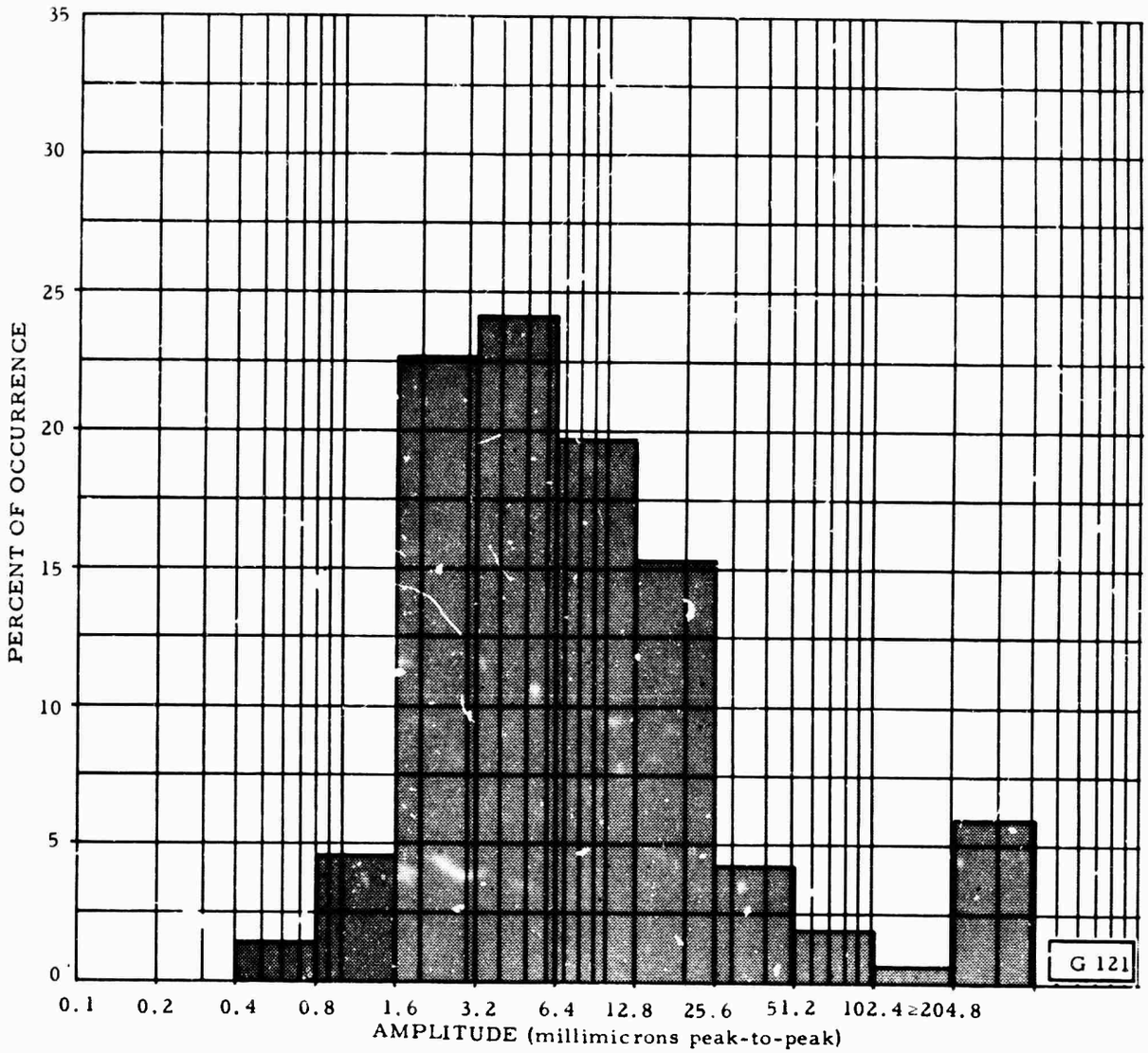

Figure 7. Frequency distribution of amplitudes of 596 signals that were recorded by the summation of the surface-array elements (ST)

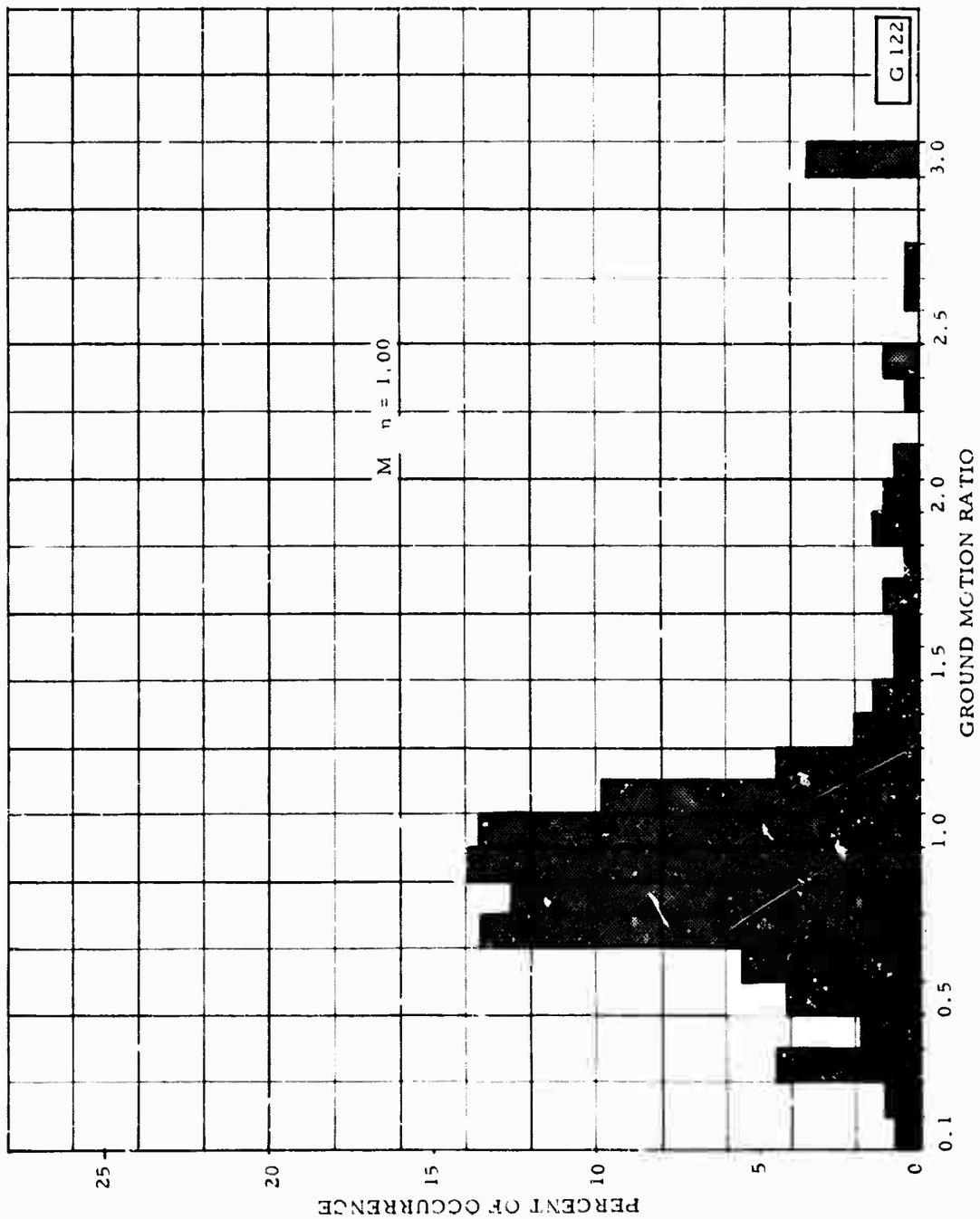

Figure 8. Frequency distribution of the ratios of the peak-to-peak ground motion as recorded by the shallow-hole (SH) system relative to Z1 for 294 signals

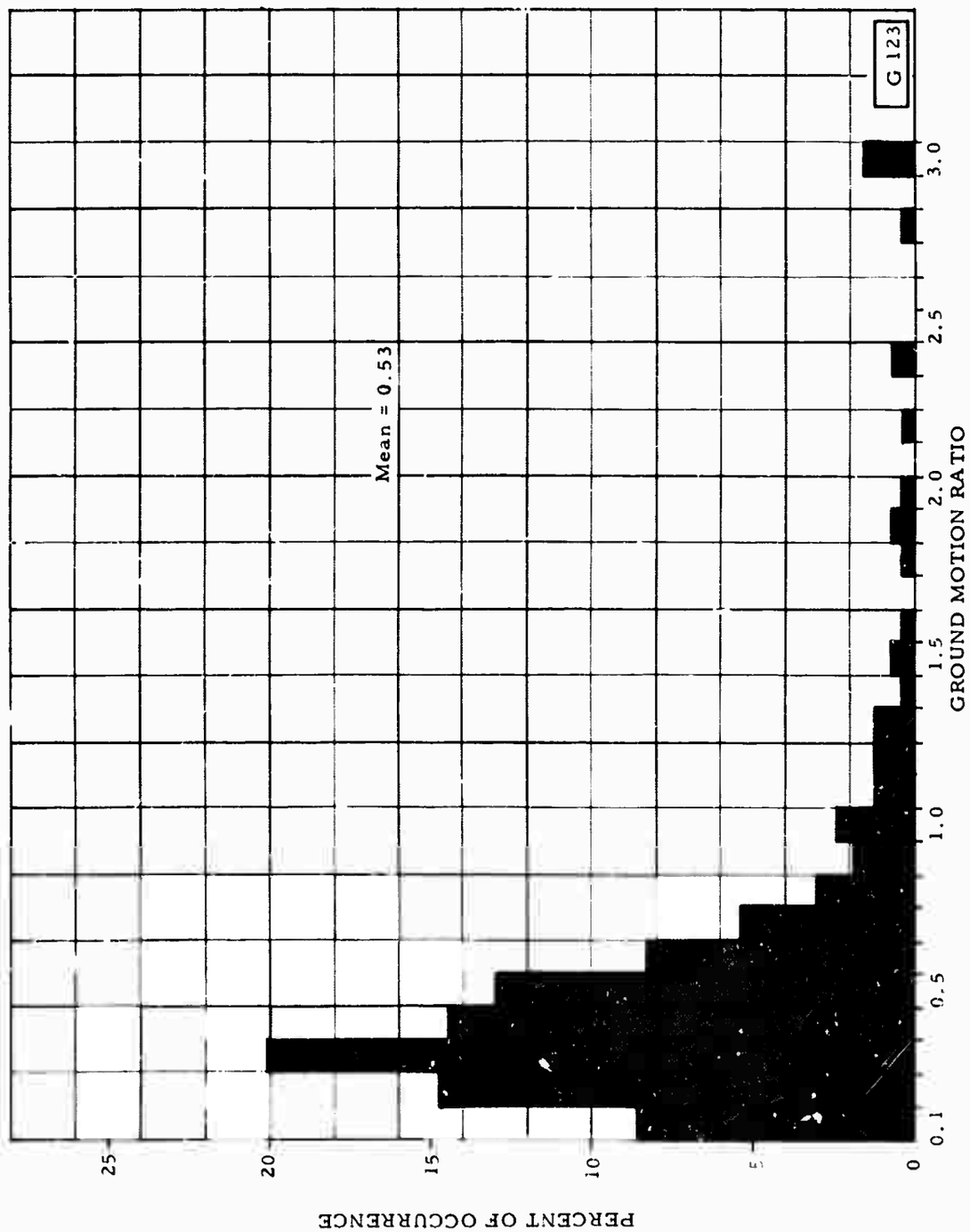

Figure 9. Frequency distribution of the ratios of the peak-to-peak ground motion as recorded by the deep-hole (DH) system relative to Z1 for 339 signals

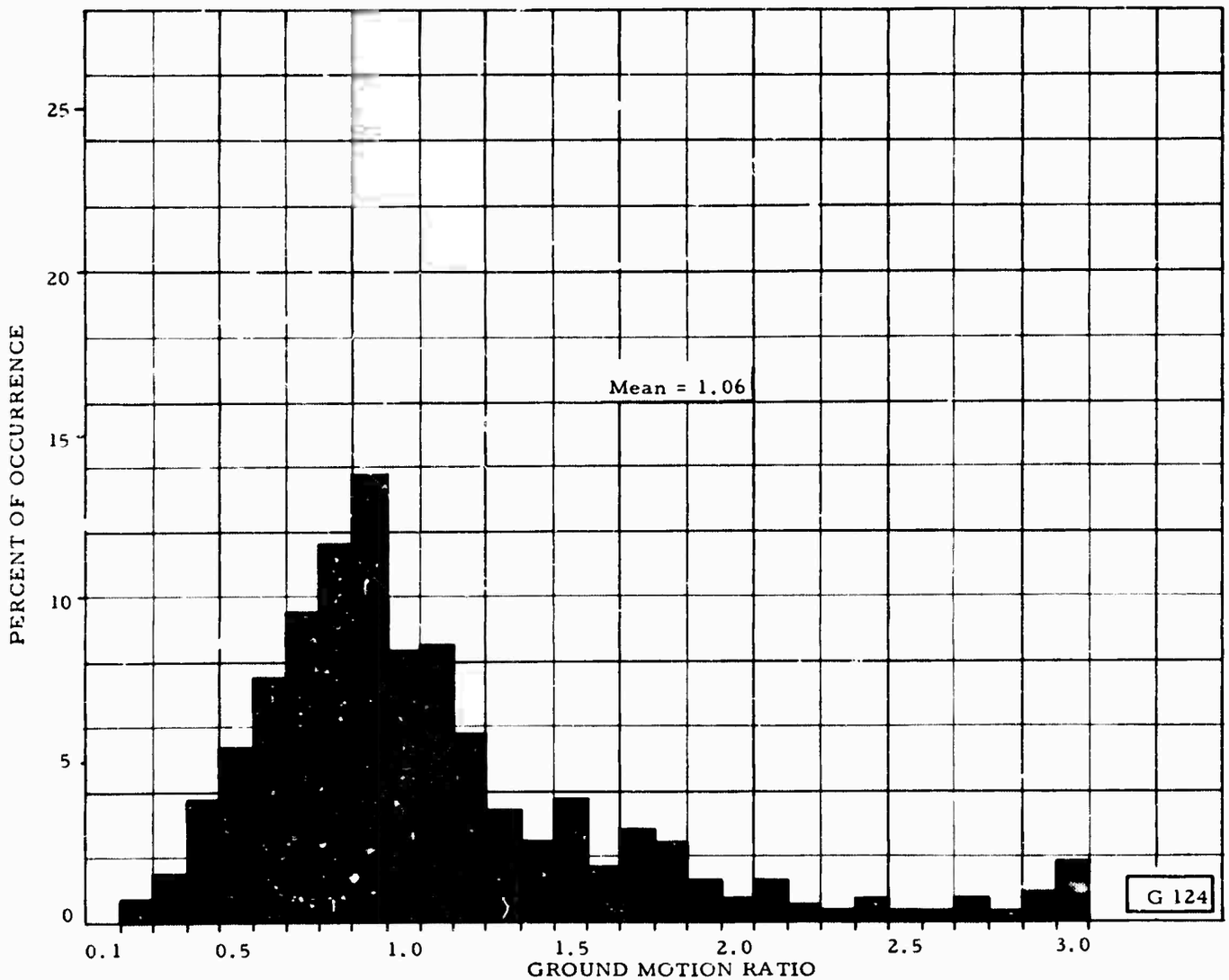

Figure 10. Frequency distribution of the ratios of the peak-to-peak ground motion as recorded by the summation of the surface-array elements (ST) relative to Z1 for 507 signals

period recorded on the SH, DH, and ST systems was observed to be less than the signal period recorded on Z1 follow.

Seismograph	Number of observations	Percent with period less than Z1
DH	339	48.4
SH	294	42.9
ST	507	26.4

The distribution of signal periods and the period ratios relative to Z1 are shown in figures 11 through 17. The prominent mode at a ratio of 0.3 on the amplitude ratio distribution curve (figure 9) for the DH system is probably a result of the tendency of the DH system to record shorter-period signals relative to Z1 (figure 16). The absence of a similar sharp mode on the plot for SH (figure 8) probably reflects the fact that the average frequency response (figure 3) of the SH system is much less sensitive to shorter signal periods than is the DH system.

The apparent ability of the ST system to resolve longer period signals is attributed to the properties of any summation of several seismographs. If all teleseismic signals recorded at UBSO were vertically incident and the background noise level negligible, the simple summation of the 10 array elements (ST) would produce a seismogram identical to Z1. However, few signals are vertically incident. In addition, ST has the ability to attenuate low-velocity, horizontally propagated microseismic noise. Primarily because of the cancellation of microseismic noise achieved by summation and secondarily because of the step-out of signals across the surface array, signal periods determined from the ST system are, in general, longer than signal periods determined from other systems.

4.2 NOISE CHARACTERISTICS

The microseismic background noise is the most important factor influencing the detection capability of any observatory. In an effort to determine the characteristics of the noise at UBSO and its effect on the DH, SH, and surface systems, 200 samples of noise from each system were analyzed. The noise samples chosen were selected because of their proximity to signals that were recorded on all systems. In each case, the 10 seconds of noise preceding

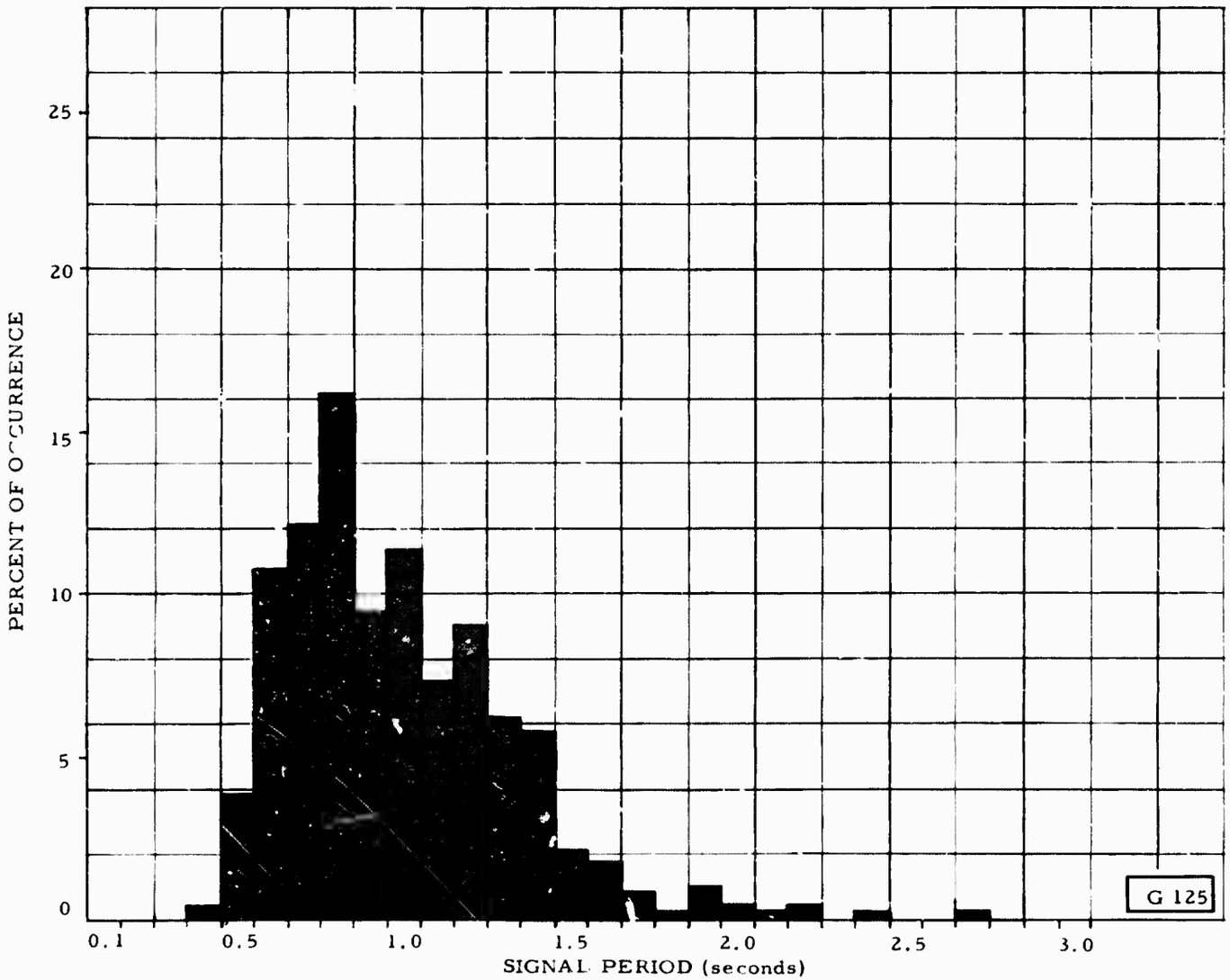

Figure 11. Frequency distribution of periods of 517 signals that were recorded by a single element (Z1) of the surface array

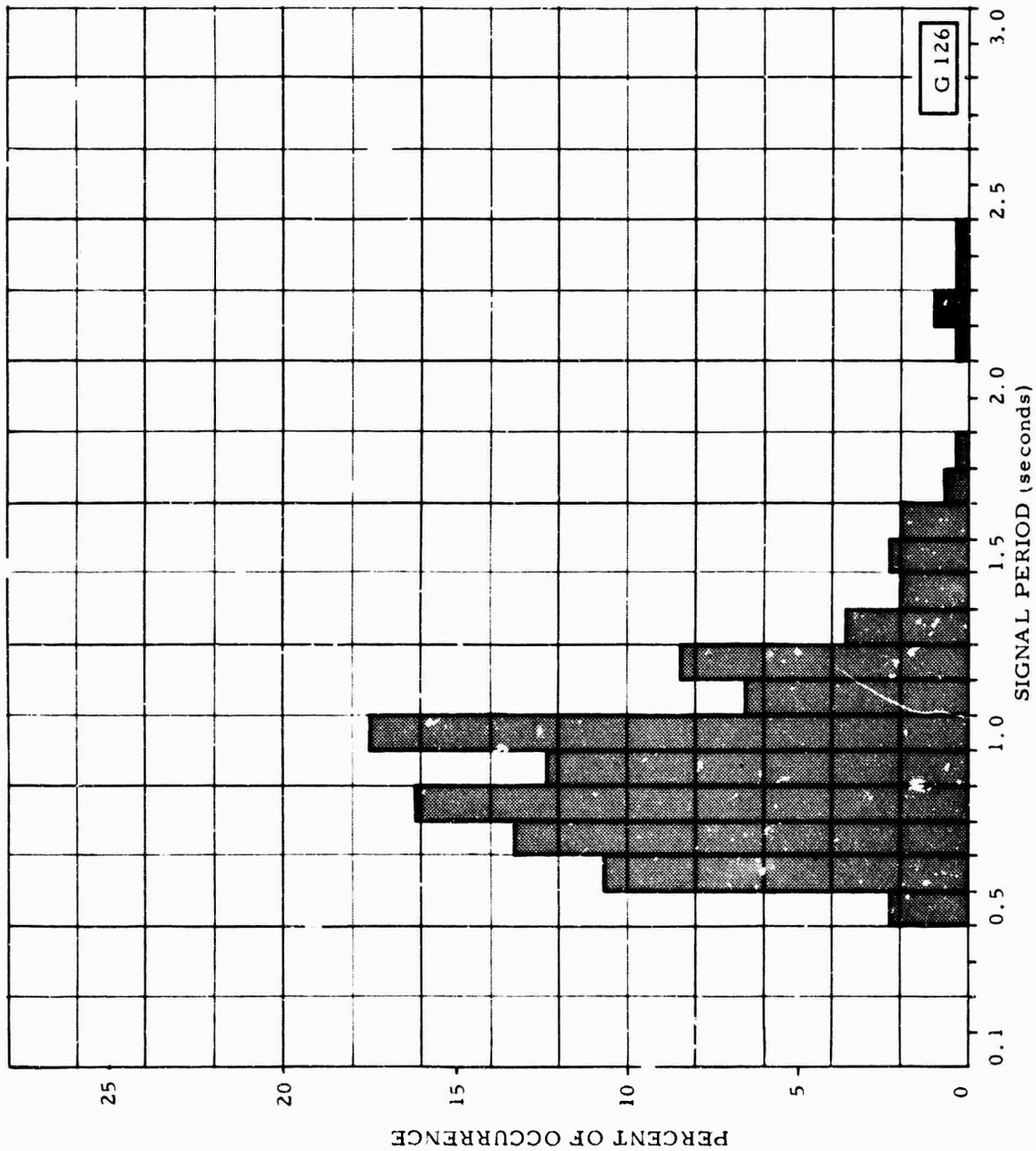

Figure 12. Frequency distribution of periods of 308 signals that were recorded by the shallow-hole (SH) system

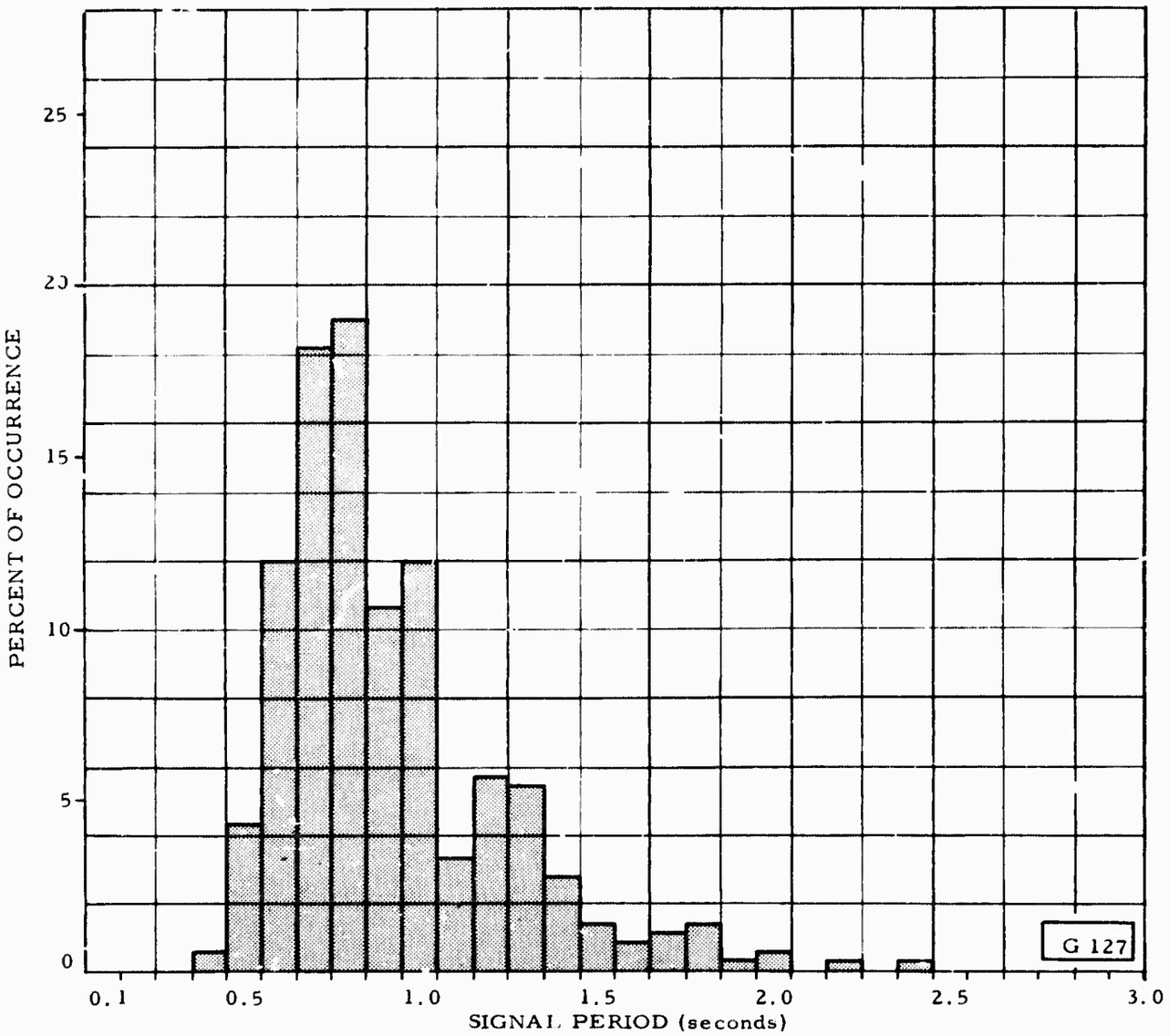

Figure 13. Frequency distribution of periods of 367 signals that were recorded by the deep-hole (DH) system

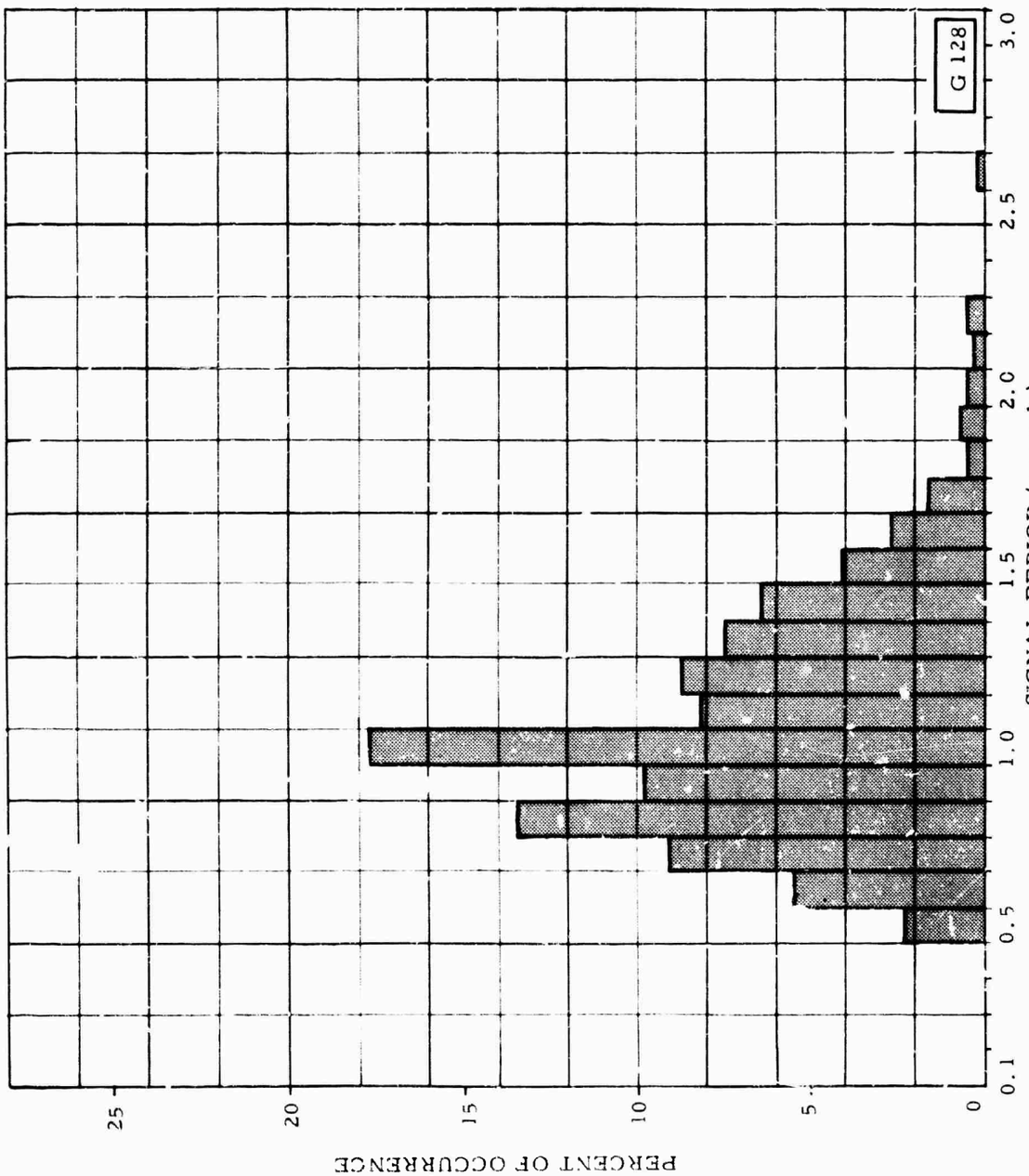

Figure 14. Frequency distribution of periods of 562 signals that were recorded by the summation of the surface-array elements (ST)

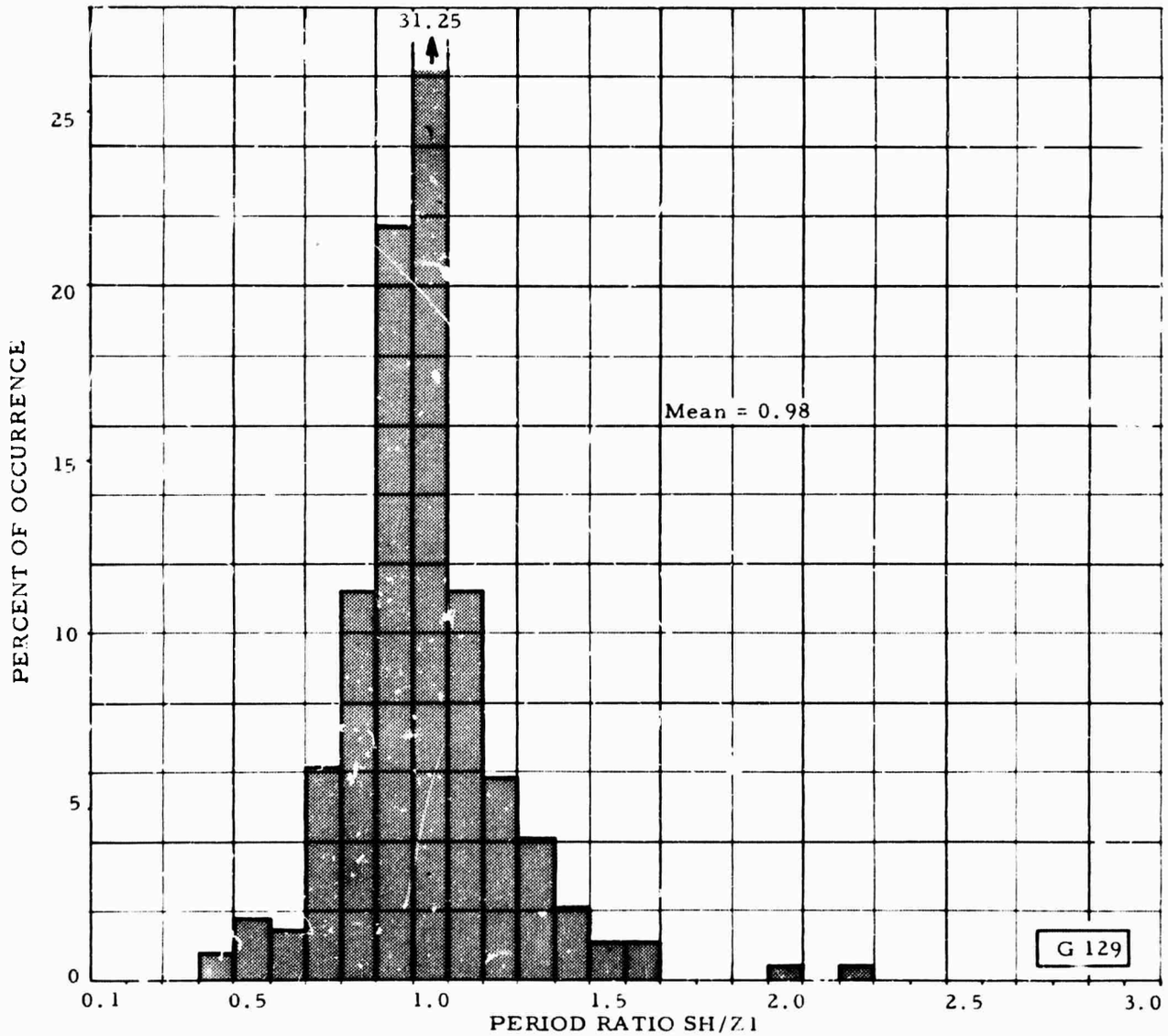

Figure 15. Frequency distribution of the ratios of periods as recorded by the shallow-hole (SH) system relative to Z1 for 294 signals

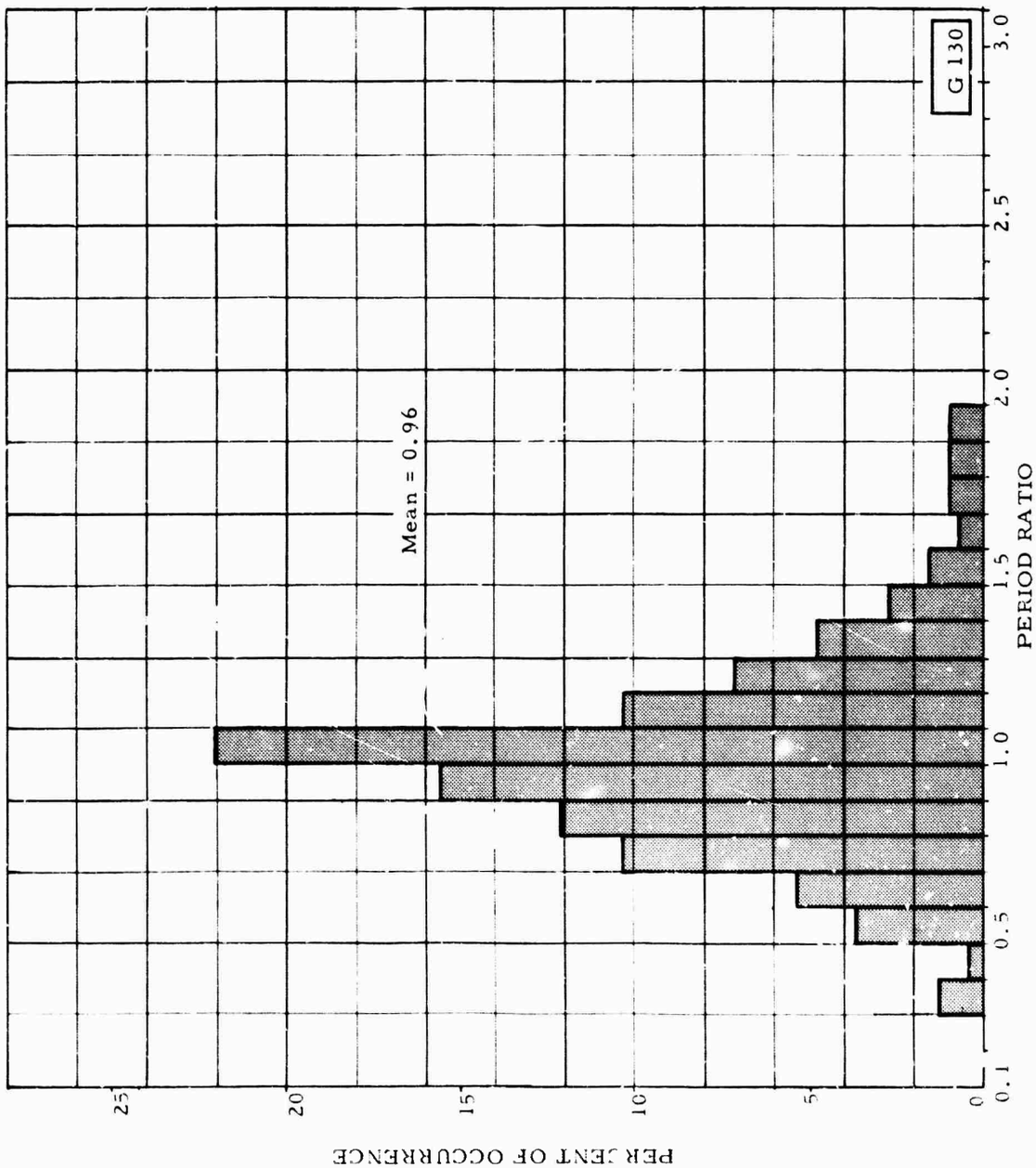

Figure 16. Frequency distribution of the ratios of periods as recorded by the deep-hole (DH) system relative to Z1 for 339 signals

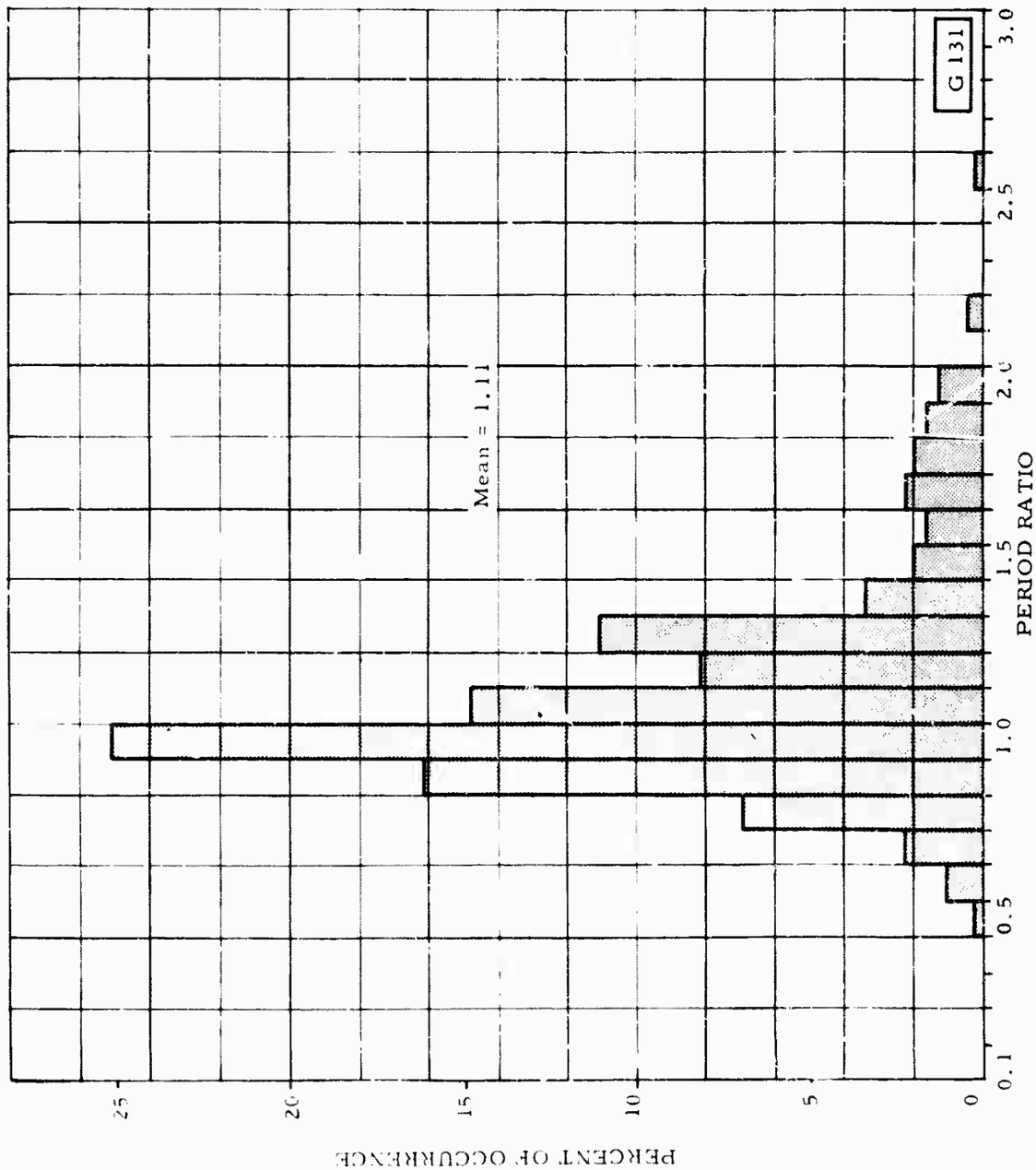

Figure 17. Frequency distribution of the ratios of period as recorded by the summation of the surface array elements (ST) relative to Z 1 for 507 signals

the signal arrival was analyzed in detail. This selection criterion served a two-fold purpose: a random sample interval over the study period was achieved (the 200th signal recorded by all systems was the 518th signal out of the total 614 events used in the study) and the close proximity of the sample time to a signal provided a convenient basis for signal-to-noise ratio comparisons

The peak-to-peak amplitude of each half-cycle of the noise in the 0.1 through 3.0 seconds period range and its associated half-period were measured. Before statistical evaluation was performed, the half-period was converted to full period. This method of measuring noise effectively acts as a low-cut filter. The shorter period noise components are superimposed on the long-period noise pulses, resulting in minimizing the effects of the longer period noise in the data.

All trace amplitude measurements were normalized to a magnification of 600K at 1 cps so that comparisons could readily be made. In addition, the measurements made from the DH and SH seismograms were normalized to the standard Benioff response. Cumulative trace amplitude distributions were compiled for two period ranges: 0.1 through 3.0 seconds and 0.4 through 1.4 seconds. The broader range was chosen so that a complete spectrum of the noise could be determined while the more restricted range was chosen because more than 90 percent of all signals recorded on the individual seismographs exhibited periods that fell within this range. Normalized trace amplitude distributions are presented in figures 18 and 19. To summarize these data, the 50 percent probability points follow:

Seismograph systems	Noise period range 0.1 - 3.0 sec	0.4 - 1.4 sec
Z1	0.60 mm	0.76 mm
SH	0.83	0.83
DH	0.14	0.19
ST	0.41	0.30

The effect of the method used to measure the noise is reflected in the values for the 50 percent probability data points in that all of these values are less than 1.0 mm. The effects of "measurement filtering" are also reflected in the period distribution curves presented in figure 20. Even though this measuring technique makes the noise appear to be of a much lower amplitude

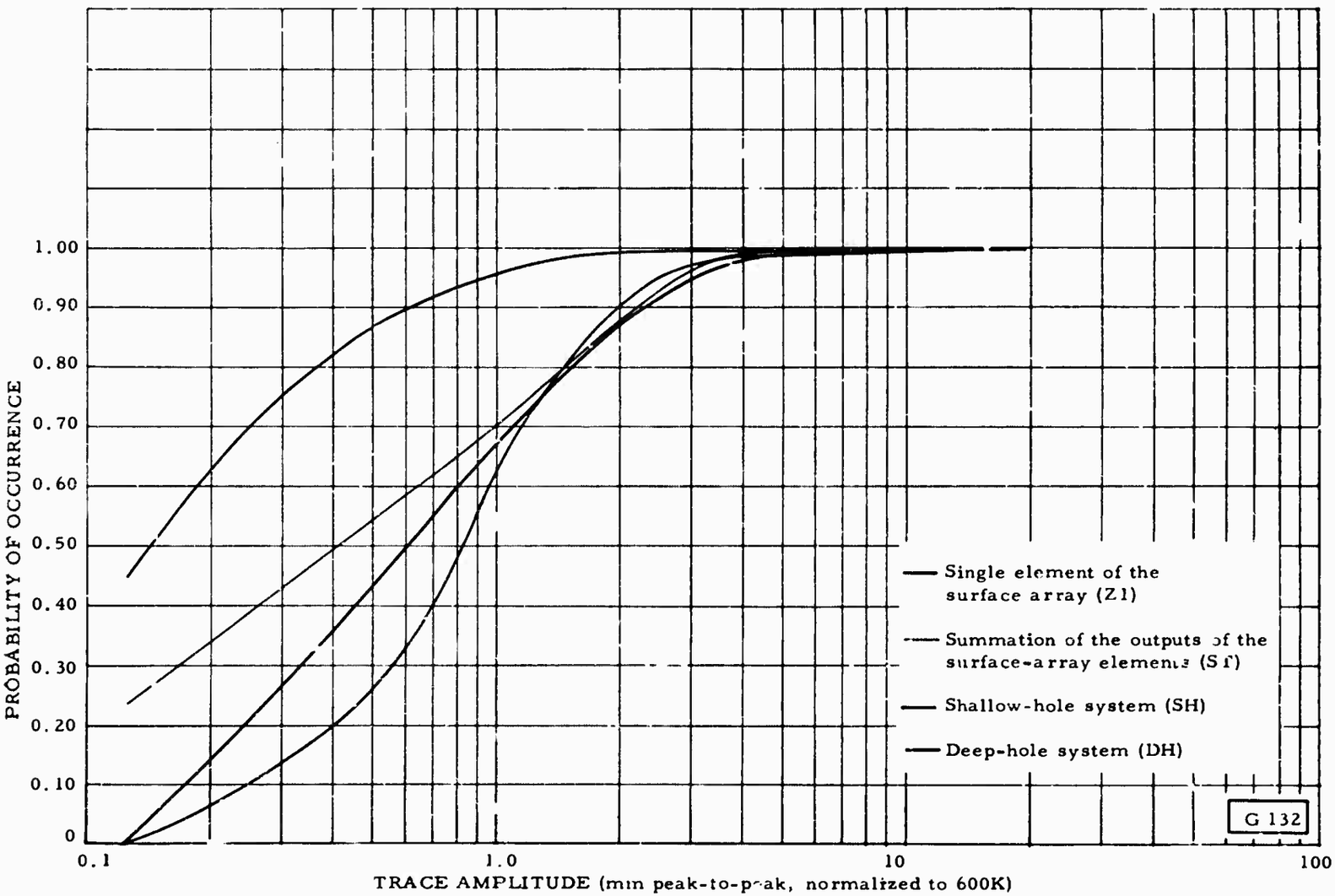

Figure 18. Probability of microseisms in the 0.1 to 3.0 second period range occurring at or less than a given trace amplitude (X10 view)

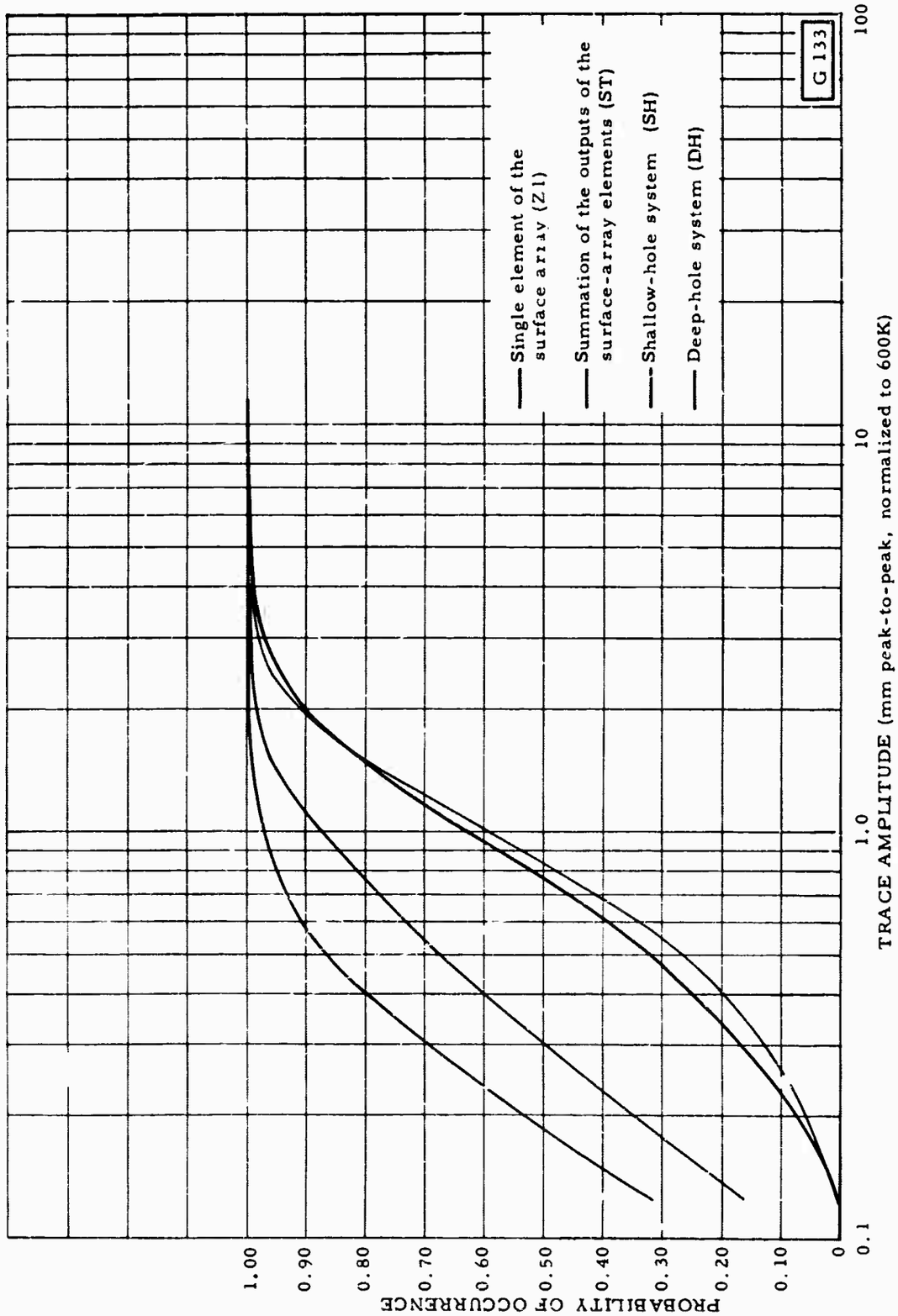

Figure 19. Probability of microseisms in the 0.4 to 1.4 second period range occurring at or less than a given trace amplitude (X10 view)

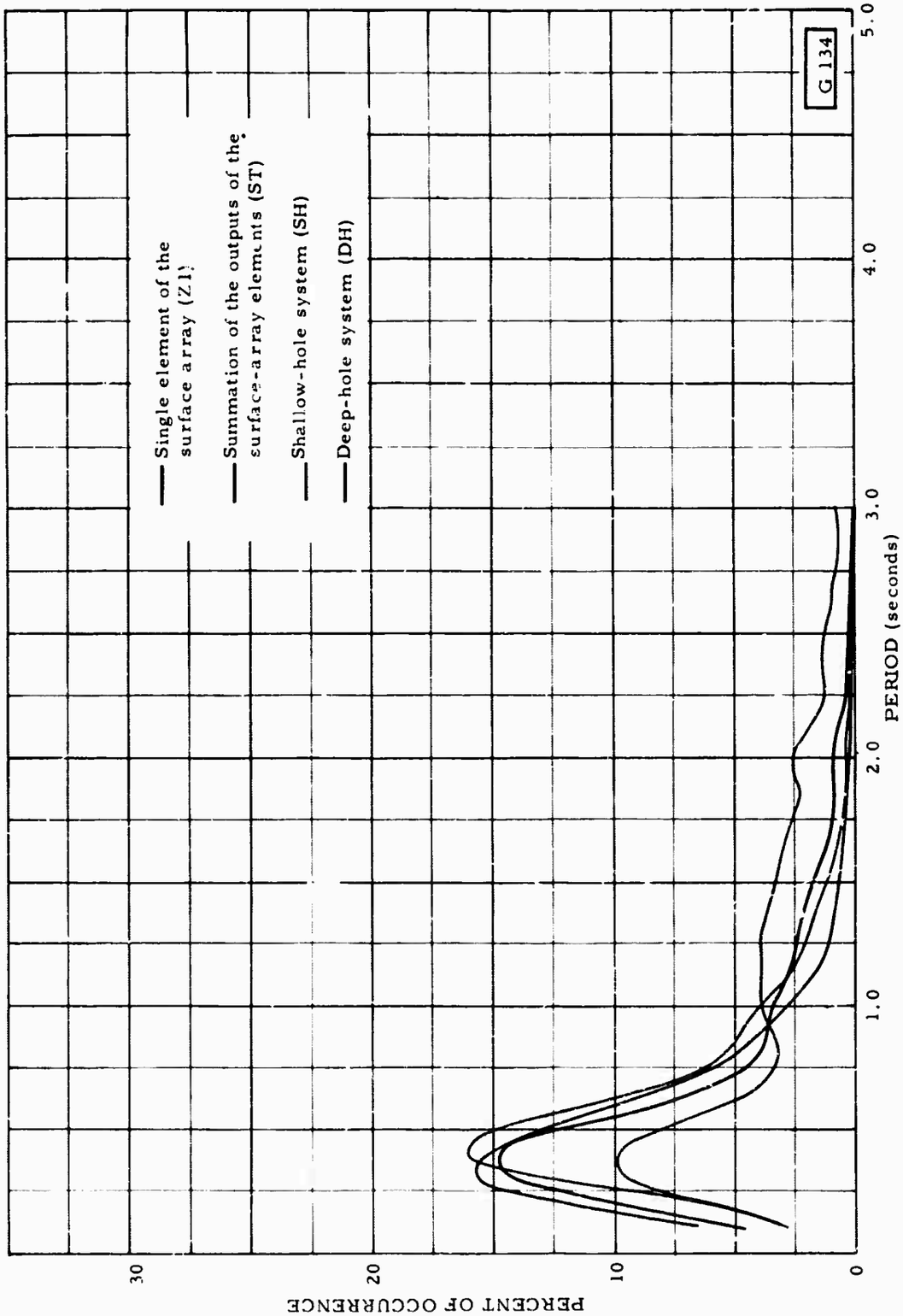

Figure 20. Frequency distribution of the periods of the microseismic background noise as recorded on the shallow-hole (SH), deep-hole (DH), single-element (Z1), and surface-summation (ST) systems

level than standard methods of visually measuring noise[1], in our opinion it provides a better estimate of the level of that portion of the background noise that has the greatest influence on signal detectability. A low-level signal is "picked" during on-line analysis solely on the basis of a change in character of the background noise. This change may be in the amplitude and/or period of a pulse on the seismogram or in the apparent coherency of a pulse, which produces a change in amplitude on a summation seismogram, when an array of instruments are used. The resulting anomalous change in the slope of a pulse in the background noise is the most easily detectable visual manifestation of the presence of a signal in the background noise. Therefore, all microseismic noise presentations in this report are based on half-cycle measurements.

The period and amplitude data were combined to produce a composite visual "spectrum" of all noise samples used in the study. The average trace amplitude in each 0.1-second period cell from 0.1 through 3.0 seconds was calculated. These data are shown in figure 21. The data for periods greater than 2.0 seconds are not as reliable as the shorter period values because of the small number of long-period data samples (see figure 20). The peaks observed on the SH and Z1 systems at the longer periods may be a reflection of the limitation of sample size; however, the peak at 1.7 to 1.8 seconds observed on all systems except ST appears to be a significant feature. The theoretical cancellation of microseismic background noise by the straight summation as a function of wave number has been calculated for the UBSO array by Texas Instruments (1963). Six strong nodes of cancellation are present at wave numbers between 0.46 and 0.62. These nodes have an azimuthal width of about 30 degrees and are centered at 60-degree intervals from north. The noise velocity corresponding to these wave numbers and the period of the observed noise peak in figure 21 is approximately 1.3 km/sec. Because this peak is not observed on ST, this portion of the spectrum is probably a low-velocity, Rayleigh-type noise component that is effectively cancelled by summing the surface-array seismographs. The ability of the ST system to cancel the low-velocity, high-frequency component of the background noise is also reflected in the noise amplitude and period distribution curves (figures 18 through 20).

[1]A more conventional method of obtaining noise amplitude distribution is to measure the largest amplitude pulse and its associated period that are present in a 10-second interval immediately following a 5-minute mark on the seismogram.

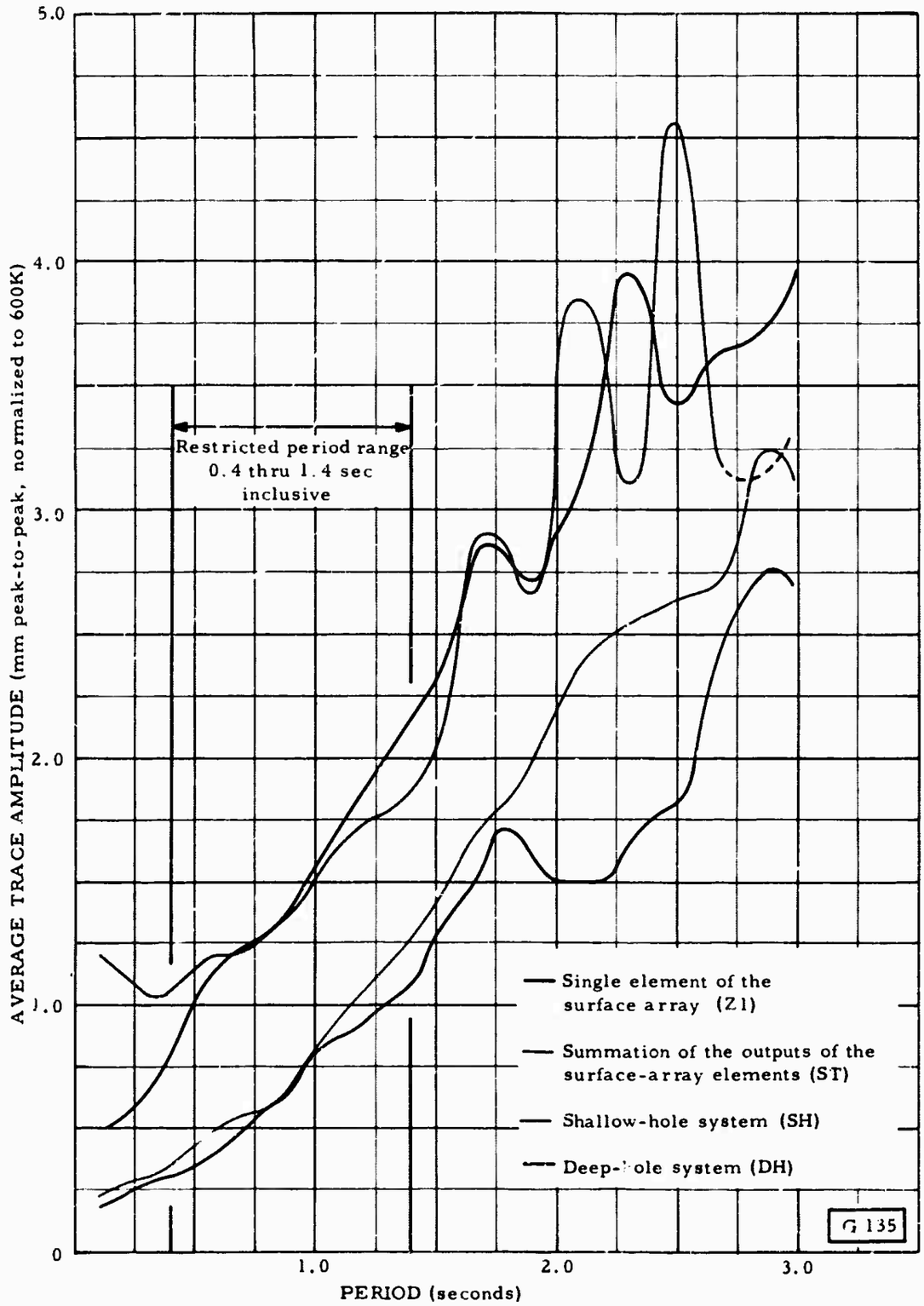

Figure 21. Average trace amplitude of the microseismic background noise as a function of noise period

Previous studies (TR 64-101) indicate that a noise attenuation factor of about 0.45 should be observed at a depth of 2700.5 meters (8860 feet). A comparison of the noise attenuation values as a function of period is shown in table 1. A degree of scatter is observed, but the average value of the attenuation factors, 0.50 is considered to be in good agreement with the depth attenuation factor previously determined for the DH system.

Table 1. Noise attenuation factors as a function of noise period for the deep-hole system

Period	Attenuation factor	Period	Attenuation factor	Period	Attenuation factor
0.1	0.34	1.1	0.50	2.1	0.47
0.2	0.38	1.2	0.49	2.2	0.42
0.3	0.40	1.3	0.49	2.3	0.41
0.4	0.35	1.4	0.50	2.4	0.46
0.5	0.32	1.5	0.54	2.5	0.52
0.6	0.34	1.6	0.53	2.6	0.58
0.7	0.38	1.7	0.54	2.7	0.67
0.8	0.44	1.8	0.60	2.8	0.72
0.9	0.49	1.9	0.59	2.9	0.73
1.0	0.51	2.0	0.51	3.0	0.68

Average factor for all periods = 0.50

4.3 SIGNAL-TO-NOISE RATIO

The signal-to-noise ratio for 200 signals received by all systems was calculated for each system. For the purpose of this report, signal-to-noise ratio is defined as the ratio of the maximum trace amplitude within the first few cycles of the signal to the average trace amplitude of the background noise in the 10 seconds prior to the signal arrival, in a period range that is equal to the signal period plus and minus 0.3 second. The method of measuring the background noise is described in sections 3 and 4.2. In the event that no measurable background noise was present in the signal period range, a minimum background amplitude of 0.49 mm (an arbitrary value less than 0.5 mm, the smallest amplitude that could be accurately resolved) was assigned. In a few

instances, this convention resulted in extremely large values of signal-to-noise ratio, particularly on the ST system when calculating the signal-to-noise ratio for relatively high-frequency signals. The signal-to-noise ratios calculated for each signal on each system are summarized in table 2. In addition, the ratios of the signal-to-noise ratios for each component relative to Z1 are included. The observed signal-to-noise ratios on Z1 compared with the observed signal-to-noise ratios on each of the other components are shown in figures 22 through 25. The distribution of the signal-to-noise ratios relative to Z1 are presented in figures 26 through 29.

Straight line equations, shown in table 3, were calculated using a "reduced major axis" (Miller and Kahn, 1962) best fit of the data points. The standard errors in the slope determinations are 0.052, 0.112, 0.142, and 0.167 for SH, DH, ST, and SF, respectively. When no signal is present, the signal-to-noise ratio is zero; therefore, the curve should pass through the origin. The intercepts of the best-fit straight lines are not zero, probably because of the large scatter in the data. In an effort to verify this conclusion, the 97.5 percent confidence limits of the slope of each line were calculated. The origin of each graph was found to be included within the limits, indicating that the intercept values are probably statistically insignificant. Therefore, the slopes of the best-fit straight lines that were constrained to the origin (figures 22 through 25) are considered to be valid estimates of the best-fit straight-line relationships for these data and, hence, a valid estimate of the signal-to-noise ratio improvement. Estimates of the signal-to-noise ratio improvement relative to Z1 based on both methods are summarized in table 3. As expected, the signal-to-noise ratio increases with increase in depth of burial of the seismometer; however, the values of signal-to-noise ratio improvement obtained in this study (table 3) are somewhat higher than those reported in TR 64-101. This apparent disagreement is probably the result of the different techniques used to measure the background noise (see section 4.2).

Table 2. Summary of the signal-to-noise ratios for 200 signals recorded by all systems

SIGNAL	SIGNAL-TO-NOISE RATIO					SIGNAL-TO-NOISE RATIOS RELATIVE TO Z1				
NUMBER	Z1	SH	DH	ST	SF	Z1/Z1	SH/Z1	DH/Z1	ST/Z1	SF/Z1
2	3.38	3.54	5.34	5.38	6.67	1.00	1.05	1.58	1.59	1.97
3	14.29	7.34	3.03	6.95	7.54	1.00	.51	.21	.49	.53
4	4.71	5.20	5.70	6.82	10.51	1.00	1.11	1.21	1.45	2.23
6	5.63	3.11	9.23	9.00	19.13	1.00	.55	1.64	1.60	3.40
7	4.53	5.52	4.61	7.64	9.68	1.00	1.22	1.02	1.68	2.14
9	3.48	3.95	5.72	3.71	4.26	1.00	1.13	1.64	1.06	1.22
16	2.50	2.89	1.94	2.06	3.11	1.00	1.15	.78	.82	1.24
19	2.17	1.65	2.32	3.13	2.57	1.00	.76	1.07	1.44	1.18
20	2.25	3.95	2.29	8.00	7.04	1.00	1.75	1.02	3.55	3.13
23	4.13	5.39	6.39	5.00	8.68	1.00	1.31	1.55	1.21	2.10
25	2.86	3.33	3.92	3.00	3.33	1.00	1.17	1.37	1.05	1.17
26	4.67	6.32	8.30	24.00	20.00	1.00	1.35	1.78	5.14	4.28
31	2.38	3.70	4.52	8.56	11.52	1.00	1.55	1.90	3.59	4.83
34	6.44	7.22	10.18	10.67	25.95	1.00	1.12	1.58	1.65	4.02
40	2.29	3.39	3.27	1.93	3.40	1.00	1.48	1.43	.84	1.48
54	4.35	6.95	9.35	4.20	13.74	1.00	1.60	2.15	.97	3.16
60	3.69	2.92	29.92	3.80	2.24	1.00	.79	8.09	1.03	.61
64	3.45	2.99	5.86	4.20	4.18	1.00	.87	1.70	1.22	1.21
69	4.42	4.06	2.21	15.31	4.92	1.00	.92	.50	3.46	1.11
73	4.50	18.57	1.24	4.20	108.16	1.00	4.12	.28	.93	24.01
77	4.13	6.09	4.07	7.52	9.67	1.00	1.47	.99	1.82	2.34
82	3.23	3.42	6.76	2.08	10.22	1.00	1.06	2.09	.65	3.16
84	3.06	2.88	3.89	5.00	4.05	1.00	.94	1.27	1.64	1.33
90	3.00	1.84	2.60	3.91	2.74	1.00	.61	.87	1.30	.91
93	2.06	7.11	4.85	10.90	7.70	1.00	3.44	2.35	5.27	3.73
101	3.00	1.75	3.73	2.12	2.00	1.00	.58	1.24	.71	.67
104	3.37	3.88	9.56	5.76	7.27	1.00	1.15	2.83	1.71	2.16
106	5.14	4.50	3.77	10.20	6.55	1.00	.88	.73	1.98	1.27
107	2.15	2.17	2.92	5.91	6.49	1.00	1.01	1.36	2.74	3.01
113	3.21	2.31	3.72	1.40	1.54	1.00	.72	1.16	.44	.48
114	7.00	6.40	7.23	9.30	22.40	1.00	.91	1.03	1.33	3.20
116	5.00	4.72	3.07	5.39	4.63	1.00	.94	.61	1.08	.93
120	3.20	3.10	2.62	4.90	7.98	1.00	.97	.82	1.53	2.49
121	4.23	3.93	3.25	2.74	4.60	1.00	.93	.77	.65	1.09
122	2.67	3.95	3.74	4.71	7.08	1.00	1.48	1.40	1.77	2.65
124	1.27	2.91	2.52	2.80	4.26	1.00	2.29	1.98	2.20	3.34
130	3.00	3.91	5.53	6.00	9.87	1.00	1.30	1.84	2.00	3.28
131	1.16	2.83	6.73	5.00	7.56	1.00	2.40	5.70	4.24	6.42
138	6.88	2.00	4.00	2.14	4.56	1.00	.29	.58	.31	.66
139	2.40	8.08	2.42	3.75	4.97	1.00	3.36	1.22	1.56	2.07
140	2.61	3.41	5.88	6.29	7.56	1.00	1.31	2.25	2.41	2.90
142	4.93	3.59	5.73	3.82	12.75	1.00	.73	1.16	.77	2.59
147	2.67	1.79	1.57	1.75	2.53	1.00	.67	.59	.66	.95
151	2.00	2.68	3.11	4.33	4.32	1.00	1.34	1.55	2.16	2.16
153	1.90	2.64	2.10	4.50	3.65	1.00	1.39	1.10	2.36	1.92
158	5.14	3.75	8.47	10.11	8.04	1.00	.73	1.65	1.96	1.56
160	3.00	4.83	2.50	3.86	5.42	1.00	1.61	.83	1.29	1.80
161	7.50	7.86	1.47	24.67	21.42	1.00	1.05	.20	3.29	2.85
162	2.60	5.33	1.75	3.50	3.10	1.00	2.05	.67	1.35	1.19
164	3.27	3.82	3.62	4.50	5.76	1.00	.92	.92	1.37	1.76

Table 2, Continued

SIGNAL	SIGNAL-TO-NOISE RATIO					SIGNAL-TO-NOISE RATIOS RELATIVE TO Z1				
NUMBER	Z1	SH	DH	ST	SF	Z1/Z1	SH/Z1	DH/Z1	ST/Z1	SF/Z1
165	1.71	3.04	2.71	2.00	4.69	1.00	1.78	1.58	1.17	2.73
168	5.85	11.38	10.48	9.25	14.96	1.00	1.94	1.88	1.58	2.56
173	4.00	4.60	5.40	5.50	18.00	1.00	1.15	1.47	1.37	4.50
175	3.60	11.23	12.34	19.00	18.61	1.00	3.12	3.42	5.27	5.16
176	18.50	17.80	12.02	35.45	40.36	1.00	.96	.65	1.92	2.18
178	2.83	2.49	3.21	4.43	5.45	1.00	.88	1.14	1.57	1.93
182	4.67	3.73	3.56	6.08	5.50	1.00	.80	.76	1.30	1.18
183	3.57	6.57	3.85	4.32	6.38	1.00	1.84	1.08	1.21	1.78
186	10.86	14.85	18.61	10.36	26.41	1.00	1.37	1.71	.95	2.48
187	1.71	2.56	4.42	2.43	3.31	1.00	1.49	2.57	1.42	1.93
188	16.20	31.00	31.06	10.29	30.88	1.00	1.91	1.92	.63	1.91
190	14.29	4.46	4.55	4.10	5.21	1.00	.31	.32	.29	.36
192	3.30	2.87	1.69	2.78	7.32	1.00	.86	.57	.93	2.44
193	1.91	6.47	2.33	3.60	3.45	1.00	3.38	1.22	1.88	1.79
194	2.22	2.40	4.43	3.03	3.45	1.00	1.08	1.99	1.36	1.54
195	2.73	3.85	3.91	15.31	9.52	1.00	1.41	1.43	5.60	3.49
196	23.57	18.64	23.12	32.73	58.46	1.00	.79	.98	1.39	2.48
199	5.44	5.12	3.71	8.89	9.60	1.00	.94	.68	1.63	1.76
200	4.62	3.30	5.37	9.06	9.82	1.00	.72	1.16	1.96	2.13
201	4.00	4.68	6.42	5.80	14.45	1.00	1.17	1.73	1.45	3.61
204	1.20	2.55	3.76	2.13	3.36	1.00	2.12	3.13	1.77	2.81
208	7.21	5.55	8.02	19.80	11.00	1.00	.77	1.11	2.74	1.52
211	6.42	5.67	6.20	8.70	20.83	1.00	.88	.97	1.36	3.25
212	1.80	2.15	1.55	5.67	5.59	1.00	1.19	.86	3.14	3.10
213	15.31	4.88	5.69	7.24	11.11	1.00	.32	.37	.47	.73
214	2.50	2.21	3.68	3.75	2.72	1.00	.88	1.47	1.50	1.09
227	4.03	1.66	4.32	3.62	6.56	1.00	.41	1.07	.90	1.63
228	13.87	11.10	10.89	20.45	28.52	1.00	.80	1.22	1.47	2.06
230	3.16	3.94	4.75	18.37	17.97	1.00	1.25	1.50	5.81	5.68
232	2.80	2.18	4.37	1.83	7.50	1.00	.78	1.56	.66	2.68
233	2.29	3.73	3.63	3.13	8.74	1.00	1.63	1.67	1.37	3.82
234	4.82	5.49	6.88	7.43	9.04	1.00	1.14	1.43	1.54	1.87
235	1.34	1.19	2.18	2.78	2.60	1.00	.88	1.62	2.06	1.93
236	6.36	4.02	5.16	9.00	8.93	1.00	.63	.81	1.41	1.40
238	1.94	1.92	4.12	2.35	4.91	1.00	.99	2.12	1.21	2.53
241	3.13	3.07	3.43	9.95	4.64	1.00	.98	1.10	3.18	1.55
244	4.20	3.54	3.91	5.68	11.43	1.00	.84	.93	1.35	2.72
248	2.42	2.25	4.07	2.00	4.40	1.00	.93	1.68	.83	1.81
250	3.00	2.48	5.43	6.18	5.20	1.00	.83	1.81	2.06	1.73
251	3.50	3.91	3.08	8.50	9.03	1.00	1.12	.88	2.43	2.58
256	14.00	11.76	12.65	11.79	15.89	1.00	.84	.90	.84	1.13
259	4.06	5.42	7.45	5.25	9.61	1.00	1.33	1.83	1.29	2.41
261	3.76	2.83	3.94	4.25	7.26	1.00	.75	1.05	1.13	1.93
262	12.22	9.67	11.29	21.50	21.14	1.00	.79	.92	1.76	1.73
264	11.76	14.46	18.47	13.71	19.60	1.00	1.23	1.61	1.17	1.67
265	2.40	10.52	32.23	47.96	9.15	1.00	4.38	13.40	19.94	3.81
266	11.50	15.90	14.75	57.14	31.98	1.00	1.38	1.28	4.97	2.78
268	11.03	10.72	17.37	19.47	41.07	1.00	.97	1.57	1.76	3.72
270	1.75	.75	2.45	3.24	3.60	1.00	.43	1.40	1.85	2.05
271	2.36	2.94	1.73	2.17	3.46	1.00	1.25	.73	.92	1.47

Table 2, Continued

SIGNAL	SIGNAL-TO-NOISE RATIO					SIGNAL-TO-NOISE RATIOS RELATIVE TO Z1				
NUMBER	Z1	SH	DH	ST	SF	Z1/Z1	SH/Z1	DH/Z1	ST/Z1	SF/Z1
275	4.86	5.40	7.26	12.92	13.19	1.00	1.11	1.49	2.66	2.71
279	2.91	3.72	4.13	6.54	11.15	1.00	1.28	1.42	2.24	3.83
283	4.86	6.90	61.22	51.02	13.00	1.00	1.44	12.74	10.62	2.71
284	2.24	3.50	3.45	3.47	5.20	1.00	1.57	1.73	1.52	2.27
289	1.71	2.09	2.32	2.60	5.73	1.00	1.22	1.35	1.69	3.34
294	5.83	3.59	2.93	3.53	3.43	1.00	.62	.50	.61	.59
295	5.60	6.37	6.47	8.00	5.87	1.00	1.14	1.16	1.43	1.05
299	4.76	15.34	6.69	7.20	13.16	1.00	3.22	1.44	1.51	2.76
304	2.60	3.33	3.47	7.76	7.73	1.00	1.28	1.53	2.98	2.97
305	6.24	7.20	12.03	16.73	19.00	1.00	1.14	1.91	2.66	3.02
307	13.34	16.49	20.90	21.38	34.13	1.00	1.23	1.56	1.60	2.55
308	6.40	4.10	3.51	12.50	17.57	1.00	.64	.55	1.95	2.74
315	2.44	3.30	5.51	4.02	4.25	1.00	1.35	2.25	1.64	1.74
316	4.00	4.21	5.11	7.64	5.00	1.00	1.05	1.28	1.91	1.25
318	3.64	3.86	8.02	4.64	8.56	1.00	1.05	2.17	1.26	2.32
319	1.71	8.79	1.96	4.44	5.14	1.00	5.12	1.14	2.59	2.99
320	4.22	4.23	7.54	5.50	5.58	1.00	1.00	1.78	1.30	1.32
323	3.86	3.94	3.57	2.50	6.07	1.00	1.02	.92	.65	1.57
326	2.72	2.67	7.14	3.25	7.27	1.00	.98	2.62	1.19	2.67
328	1.75	3.45	8.93	4.29	15.24	1.00	1.97	5.09	2.44	8.69
334	4.80	3.11	4.37	6.46	6.34	1.00	.65	.91	1.35	1.32
340	3.00	3.15	5.64	3.64	6.00	1.00	1.05	1.88	1.21	2.00
344	2.83	3.36	1.27	4.44	4.36	1.00	1.19	.45	1.57	1.54
345	1.74	2.23	9.43	1.50	4.96	1.00	1.28	5.41	.86	2.84
347	2.54	1.05	2.80	2.68	5.44	1.00	.41	1.08	1.03	2.12
349	15.00	12.51	15.11	10.26	15.72	1.00	.83	1.01	.68	1.05
351	1.43	2.13	3.56	5.00	6.52	1.00	1.49	2.49	3.49	4.55
352	2.50	2.91	2.67	8.16	4.61	1.00	1.16	1.07	3.26	1.84
354	3.37	3.46	5.64	13.65	19.70	1.00	1.03	1.67	4.05	3.17
360	2.81	5.47	5.04	6.74	9.21	1.00	1.94	1.79	2.39	3.27
367	2.27	2.38	15.03	4.20	9.35	1.00	1.05	6.60	1.85	4.11
371	1.41	1.60	35.14	1.36	1.84	1.00	1.13	24.82	.96	1.34
372	1.23	1.67	2.37	1.76	3.08	1.00	1.35	1.93	1.43	2.49
375	9.60	6.61	11.70	13.45	20.74	1.00	.69	1.22	1.40	2.16
384	2.73	2.32	4.84	5.00	8.41	1.00	.85	1.77	1.83	3.08
387	3.37	3.29	3.77	3.80	5.95	1.00	.98	1.12	1.13	1.76
390	1.97	2.57	4.61	5.42	7.72	1.00	1.30	2.04	2.75	3.92
393	2.13	8.69	4.06	3.25	9.13	1.00	4.07	1.90	1.52	4.27
397	14.17	12.22	18.30	39.00	45.46	1.00	.86	1.29	2.75	3.21
399	4.80	6.45	17.62	27.00	10.29	1.00	1.34	3.71	5.62	2.14
401	2.82	3.20	4.92	17.35	8.16	1.00	1.13	1.74	6.14	2.89
402	3.09	14.41	4.75	10.06	9.60	1.00	4.66	1.54	3.25	3.10
405	7.00	8.80	7.27	9.00	7.87	1.00	1.26	1.04	1.29	1.12
407	9.03	7.46	11.92	12.24	23.15	1.00	.83	1.32	1.35	2.56
408	6.86	7.40	9.06	10.67	14.00	1.00	1.08	1.32	1.56	2.04
409	4.80	5.41	4.17	4.13	9.50	1.00	1.13	.87	.86	1.98
410	4.40	4.51	5.60	5.00	11.25	1.00	1.03	1.14	1.34	2.55
411	8.40	7.44	7.18	16.50	34.57	1.00	.89	.85	1.96	4.11
413	2.46	2.76	1.71	6.00	6.36	1.00	1.12	.70	2.44	2.57
416	4.04	4.43	4.62	11.22	11.57	1.00	1.08	1.13	2.74	2.83

Table 2, Continued

SIGNAL NUMBER	SIGNAL-TO-NOISE RATIO					SIGNAL-TO-NOISE RATIOS RELATIVE TO Z1				
	Z1	SH	DH	ST	SF	Z1/Z1	SH/Z1	DH/Z1	ST/Z1	SF/Z1
418	27.55	23.87	2.67	6.34	11.00	1.00	.87	.10	.23	.40
420	17.35	12.73	6.20	3.28	4.37	1.00	.73	.36	.19	.25	
421	12.24	2.50	1.69	3.00	6.99	1.00	.20	.14	.25	.57
423	12.24	3.75	2.78	7.20	7.66	1.00	.31	.23	.59	.63
427	1.33	1.80	2.19	4.64	6.08	1.00	1.35	1.64	3.47	4.55
428	2.17	2.18	14.61	4.20	4.66	1.00	1.00	6.80	1.93	2.15
429	2.50	1.82	4.42	3.42	3.35	1.00	.73	1.67	1.37	1.34
431	2.18	4.02	6.07	4.43	5.00	1.00	1.84	2.78	2.03	2.29
434	6.50	8.17	7.12	20.00	22.98	1.00	1.26	1.10	3.08	3.53
436	2.86	2.13	3.69	3.94	7.33	1.00	.74	1.29	1.38	2.56
438	1.40	1.75	1.12	1.38	2.26	1.00	1.25	.80	.98	1.61
439	2.23	7.27	2.94	2.03	1.91	1.00	3.26	1.32	.91	.86
442	3.71	3.56	3.40	2.57	4.19	1.00	.96	.92	.69	1.13
443	1.25	2.77	2.44	1.93	3.64	1.00	2.21	1.94	1.54	2.90
444	4.29	3.93	5.83	15.00	18.75	1.00	.92	1.36	3.50	4.37
448	4.00	3.24	2.13	6.80	7.06	1.00	.81	.53	1.70	1.76
449	1.36	2.25	2.86	12.24	3.16	1.00	1.65	2.10	8.95	2.33
450	6.67	4.49	8.54	14.60	13.60	1.00	.67	1.28	2.10	2.04
451	8.40	11.28	8.05	22.00	33.27	1.00	1.34	.96	2.62	3.96
455	3.90	3.33	3.18	4.04	9.29	1.00	.85	.81	1.04	2.38
456	7.14	1.23	2.10	1.76	3.94	1.00	.17	.30	.25	.55
458	2.31	4.53	2.72	3.55	5.75	1.00	1.96	1.17	1.53	2.48
462	6.00	6.82	10.04	11.50	14.56	1.00	1.14	1.67	1.92	2.43
463	6.86	7.52	5.11	33.67	19.05	1.00	1.10	.75	4.91	2.78
464	6.60	5.16	4.76	6.00	13.87	1.00	.78	.72	.91	2.10
465	3.53	4.43	3.37	4.71	6.85	1.00	1.26	.95	1.34	1.94
469	1.82	2.23	2.56	12.24	13.00	1.00	1.23	1.41	6.72	7.13
471	4.50	4.50	5.28	18.00	5.60	1.00	1.00	1.17	4.00	1.24
472	2.33	1.42	5.66	2.44	4.62	1.00	.61	2.42	1.05	1.98
477	12.60	11.97	16.52	18.00	18.84	1.00	.95	1.31	1.43	1.50
478	2.86	2.54	3.72	3.00	7.05	1.00	.89	1.30	.05	2.47
482	2.84	4.50	3.41	2.00	5.76	1.00	1.58	1.35	.69	1.99
483	1.71	9.43	5.16	3.60	3.50	1.00	5.49	3.00	2.10	2.04
484	5.36	4.47	6.41	14.80	19.25	1.00	.83	1.20	2.76	3.59
486	6.50	8.26	8.08	5.18	15.20	1.00	.95	1.23	.79	2.33
488	8.33	7.05	10.64	16.00	20.25	1.00	.85	1.30	1.92	2.43
489	2.13	13.17	4.52	3.59	4.62	1.00	6.18	2.13	1.69	2.17
490	1.90	2.00	5.44	3.47	7.20	1.00	1.05	2.85	1.82	3.81
494	5.00	3.77	4.35	45.92	7.20	1.00	.75	.87	9.18	1.44
495	2.63	2.78	2.68	7.43	9.60	1.00	1.06	1.02	2.83	3.65
499	3.75	2.82	2.67	2.50	3.91	1.00	.62	.77	.67	1.04
501	5.33	2.57	5.37	5.14	14.64	1.00	.48	1.01	.96	2.75
502	2.86	3.18	4.63	4.75	5.76	1.00	1.11	1.62	1.66	2.01
503	2.50	3.23	4.15	3.94	7.00	1.00	1.29	1.66	1.57	2.80
504	2.80	2.21	7.67	9.50	11.03	1.00	.79	2.81	3.39	3.94
507	3.23	5.07	5.47	9.25	12.36	1.00	1.57	1.69	2.86	3.83
509	4.00	5.50	6.17	21.43	27.64	1.00	1.37	1.54	5.35	6.97
511	4.27	4.20	3.67	11.00	11.65	1.00	.98	.91	2.58	2.73
516	3.50	2.74	3.63	7.00	5.71	1.00	.78	1.09	2.00	1.63
518	10.95	10.65	21.45	14.32	22.74	1.00	.97	2.00	1.31	2.08

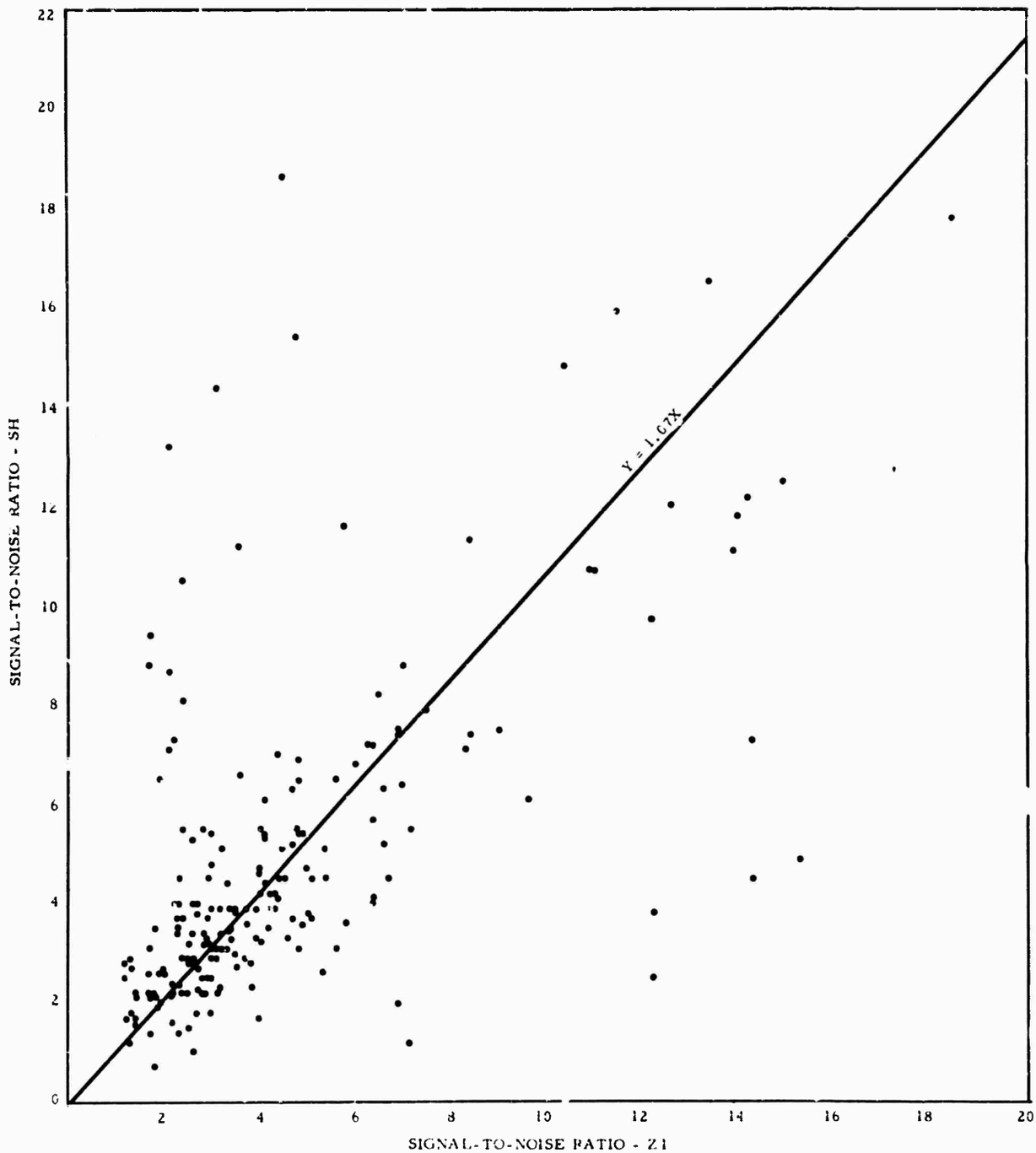

Figure 22. Distribution of signal-to-noise ratios calculated from the shallow-hole (SH) system versus the signal-to-noise ratio calculated from Z1

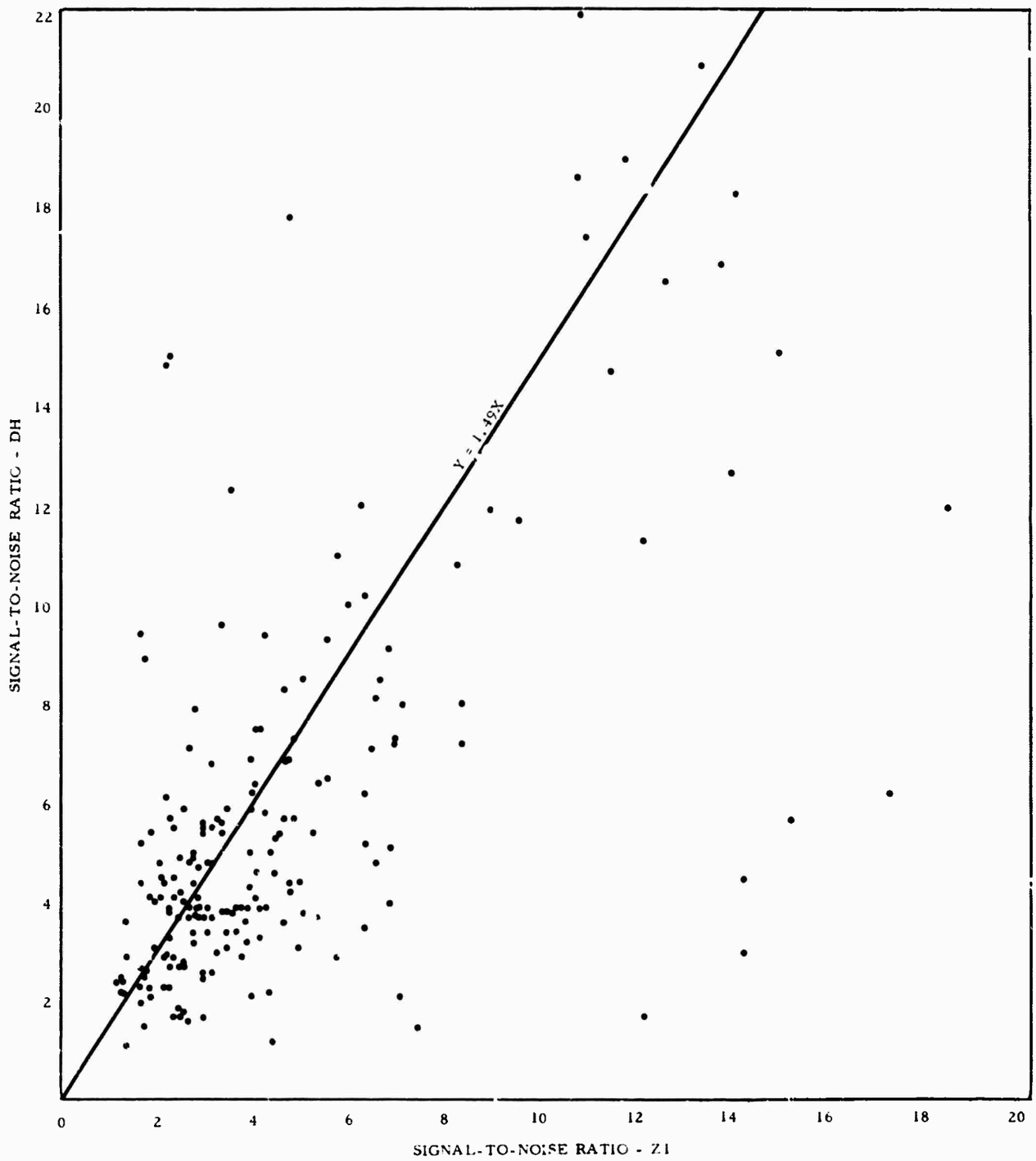

Figure 23. Distribution of signal-to-noise ratios calculated from the deep-hole (DH) system versus the signal-to-noise ratio calculated from Z1

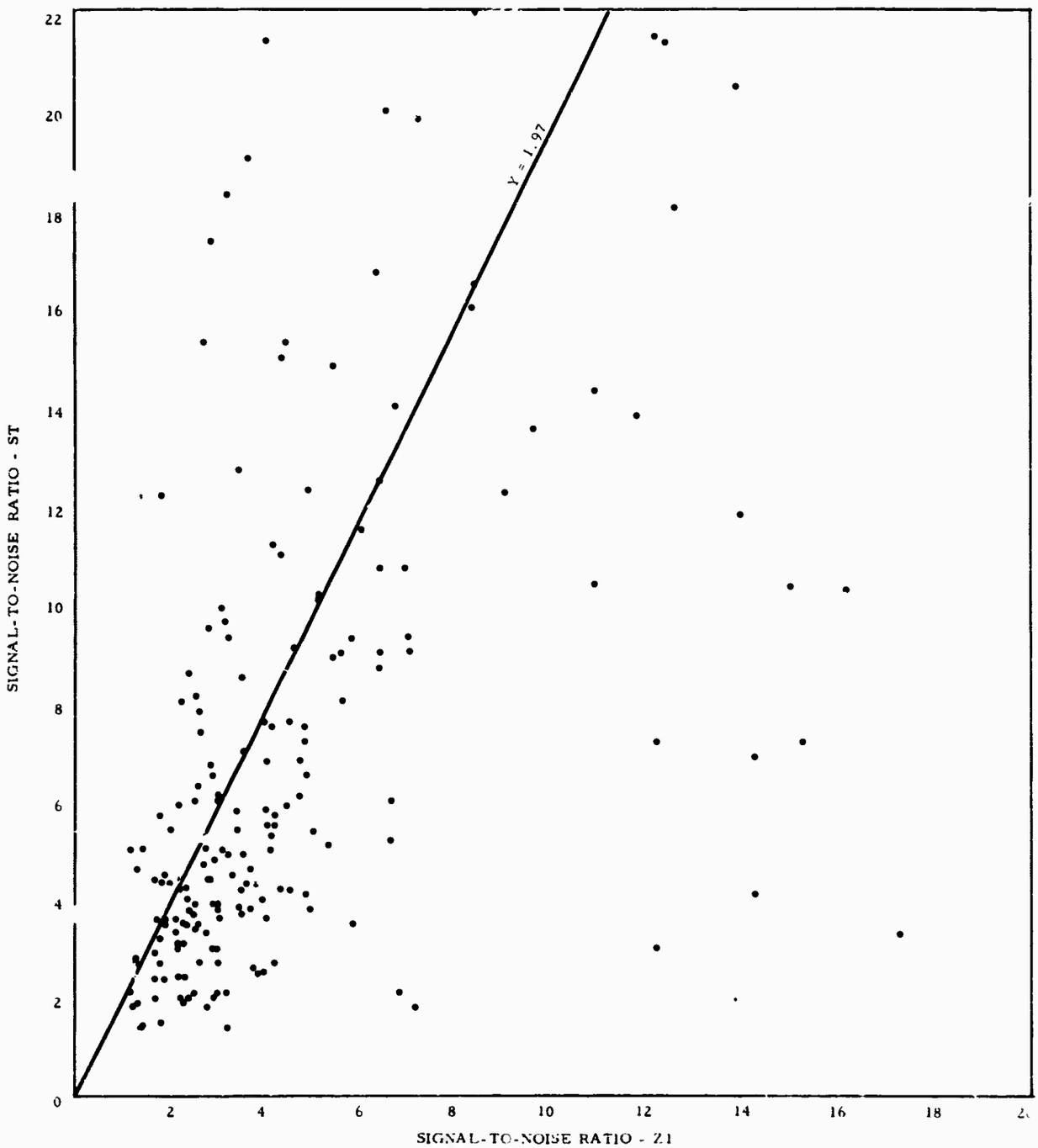

Figure 24. Distribution of signal-to-noise ratios calculated from the summation of the surface-array elements (ST) versus the signal-to-noise ratio calculated from Z1

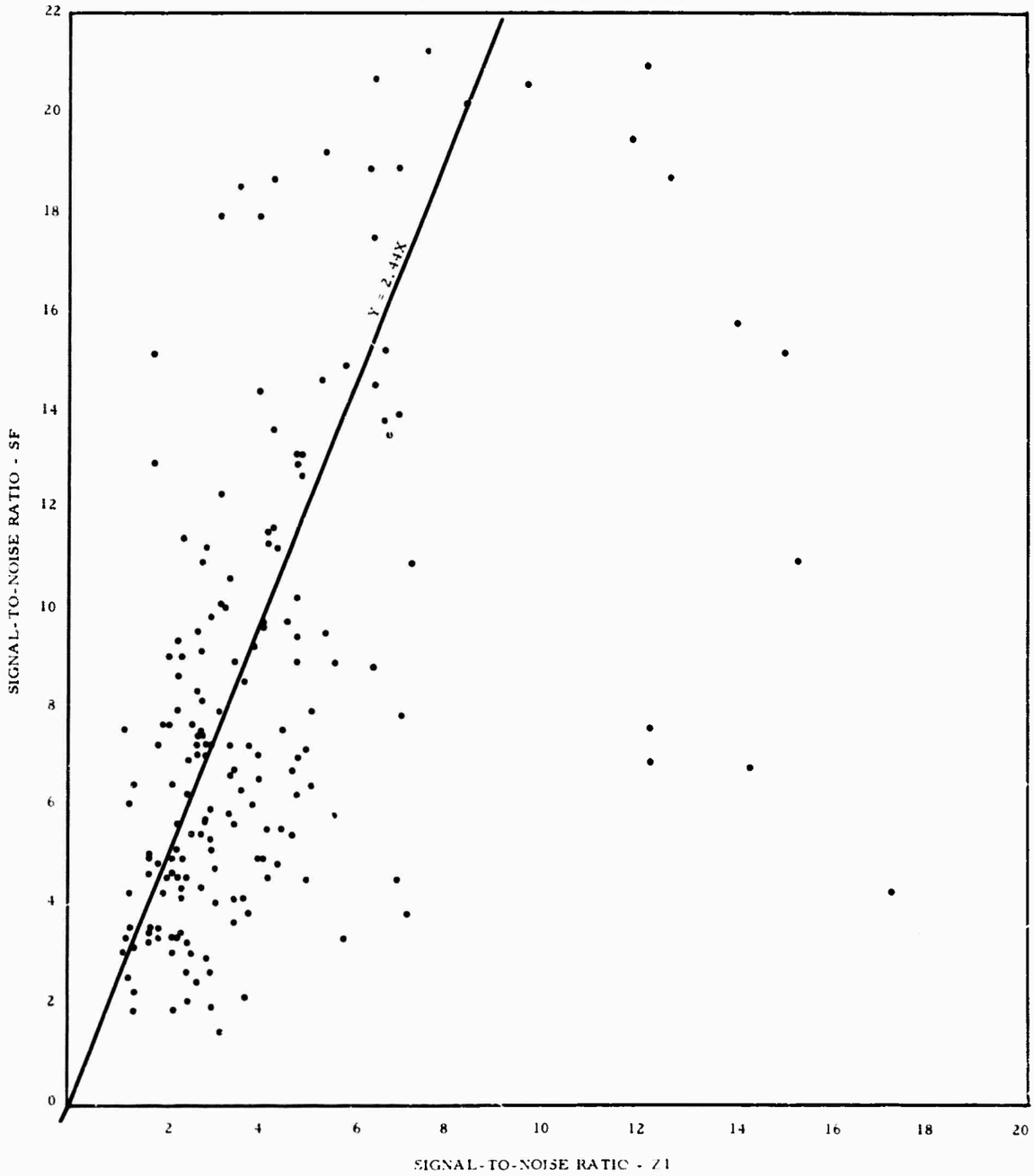

Figure 25. Distribution of signal-to-noise ratios calculated from the filtered summation of the surface-array elements (SF) versus the signal-to-noise ratio calculated from Z1

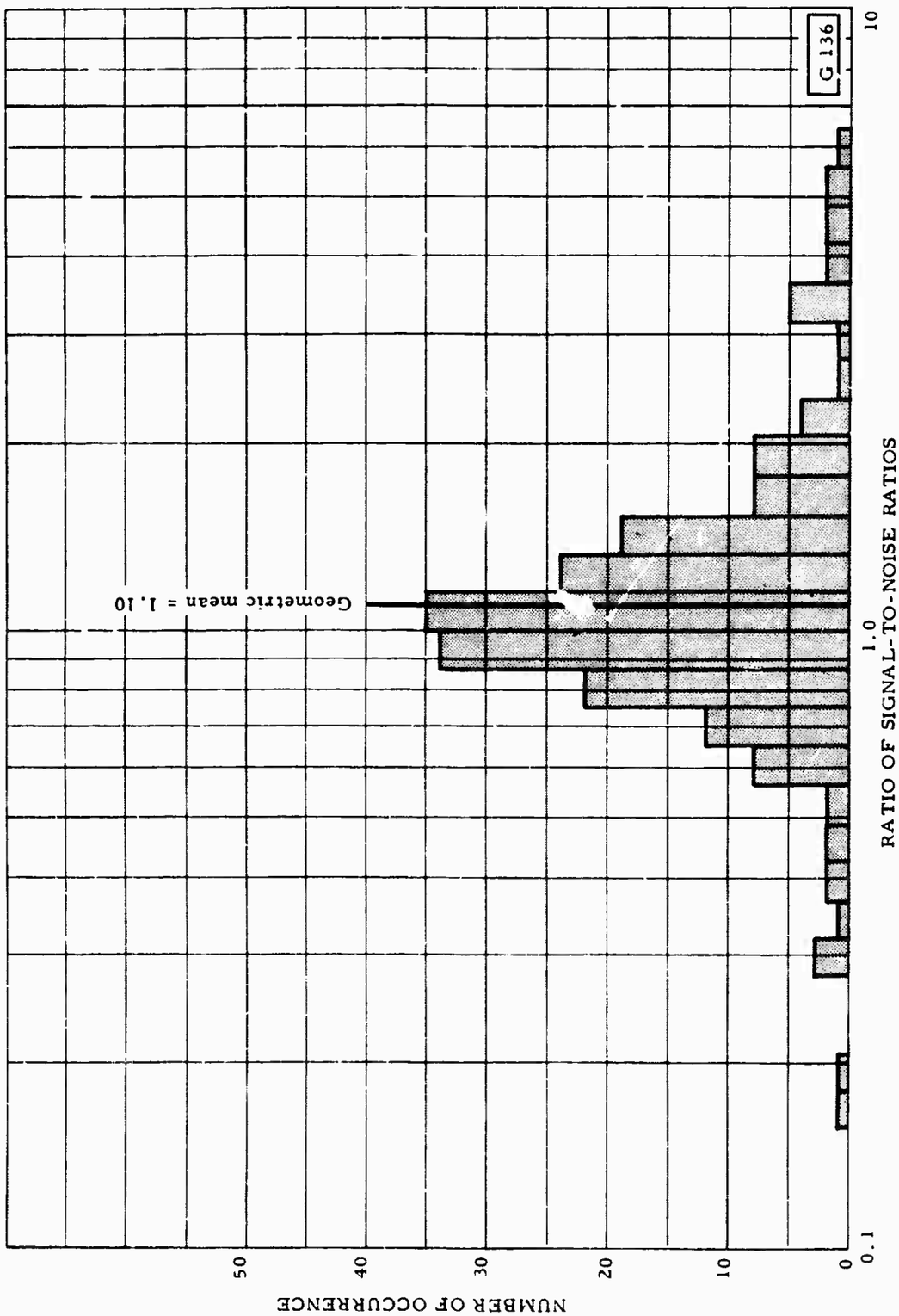

Figure 26. Frequency distribution of the ratio of signal-to-noise ratios calculated on the shallow-hole (SH) system relative to Z1

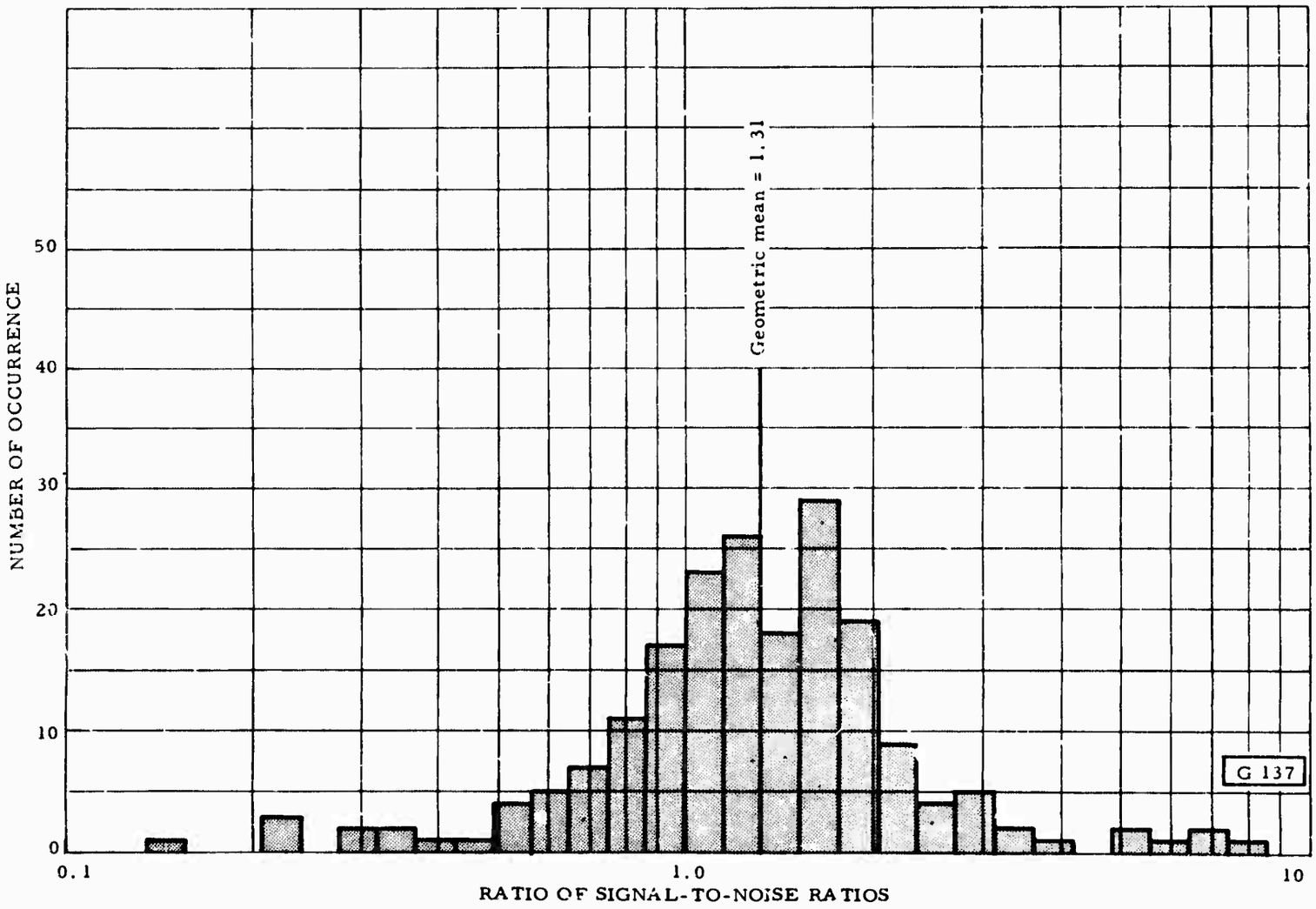

Figure 27. Frequency distribution of the ratio of signal-to-noise ratios calculated on the deep-hole (DH) system relative to Z1

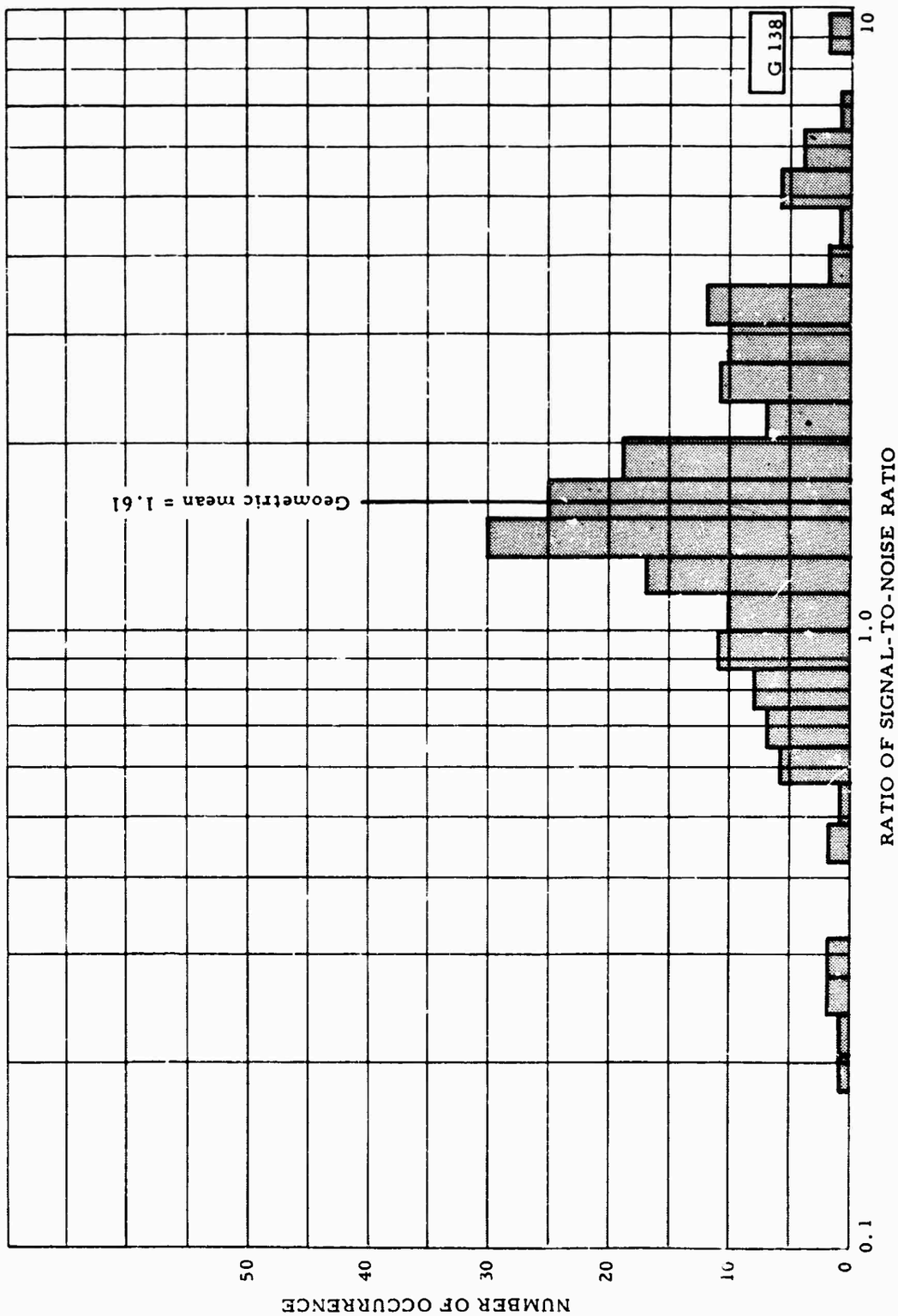

Figure 28. Frequency distribution of the ratio of signal-to-noise ratios calculated on the unfiltered summation of the surface-array elements (ST) relative to Z1

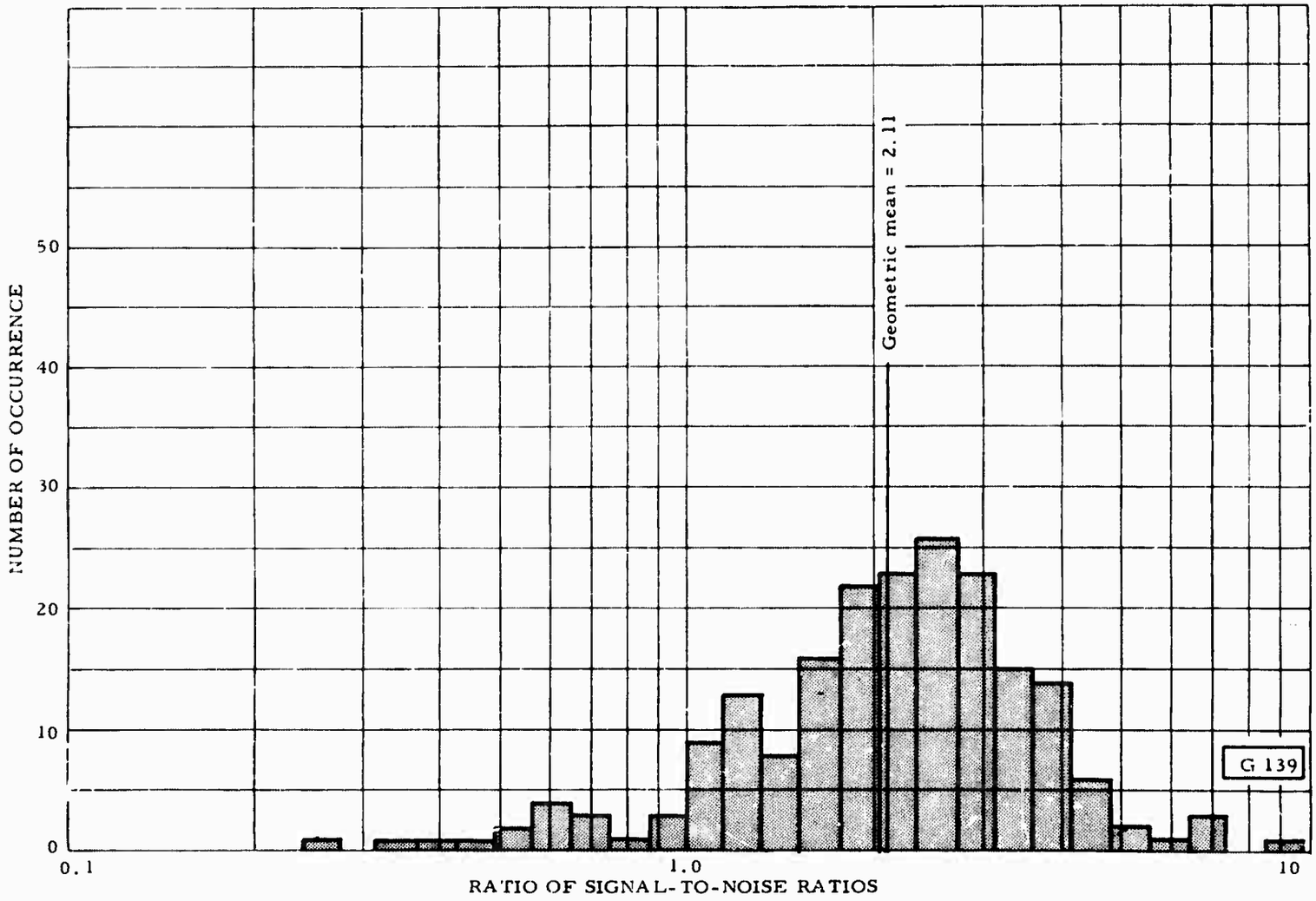

Figure 29. Frequency distribution of the ratio of signal-to-noise ratios calculated on the filtered summation of the surface-array elements (SF) relative to Z1

Table 3. Summary of signal-to-noise ratio improvement relative to Z1

Component relative to Z1	Signal-to-noise ratio improvement by slope of best-fit straight line		Signal-to-noise ratio improvement by slope of best-fit straight line through the orgin
	Equation	97.5% confidence limits of slope	
SH	Y = 0.21 + 1.04X	0.90 - 1.19	1.07
DH	Y = 1.52 + 1.67X	1.04 - 2.30	1.49
ST	Y = 2.03 + 2.21X	1.52 - 2.89	1.97
SF	Y = 2.41 + 2.72X	2.06 - 3.38	2.44

4.4 MAGNITUDE COMPARISONS

P-wave magnitudes were computed from data recorded by each system for each event for which the United States Coast and Geodetic Survey (USC&GS) reported a magnitude. These P-wave magnitudes were calculated using the following equation:

$$m = \log_{10}\frac{A}{T} + B + S$$

where:

m = body wave magnitude

A = maximum peak-to-peak ground displacement, in millimicrons, within the first few cycles of the P-wave arrival

T = the associated period in seconds, of the pulse used to determine A

B = combined depth-distance correction factor

S = station correction factor

Because the station correction factor for UBSO has not been established relative to the magnitudes reported by the USC&GS, no station correction factor was applied to the calculations. System magnitude residuals relative to USC&GS magnitudes were calculated and plotted as a function of USC&GS magnitude. These data are presented in figures 30 through 33. In addition, the USC&GS magnitude distribution of the events detected by each system are included in these figures. For each 0.1 USC&GS magnitude increment, the maximum residual values as well as the average values are shown. Because of the limited sample, no attempt was made to fit a curve to the data points; however, a definite negative trend is apparent on the plots for each system. As the USC&GS magnitude increases, the average residual values become negative. A part of this trend may be attributed to high UBSO system magnifications relative to the majority of stations reporting to the USC&GS. Many large signals are preceded by a few low-level pulses prior to the arrival of the larger amplitude wave train. Observatories operating with much lower system magnifications and slower recording rates will not be able to resolve these first few low-level pulses and, therefore, report only the larger amplitude. The extent to which this first arrival bias affects the results of this study is unknown. A more extensive investigation of this subject is currently in progress and the results will be published at a later date.

An intersystem comparison of magnitude determination was also made. For this portion of the evaluation, the ground amplitude-to-period ratio for each signal that was recorded by Z1 and one of the other systems was calculated. The distribution of the ratio values for each system relative to Z1 is presented in figure 34. The geometric mean values for all systems are less than 1.0, indicating that, on the average, magnitudes computed on the other systems will be less than the values computed from Z1. Magnitudes calculated from DH, ST, and SH data differed from magnitudes calculated from Z1 data by 0.34, 0.05, and 0.06 magnitude unit, respectively. It is doubtful that the difference observed on SH and ST are significant; however, a certain amount of signal attenuation, caused by step-out across the surface array, should be observed on ST. The attenuation factor resulting from depth of burial of the seismometer observed on the DH system is in close agreement with the values previously discussed (section 4.1).

4.5 RELATIVE DETECTION CAPABILITY

In an effort to evaluate the data recorded by each of the seismograph systems (see section 2), portions of the seismograms were masked by covering part of

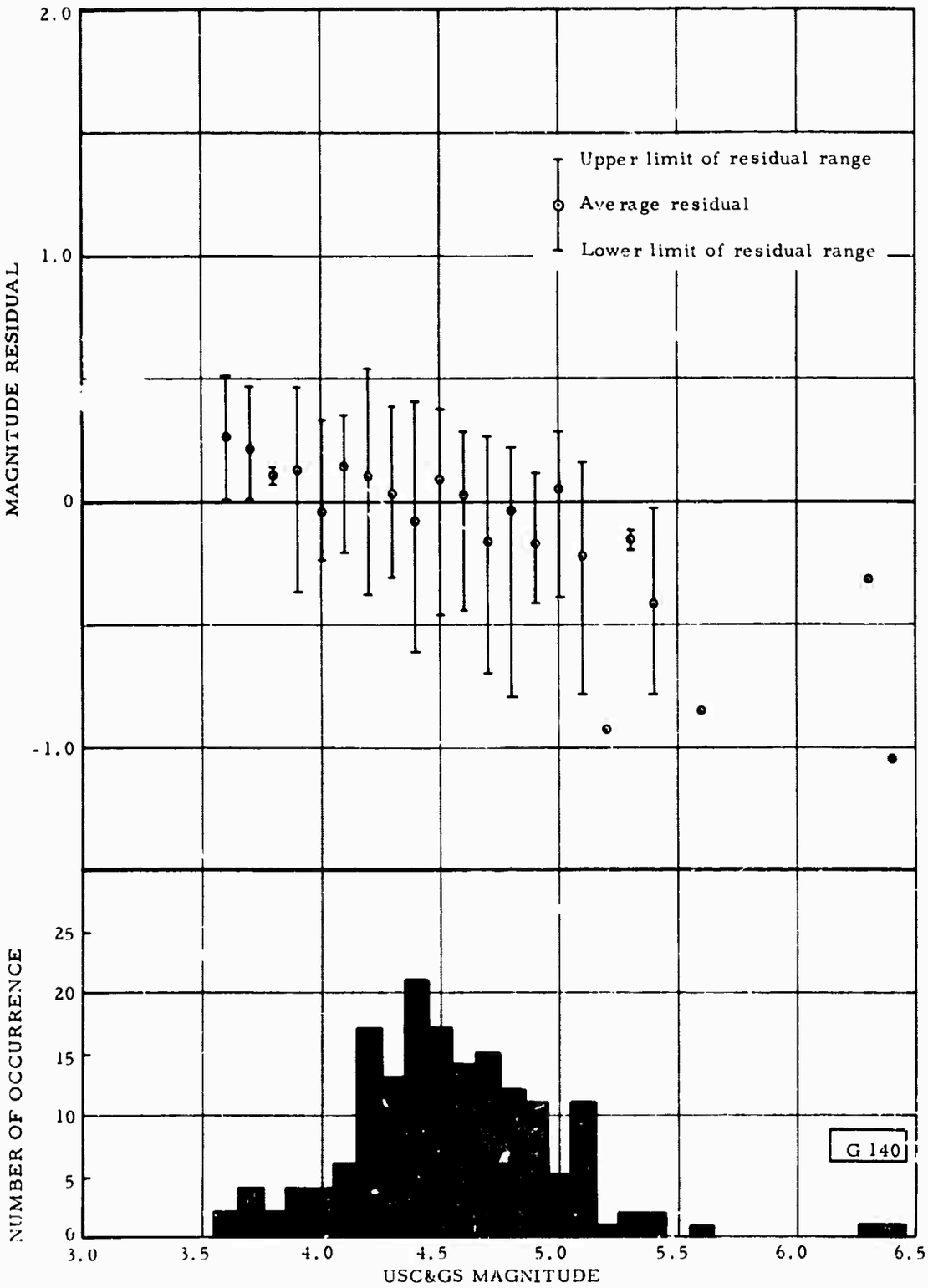

Figure 30. Mean magnitude residuals for a single surface-array element (Z1) relative to the magnitudes reported by the USC&GS and the number of events detected by Z1 as a function of USC&GS magnitude

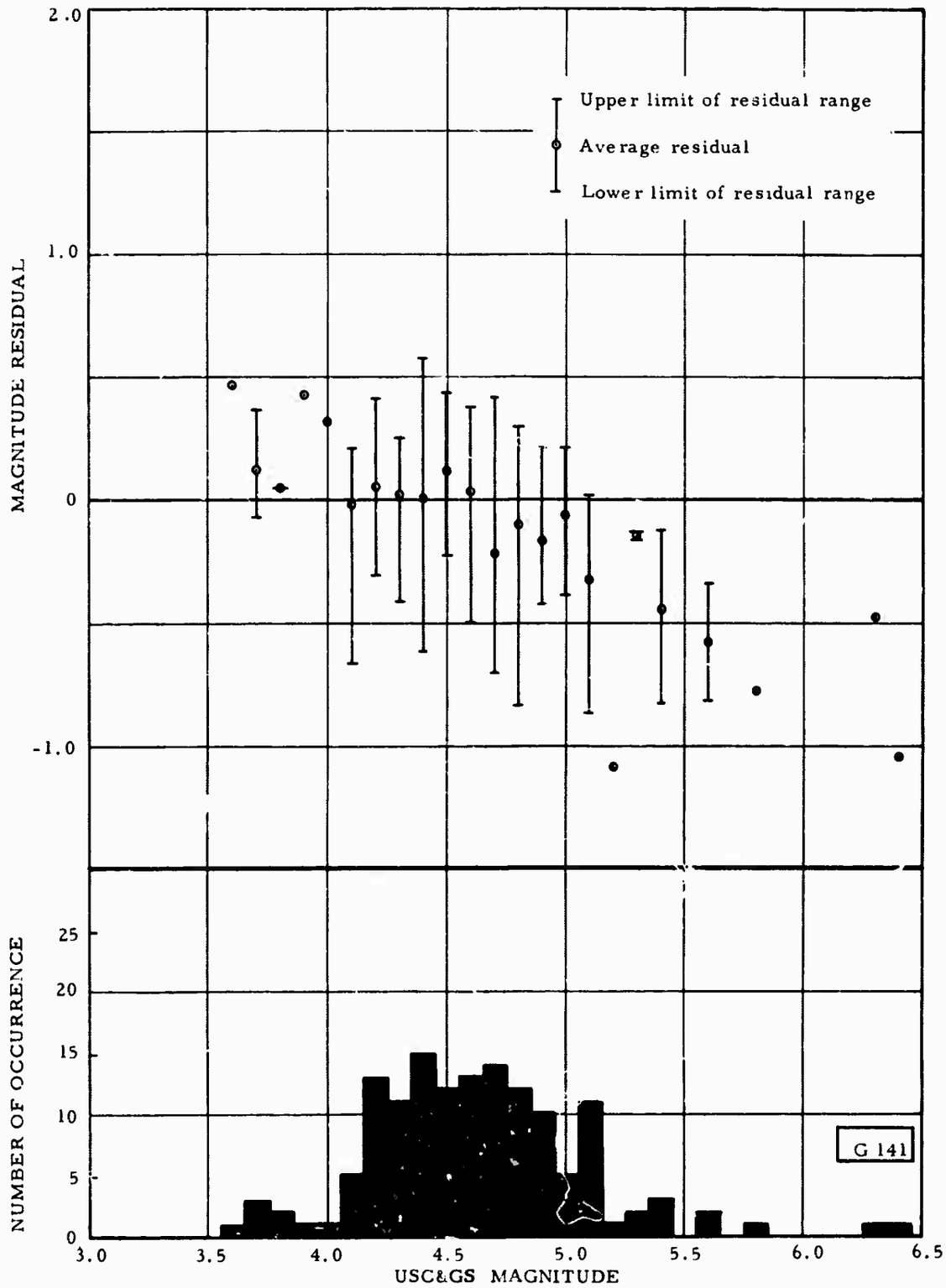

Figure 31. Mean magnitude residuals for the shallow-hole (SH) system relative to the magnitudes reported by the USC&GS and the number of events detected by SH as a function of USC&GS magnitude

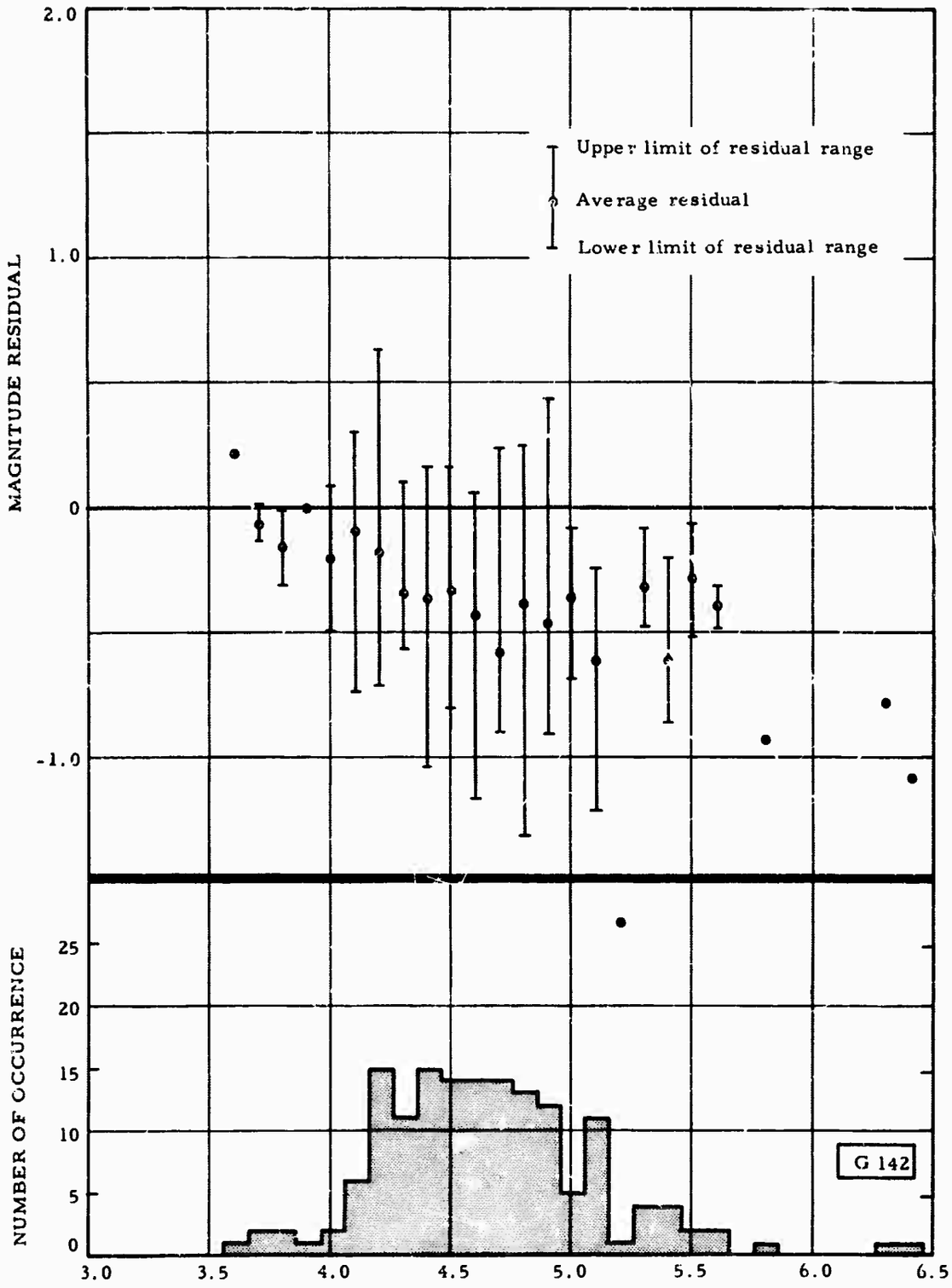

Figure 32. Mean magnitude residuals for the deep-hole (DH) system relative to the magnitudes reported by the USC&GS and the number of events detected by DH as a function of USC&GS magnitude

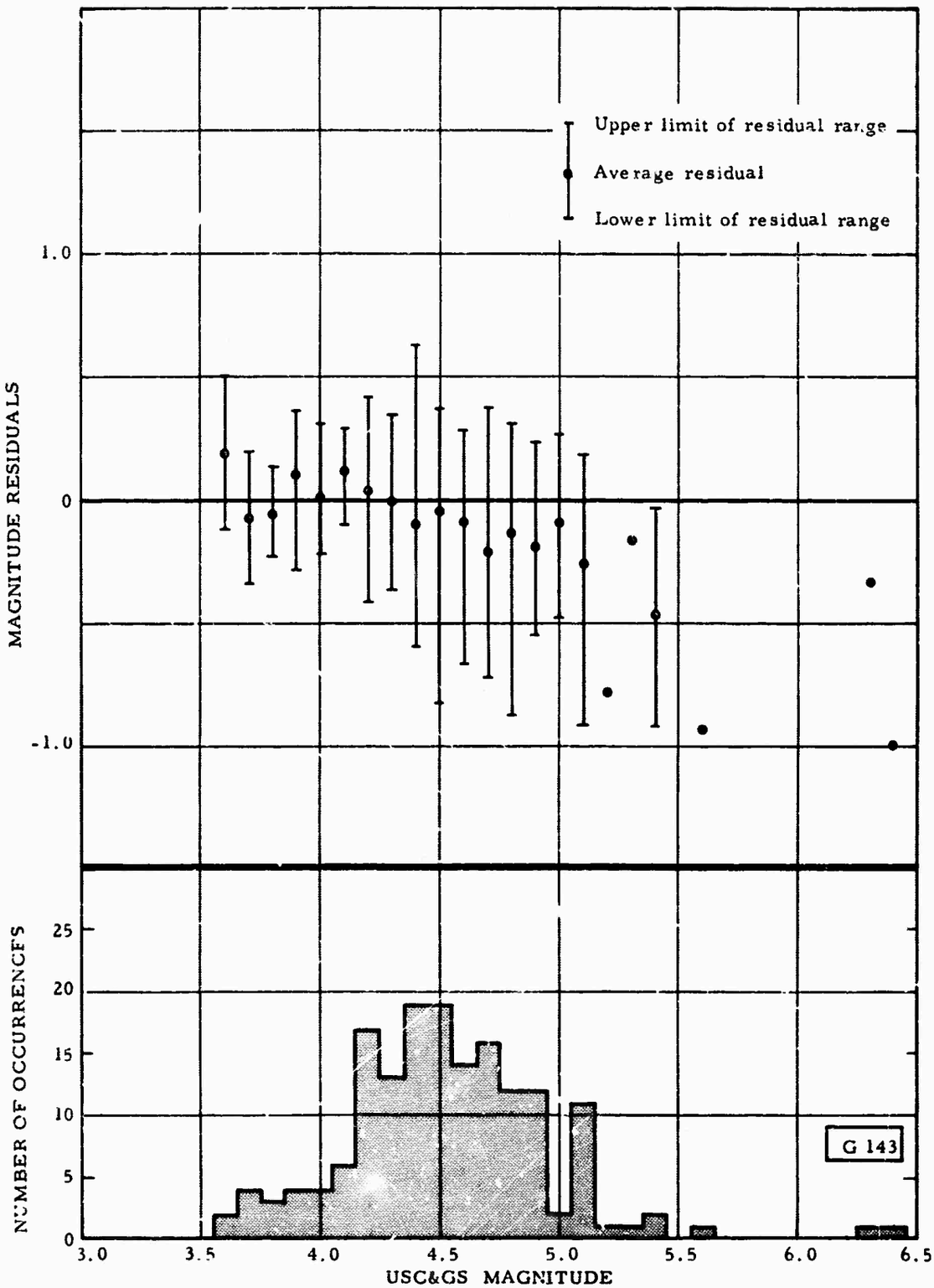

Figure 33. Mean magnitude residuals for the unfiltered summation of the surface array (ST) relative to the magnitudes reported by the USC&GS and the number of events detected by ST as a function of USC&GS magnitude

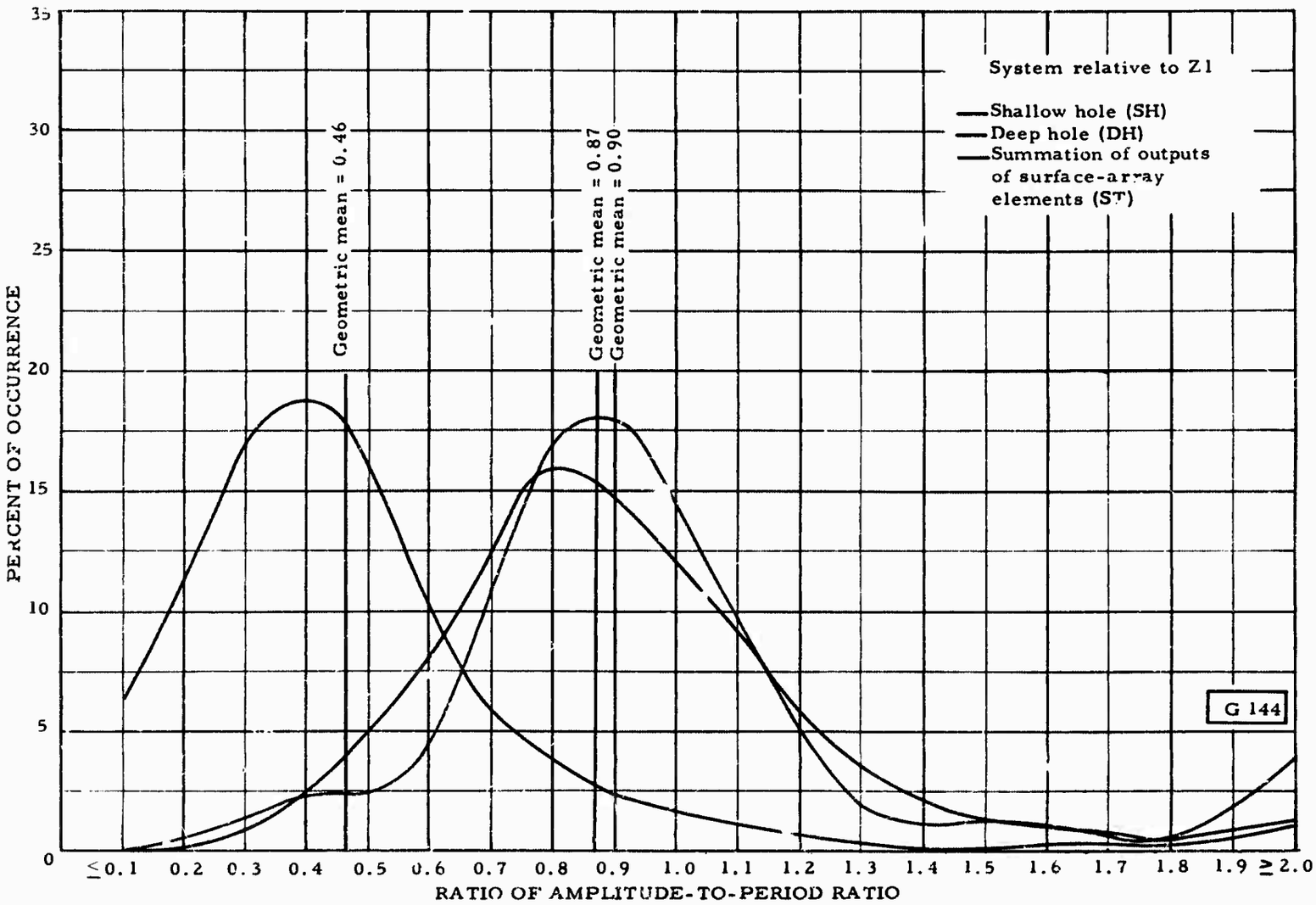

Figure 34. Frequency distribution of the ratios of the amplitude-to-period ratios as computed from the shallow-hole (SH), deep-hole (DH), and surface-array summation (ST) systems relative to Z1

the viewer screen, leaving only the desired seismograms visible. The records were then analyzed, and each event detected was credited to the appropriate system. Because UBSO records many events that are not reported by the USC&GS, system 4 (the full surface complement) was selected as the reference system. If an event was picked on system 4, it was considered to be a valid event; however, if an event was picked on another system and that event was confirmed by the USC&GS, the system was given credit for the detection. A system was not penalized for a mispick, but the "detection credit" previously awarded to that system was revoked. A total of 614 teleseismic events was recorded and analyzed during the test interval.

A summary of the detection credits awarded to each system and the number of events detected by each system that were located by the USC&GS are shown in tables 4 and 5.

A comparison was also made to determine how well (clarity of phase, signal-to-noise ratio, etc.) each event was detected by each system. Each of the 614 events used in this study was compared on the 4 systems. The system which, in the analyst's opinion, recorded the signal best was awarded a grade of 4, the second best 3, etc. If two systems recorded the signal with equal clarity, the same grade was given to both systems. If a system failed to record a signal, no grade was assigned. The total grade for each system for the study interval was obtained and a ratio of the grades relative to system 4 was computed. These data are presented in table 6.

Table 4. Summary of detection credits awarded to each system

System	1	2	3	4
Detection credits	285	325	378	614
Ratio of detection capability of each system relative to system 1	1.00	1.14	1.33	2.15
Percentage of system and detection capability possessed by each system	46.4%	52.9%	61.6%	100.0%

Table 5. Number of events detected by each system for which the USC&GS reported an epicenter

Date	System 1	2	3	4	Number events located by the USC&GS
16 August 1964	5	4	5	7	11
17 August 1964	12	11	12	15	19
18 August 1964	3	3	3	4	8
19 August 1964	0	0	0	1	7
20 August 1964	8	10	8	11	20
21 August 1964	2	4	3	6	11
22 August 1964	4	4	4	4	9
23 August 1964	6	6	6	8	10
24 August 1964	7	8	8	8	14
25 August 1964	4	6	7	7	15
26 August 1964	3	5	5	6	11
27 August 1964	8	8	8	10	17
28 August 1964	2	2	4	4	11
29 August 1964	8	7	8	10	12
30 August 1964	4	4	7	7	13
31 August 1964	3	3	2	4	9
01 September 1964	1	1	1	2	6
02 September 1964	2	2	2	4	4
03 September 1964	7	7	7	7	20
04 September 1964	1	1	1	1	21
05 September 1964	4	4	4	5	14
06 September 1964	9	10	11	11	21
07 September 1964	3	3	3	3	7
08 September 1964	7	7	7	7	14
09 September 1964	3	3	4	4	8
10 September 1964	2	2	2	4	6
11 September 1964	3	3	3	3	4
12 September 1964	5	5	5	8	13
13 September 1964	7	8	8	11	20
14 September 1964	8	7	7	8	14
15 September 1964	4	4	5	6	14
Total	145	152	160	196	383
Percent of USC&GS events detected by each system	37.9%	39.7%	41.8%	51.2%	

Table 6. Summary of the number of detection grade points awarded to each system

	System 1				System 2				System 3							
Grade point	4	3	2	1	4	3	2	1	4	3	2	1	4	3	2	1
Number of each grade value awarded to each system	40	39	79	127	44	124	149	8	81	244	44	9	604	10	0	0
Total value in each grade point cell	160	117	158	127	176	372	298	8	324	732	88	9	2416	30	0	0
Total of all grade points awarded to each system		562				854				1153				2446		
Ratio of the grade points of each system relative to system 4		0.23				0.35				0.47				1.00		

4.6 APPARENT FIRST-MOTION AND ARRIVAL-TIME RESIDUALS

The apparent first motion of 298 events that were mutually recorded by the surface, shallow-hole, and deep-hole seismograph systems was evaluated to determine the degree of agreement among the systems. Of the 298 signals, all systems agreed on the direction of first motion for 140 events (47.0 percent). The degree of agreement among the three systems for the remaining 158 signals is shown in table 7. In addition, the number of times that each system recorded a positive and negative direction of first motion is included.

Table 7. Summary of apparent first-motion determination

Systems in agreement on the direction of first motion	DH and SUR	DH and SH	SH and SUR
Number of times that the indicated systems agree	45	51	62
Probability that the indicated systems will agree when there is not a unanimous determination of direction	0.285	0.323	0.392
System	SH	DH	SUR
Number of times that the indicated system recorded a positive direction of first motion	175	178	175
Number of times that the indicated system recorded a negative direction of first motion	123	120	123

The accuracy of first-motion determination is impossible to establish because the actual first motion of any signal can be distorted by the microseismic background noise even if the true first motion is large enough to be recorded. The three systems agreed on less than one-half of all signals considered during this study; however, the surface and near surface systems appear to give the best estimate of the direction of first motion.

The ST system detected 596 of the 614 events used in this study, and of these 596 events, the DH and SH systems detected 372 and 322 signals, respectively. The arrival-time residuals relative to the surface array as a function of ground motion as recorded on the ST system for the SH and DH systems are shown in figures 35 and 36. The average arrival-time residuals, the number of occurrences, and the maximum and minimum residuals are plotted for each 5-mμ increment. All events recorded on ST whose amplitudes were too large to measure were included in the largest amplitude group.

Because of the depth of the DH seismometer, the arrival-time residuals show a consistant negative trend; however, a considerable scatter of data points was observed in the lower amplitude increments. Compressional wave velocities (obtained from sonic well logs) in the 2700.5 meter (8860-foot) section indicate that a vertically incident P-wave would take 0.70 second to travel from the DH seismometer to the surface. The apparent time differential will decrease as the angle of incidence increases, but this factor is not of sufficient magnitude to explain the average residual of -0.46 second observed on the DH system. At intermediate teleseismic distances, the angle of incidence affects the time residual by less than 0.1 second. The discrepancy between observed and predicted arrival-time residuals is probably due to a combination of factors. Because of the ability of the filtered summation seismograph to enhance signals and suppress microseismic background noise, events will tend to be picked earlier on the full-surface complement than on any single seismograph. The predicted time lapse between the DH and SH systems is essentially the same as for the DH and surface systems. The average observed time difference between the DH and SH systems, 0.73 second, agrees well with the predicted time difference. From these data, it appears that events detected on the surface system are timed on an average of from 0.25 to 0.27 second earlier than on a single seismograph.

5. CONCLUSIONS

The results of the several comparative methods of evaluation of the DH, SH, and surface systems indicate that the full-surface complement of seismographs is superior in every respect to either of the single buried systems. However, when only the single surface seismograph is compared with the two buried systems, the DH seismograph becomes the most effective system for detecting

teleseismic events. Even though the SH system is not affected by certain types of surface generated noise, it appears to be a less satisfactory system than the DH. This is probably due to the presence of certain types of microseismic noise trapped in the low-velocity upper layers. The biggest advantage of the SH system is realized during windy periods when the surface systems become unreadable. It was impossible to quantitatively evaluate the attenuation of wind-generated noise during the course of this study; however, a comparison of the seismograms in figures 37 through 46 illustrate the effectiveness of the recently installed shallow-buried array of seismometers in attenuating wind-generated noise. The seismometers of this array are buried to a depth of 61 meters (200 feet), about the same depth as that at which the SH system was operated during the study interval.

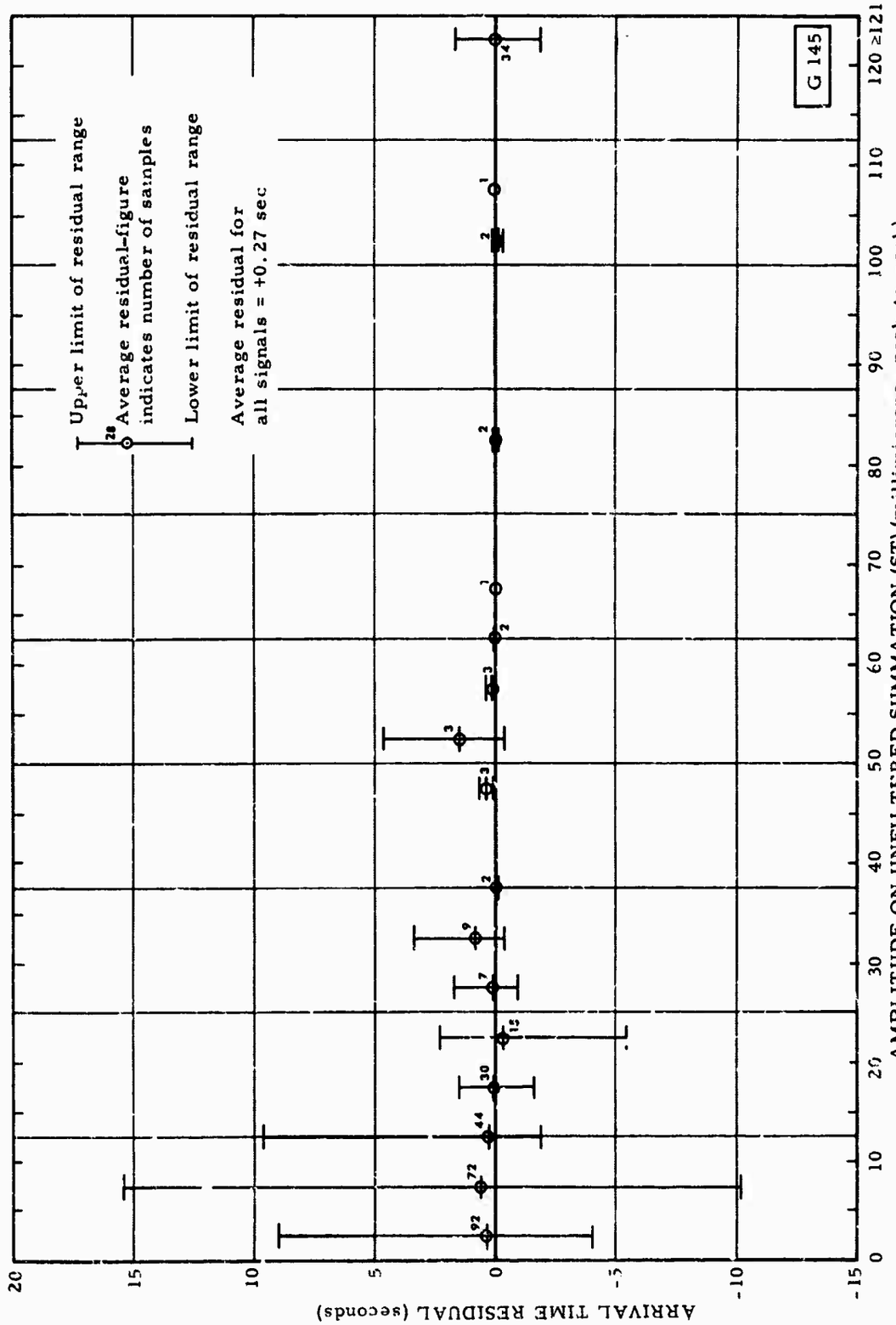

Figure 35. Shallow-hole arrival-time residuals relative to the surface array as a function of signal amplitude on the ST system

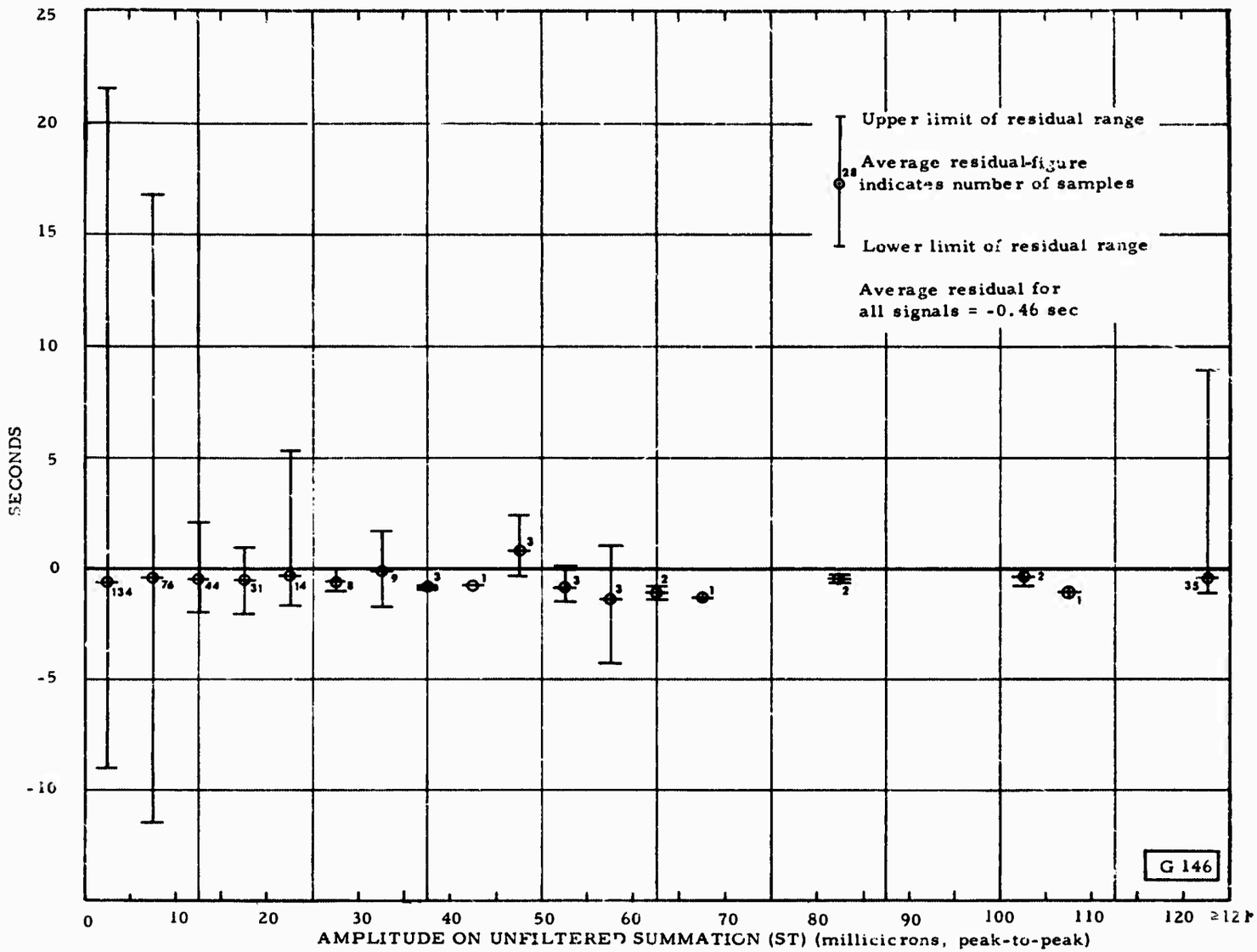

Figure 36. Deep-hole arrival-time residuals relative to the surface array as a function of signal amplitude on the ST system

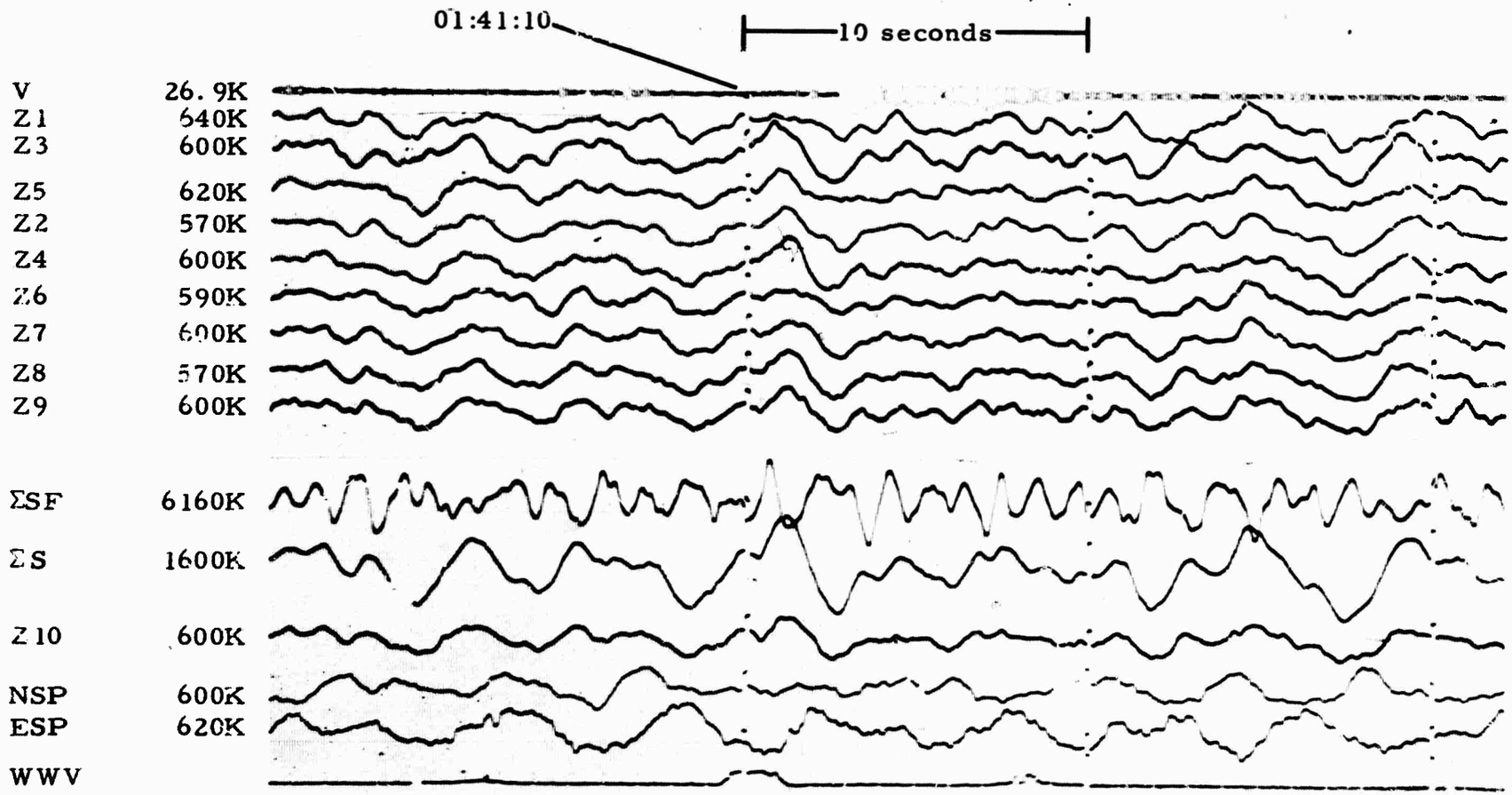

UBSO
Run 076
17 Mar 65
Data group 5000

Figure 37. Surface array, UBSO, Wind = 18 mph. Dir = SW
(X10 enlargement of 16-mm film)

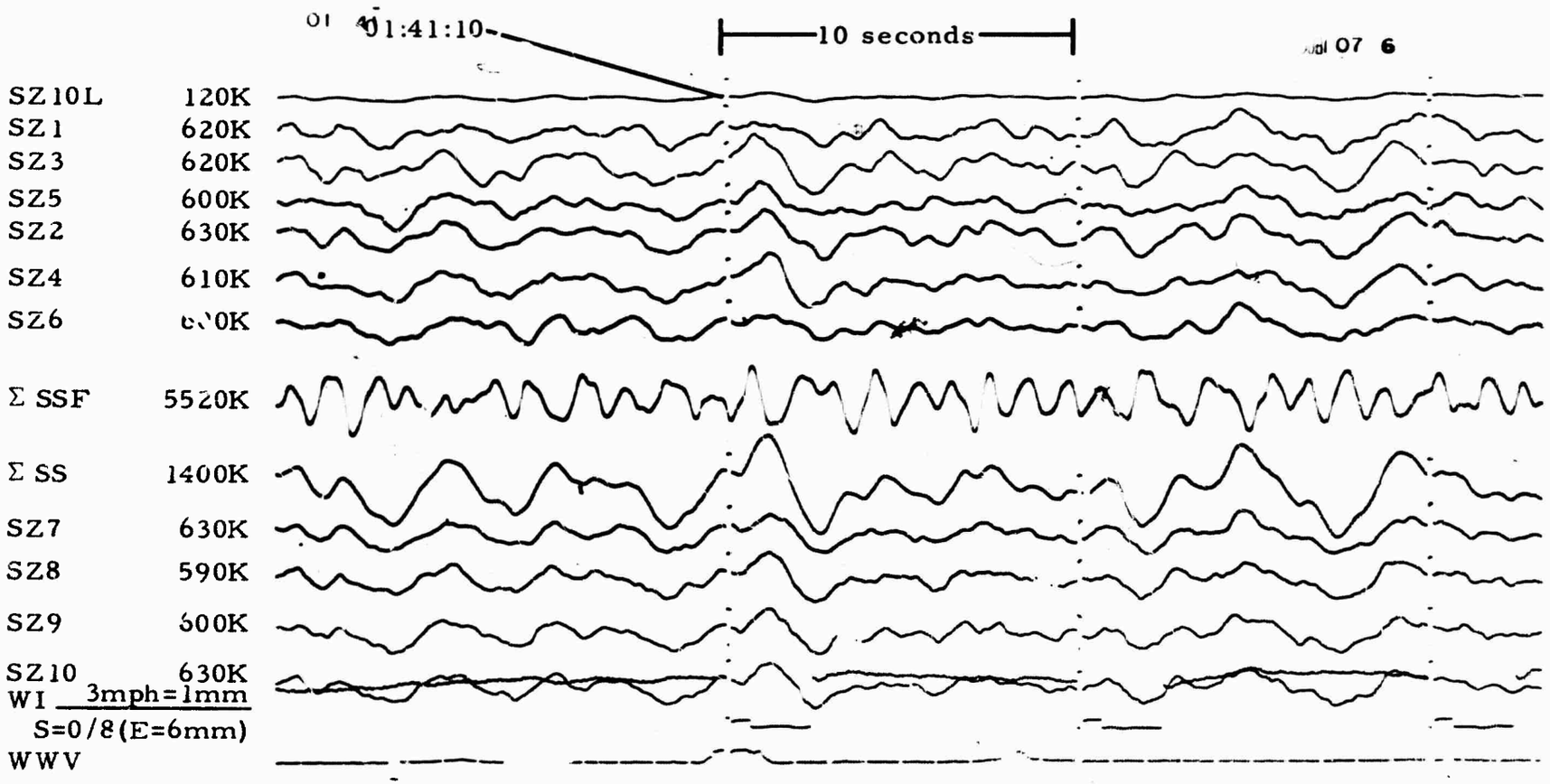

UBSO
Run 076
17 Mar 65
Data group 5016

Figure 38. Shallow-buried array, UBSO. Wind = 18 mph. Dir = SW
(X10 enlargement of 16-mm film)

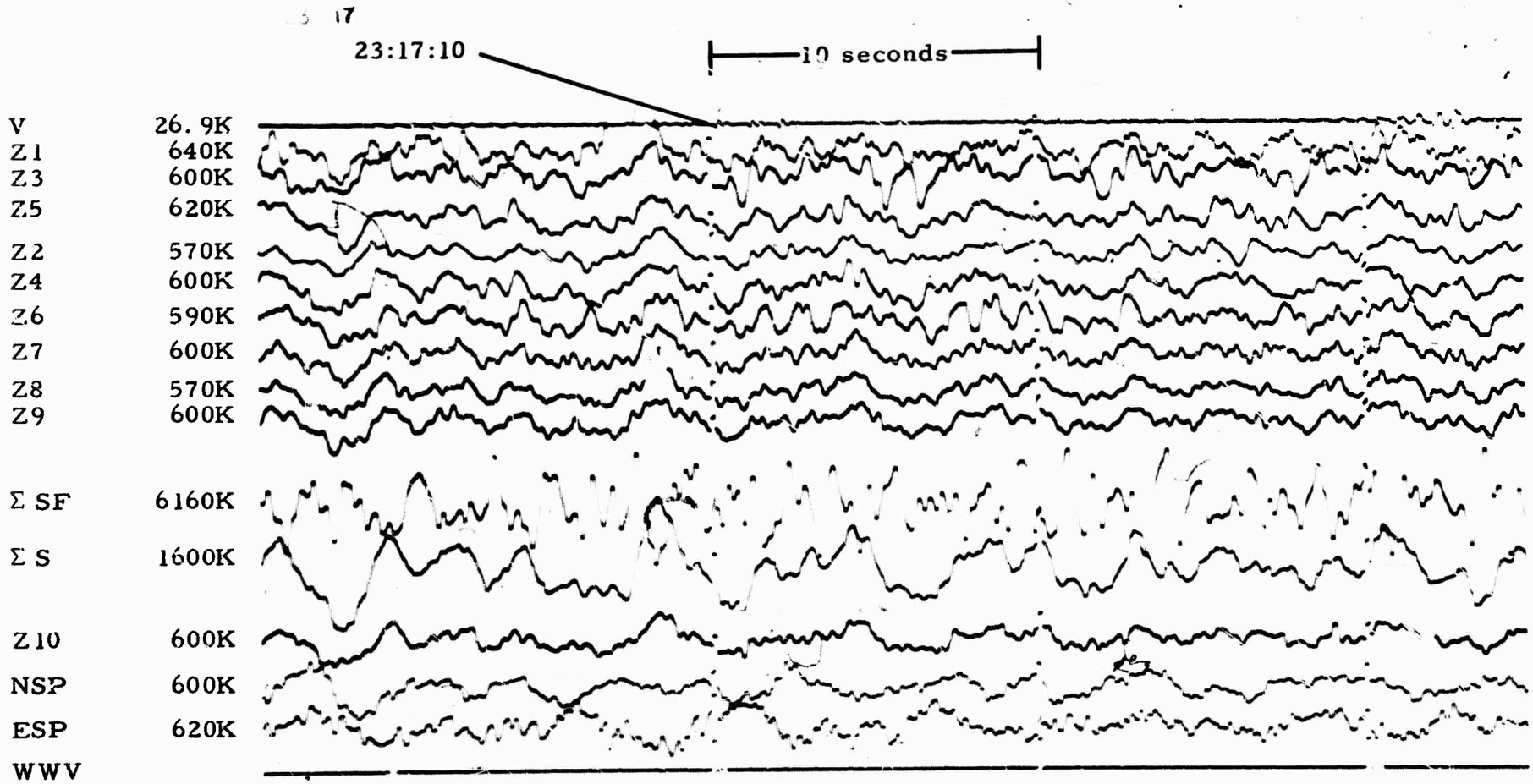

UBSO
Run 076
17 Mar 65
Data group 5000

Figure 59. Surface array, UBSO. Wind = 25 mph. Dir = W
(X10 enlargement of 16-mm film)

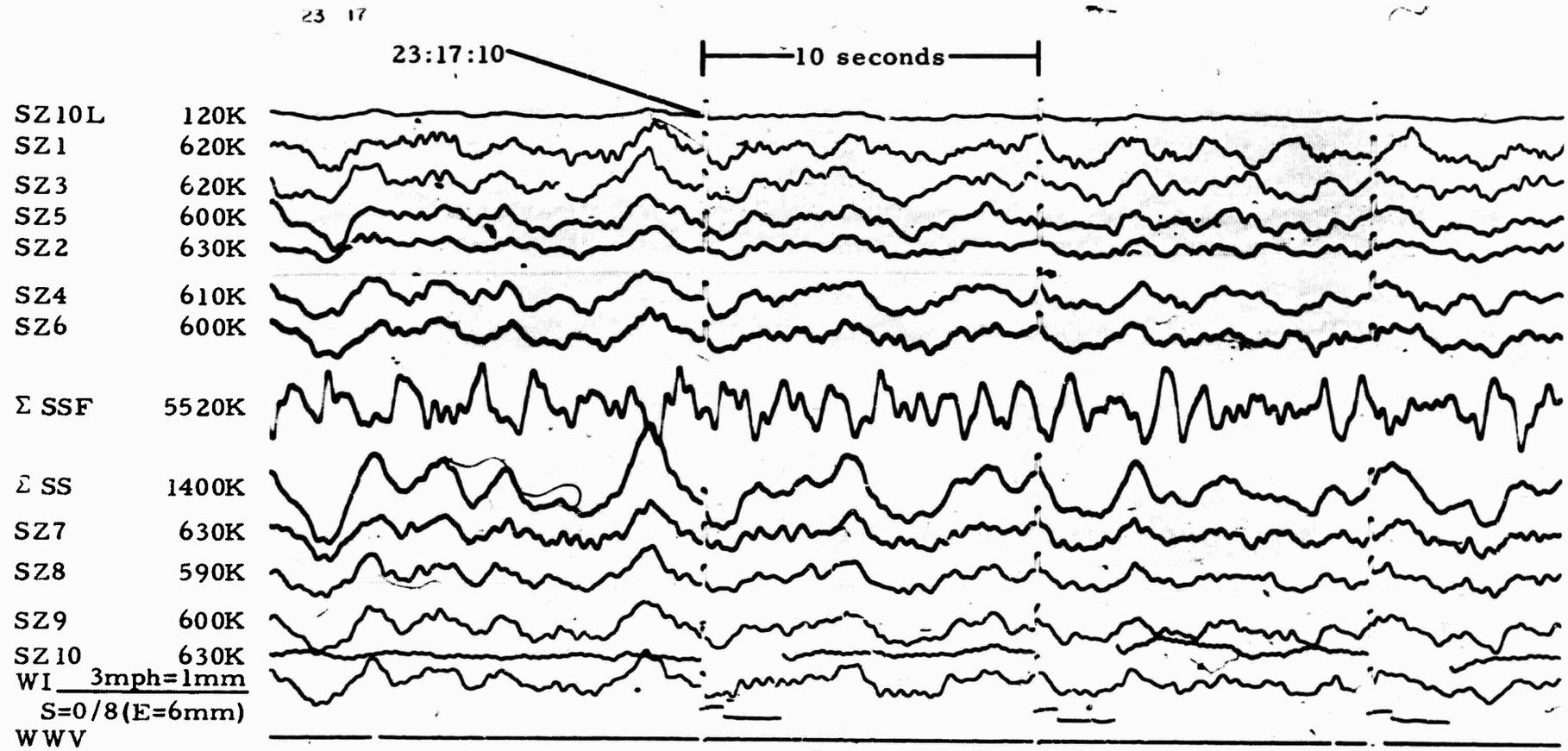

UBSO
Run 076
17 Mar 65
Data group 5016

Figure 40. Shallow buried array, UBSO. Wind = 25 mph. Dir = W
(X10 enlargement of 16-mm film)

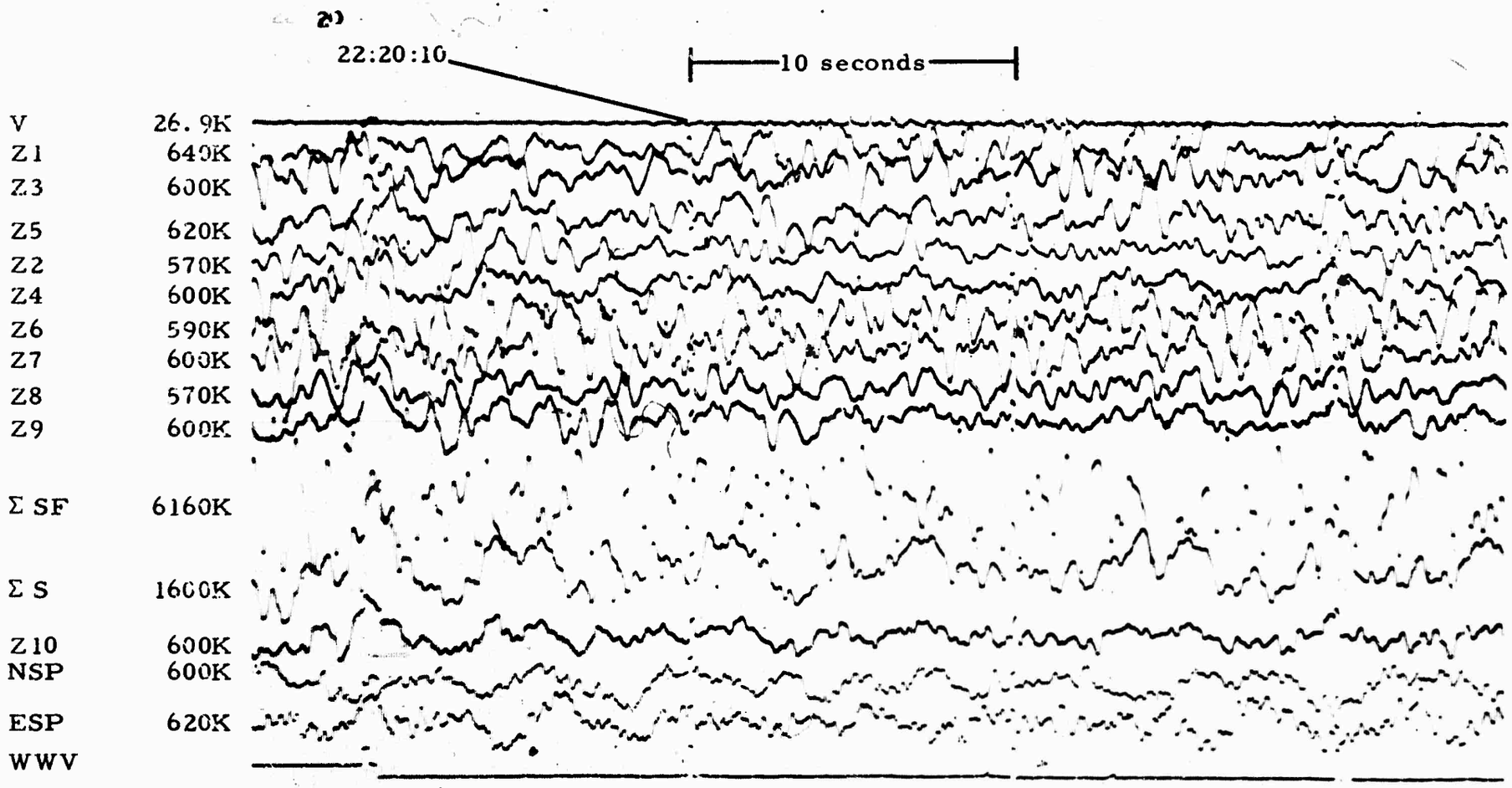

UBSO
Run 076
17 Mar 65
Data group 5000

Figure 41. Surface array, UBSO. Wind = 30 mph. Dir = WSW
(X10 enlargement of 16-mm film)

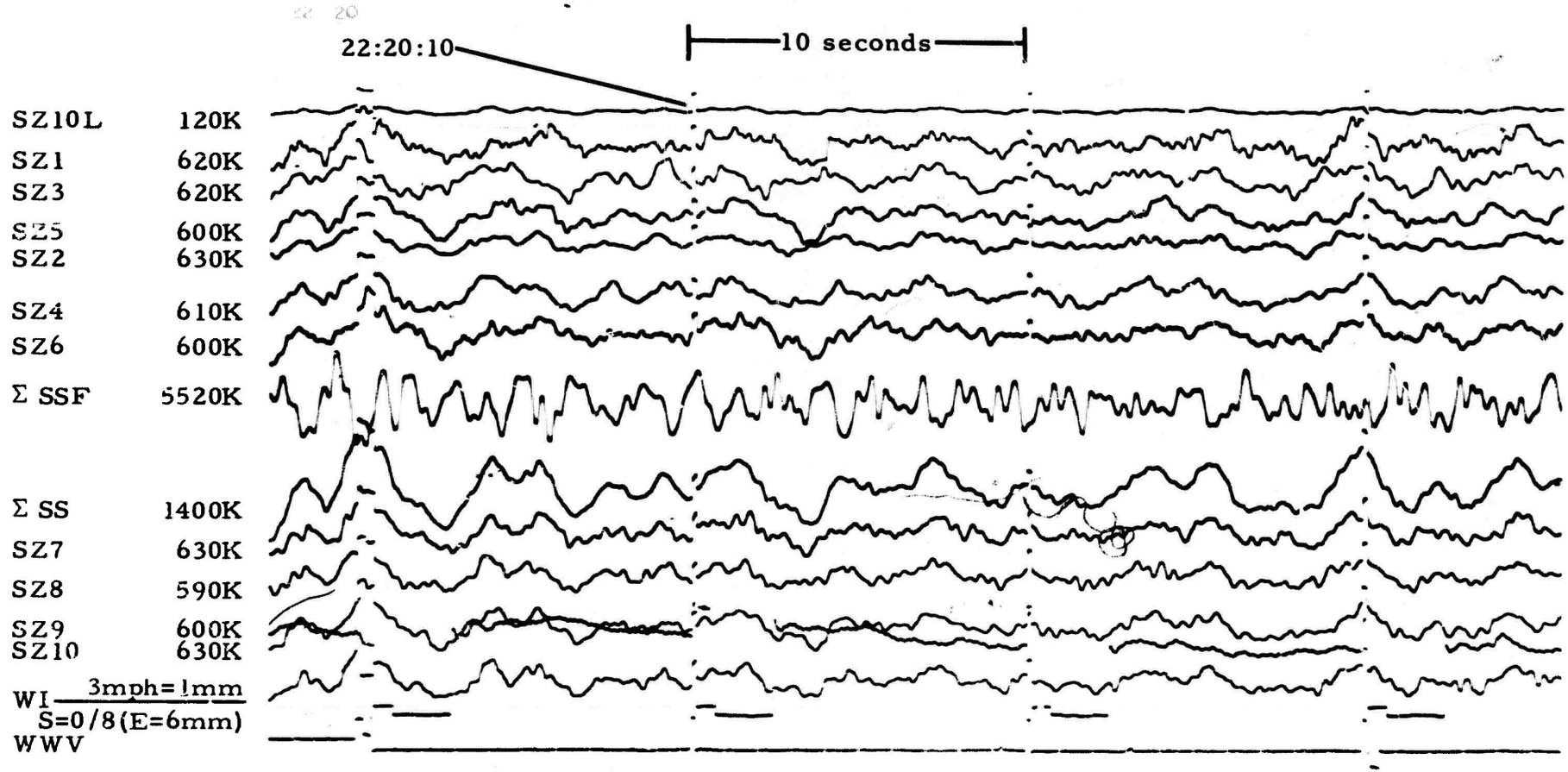

UBSO
Run 076
17 Mar 65
Data group 5016

Figure 42. Shallow buried array, UBSO. Wind = 30 mph. Dir = WSW
(X10 enlargement of 16-mm film)

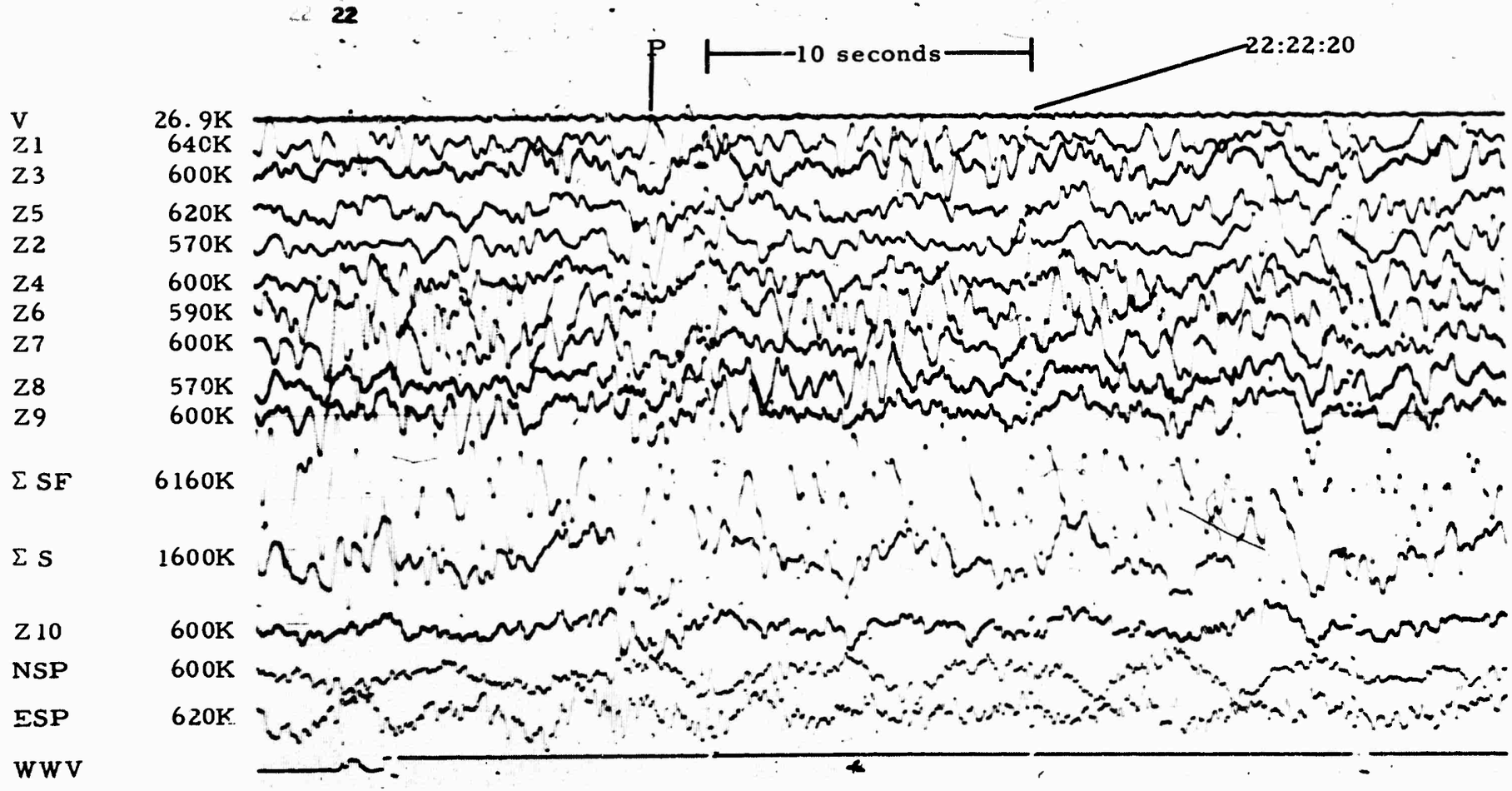

UBSO
Run 076
17 Mar 65
Data group 5000

Figure 43. Surface array, UBSO. Wind = 30 mph. Dir = SW
Teleseismic P phase; epicenter unknown
(X10 enlargement of 16-mm film)

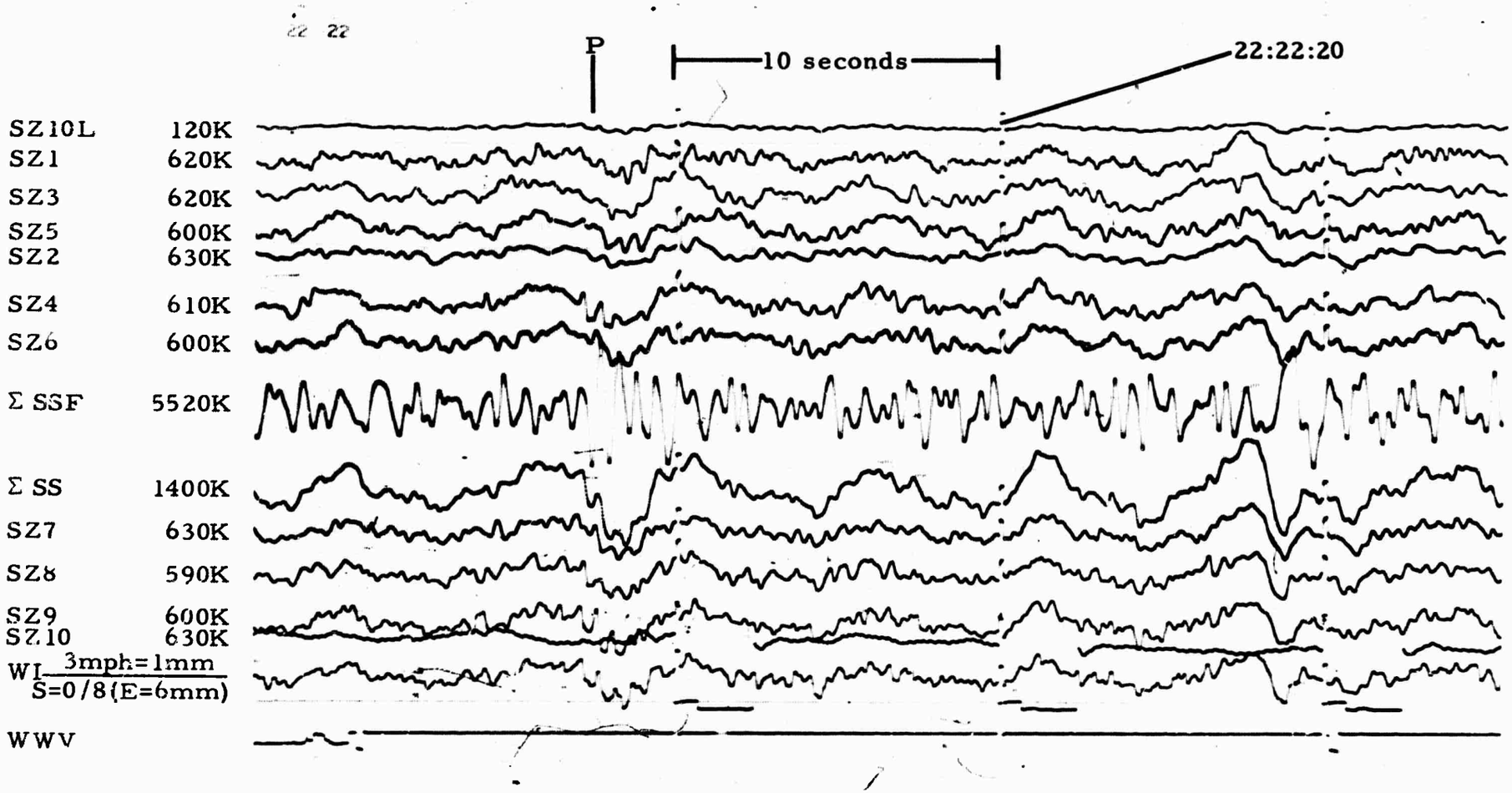

UBSO
Run 076
17 Mar 65
Data group 5016

Figure 44. Shallow buried array, UBSO. Wind = 30 mph. Dir = SW
Teleseismic P phase; epicenter unknown.
(X10 enlargement of 16-mm film)

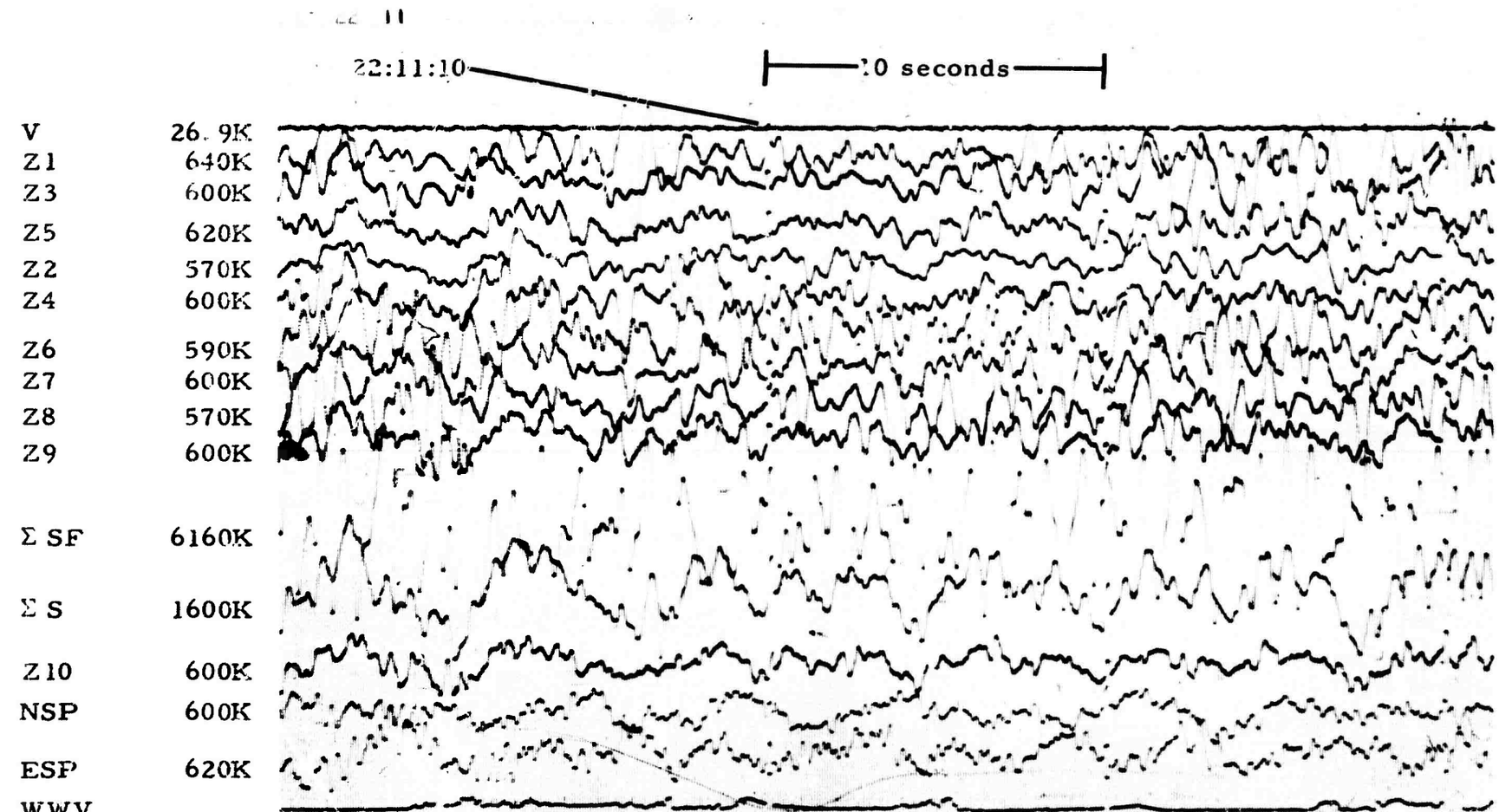

UBSC
Run 076
17 Mar 65
Data group 5000

Figure 45. Surface array, UBSO. Wind = 39 mph. Dir = WSW
(X10 enlargement of 16-mm film)

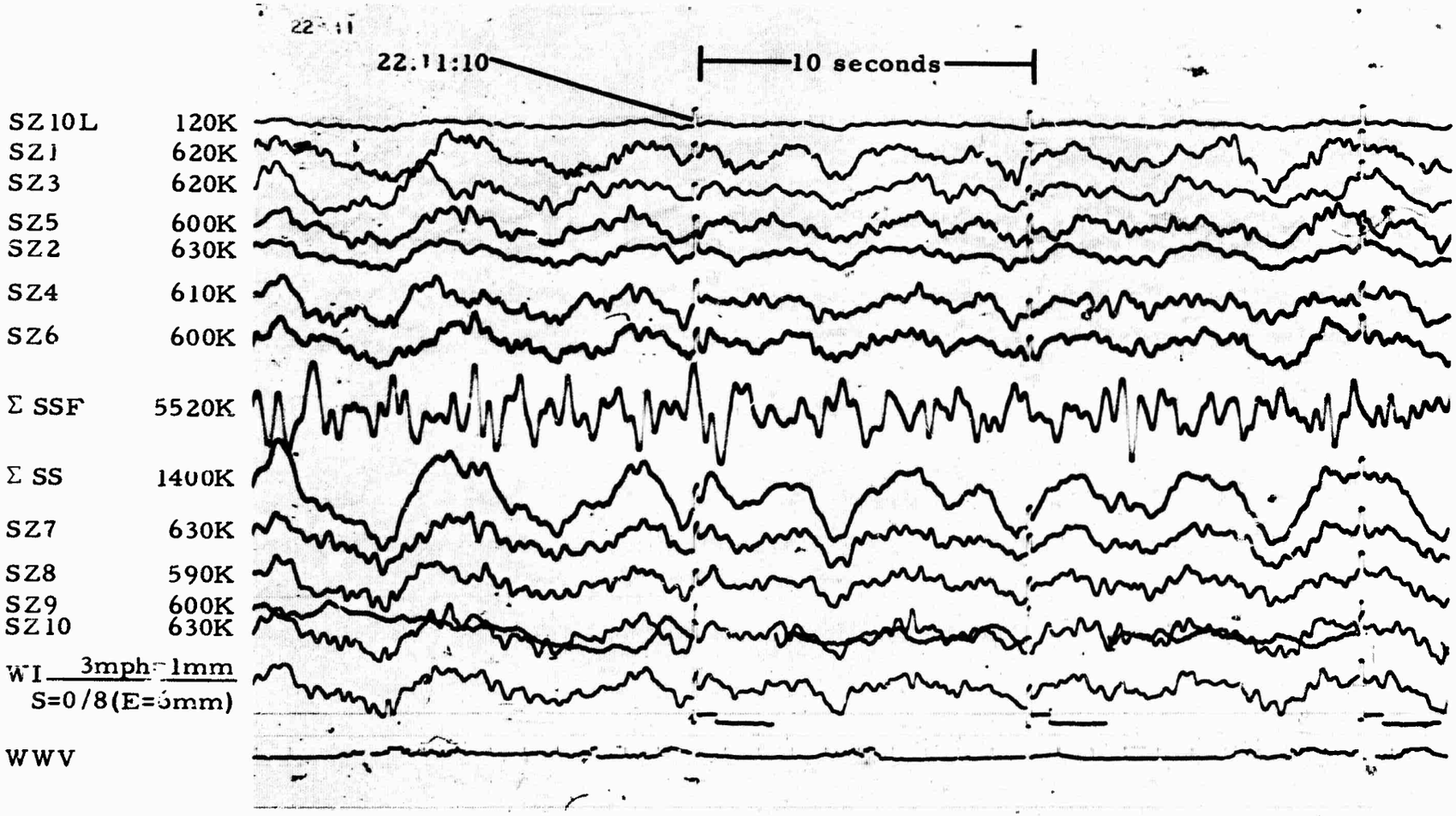

UBSO
Run 076
17 Mar 65
Data group 5016

Figure 46. Shallow buried array, UBSO. Wind = 39 mph. Dir = WSW
(X10 enlargement of 16-mm film)

REFERENCES

Geotechnical Corporation, 1964, Technical Report No. 64-101, Deep-hole site report U.S.A No. 1, Uintah County, Utah.

Texas Instruments Inc., 1963, Final report on Project VT/1124 to construct, equip, and operate three seismological observatories.

Miller, Robert L., and Kahn, James Steven, 1962, Statistical analysis in the geological sciences.

APPENDIX 1 to TECHNICAL REPORT NO. 65-124

ANALYSIS ASSIGNMENT SEB-3-64

AIR FORCE TECHNICAL APPLICATIONS CENTER
Headquarters United States Air Force
Washington DC 20333

Project VELA T/1124
Project VELA-UNIFORM

Analysis Assignment SEB-3-64
23 April 1964

Title: Comparison of Surface Array, Deep-Well, and Shallow-Well Capabilities in Detecting Teleseismic P Arrivals at the Uinta Basin Seismological Observatory.

Analysis Assignment: Perform analysis of Uinta Basin Seismological Observatory (UBSO) seismic data, including deep-well (DW) and shallow-well (SW) data, to determine relative capabilities of the standard UBSO instrumentation (Z1, $\sum$Z1-10, $\sum$Z1-10 filtered) and of the DW and SW seismographs to detect teleseismic P arrivals. Analysis should include, but need not be limited to:

a. Amplitude distribution of signals for all teleseismic events.

b. Amplitude distribution as a function of magnitude (US Coast and Geodetic Survey computed) for teleseismic events.

c. Comparison of UBSO magnitude computations for surface, DW, and SW systems.

d. Comparison of number of teleseismic events detected by UBSO standard instrumentation and by DW and SW seismographs.

e. Comparison of detection of apparent first motion by UBSO standard instrumentation and by DW and SW seismographs.

f. Comparison of signal-to-noise (S/N) ratios computed from seismograms of standard UBSO instrumentation and of DW and SW systems for P arrivals common to all systems under study.

g. Examine and analyze short-period microseismic noise recorded by DW and SW systems and standard UBSO instrumentation; include an examination of wind generated noise. Compute attenuation factors versus depth for specific periods (0.1 - 3 sec) as measured visually.

Reports:

1. An interim letter-type report may be requested, depending on the length of routine operation of the DW and SW seismographs at UBSO. Content will be specified by the project officer after discussion with the contractor.

2. A final report should be submitted to AFTAC in draft form in 2 copies and should present the following:

a. Evaluation of the relative capabilities of Z1, $\sum$Z1-10, and $\sum$Z1-10 filtered, SW, and DW seismographs.

b. Evaluation of the relative capabilities of SW, DW, and the combined UBSO systems.

c. Presentation of data analysis performed under assignment paragraph.

Following a review and acceptance of the final report by AFTAC, distribution instructions will be provided.

Time Schedule:

1. An interim report should be submitted within 15 days after request is received from the project officer.

2. A final report should be submitted not later than 30 days after routine operation of the DW and SW seismographs has ended at UBSO.

Clent Houston

CLENT HOUSTON, Captain, USAF
VELA Seismological Center
AF Technical Applications Center
DCS/Plans and Operations